"Dunărea de Jos" University of Galati

Doctoral School of Mechanical and Industrial Engineering

DOCTORAL THESIS

EXTENDED ABSTRAT

AN EXPERIMENTAL AND THEORETICAL STUDY ON STABBING AND PUNCTURE RESISTANCE OF STRATIFIED PANELS

Doctoral student

eng. Viorel TOTOLICI-RUSU

Scientific coordinator

prof. eng. Lorena DELEANU, PhD

Series I6: Mechanical Engineering No 73

Galati

2023

"Dunărea de Jos" University of Galati
Doctoral School of Mechanical and Industrial Engineering

DOCTORAL THESIS

EXTENDED ABSTRACT

AN EXPERIMENTAL AND THEORETICAL STUDY ON STABBING AND PUNCTURE RESISTANCE OF STRATIFIED PANELS

Doctoral student
eng. Viorel TOTOLICI-RUSU

President	**Prof. eng. Eugen Victor RUSU, PhD** President of the Doctoral School - Universitatea "Dunărea de Jos" din Galați
Scientific coordinator	**Prof. eng. Lorena DELEANU, PhD** "Dunărea de Jos" University of Galati
Official Referent	**Prof. eng. Adrain ROTARIU, PhD** Technical Military Academy "Ferdinand I", Bucharest
Official Referent	**Scientific researcher (CS) II, dr. . Simona Maria SANDU, PhD** Research and Innovation Centre for Chemical, Biological, Radiological and Nuclear Defence and Ecology, Bucharest, Romania
Official Referent	**Prof. phys. Gabriel MURARIU, PhD** "Dunărea de Jos" University of Galati

Series I6: Mechanical Engineering No 73
Galati
2023

The PhD thesis series publicly defended in UDJG since October 1, 2013 are:

Field of **ENGINEERING SCIENCES**

Series I 1:	**Biotechnologies**
Series I 2:	**Computers and information technology**
Series I 3:	**Electrical engineering**
Series I 4:	**Industrial engineering**
Series I 5:	**Materials engineering**
Series I 6:	**Mechanical engineering**
Series I 7:	**Food engineering**
Series I 8:	**Systems engineering**
Series I 9:	**Engineering and management in agri-culture and rural development**

Field **ECONOMIC SCIENCES**

Series E 1:	**Economy**
Series E 2**:**	**Management**

Field **HUMAN SCIENCES**

Series U 1:	**Philology - English**
Series U 2:	**Philology - English**
Series U 3:	**History**
Series U 4:	**Philology - French**

Field **MATHEMATICS AND NATURAL SCIENCES**

Series C:	**Chemistry**

Many Thanks

I would like to express my warm thanks to those who have given me all their support and guidance during this PhD thesis.

First of all, I would like to thank professor eng. Lorena Deleanu, PhD, whom, as my scientific supervisor, with great patience, dedication and professionalism, offered me guidance and permanent encouragement throughout the years of elaboration of my PhD thesis.

I would also like to thank he supervision commission of the thesis, composed of prof. phys. Gabriel Murariu, PhD, associated prof. eng. Boazu Doina, PhD and associated prof. eng. Constantin Georgescu, PhD, for their support, for the professionalism and objectivity with which they analysed the reports and the thesis, for all the constructive criticisms, for the competent recommendations that only guided me towards the expected result.

In the experimental approach, I was supported by phys. Simona Maria Sandu, PhD, eng. Cristian Popescu and the staff of CCIACBRNE - Research and Innovation Centre for CBRN Defence and Ecology, Bucharest, to whom I thank and assure them of my full consideration.

I would also like to thank eng. Mihai Boțan, PhD, eng. Cătălin Pîrvu, PhD and eng. George Cătălin Cristea, PhD, from the National Institute for Aerospace Research and Development "Elie Carafoli" - INCAS Bucharest, for all their support and pertinent recommendations made during the experiments.

I would like to thank the welding technician Mironov Paul for the masterful processing of the sharp-edged weapons according to NIJ 0115.00 standard.

Last but not least, with gratitude, I thank my entire family, who with great patience and understanding, stood by me, encouraged and supported me throughout this trial.

Eng. Viorel Totolici-Rusu

Galati, 24.11.2023

Table of Contents

	Thesis	Summary
Many Thanks	3	3
Table of Contents (in Romanian)	5	-
Table of Contents (in English)	7	5
Introduction (in Romanian)	9	-
Introduction (in English)	11	-
Notations and abbreviations	13	-
List of figures. List of tables	14	-
Chapter 1. Current status on the structure, testing and evaluation of material characteristics at edged weapon impact	21	7
1.1. Introduction	21	7
1.2. A short history of edged and pointed weapons and armour	21	7
1.3. Stab protection materials	27	8
1.4. High performance fibres used in personal protection	29	8
1.5. Test methods for stab resistance assessment	29	9
1.6. Research directions for this studyu	51	14
Chapter 2. Organisation of the thesis	53	-
2.1. Importance of the theme and main objectives	53	-
2.2. Organisation of the thesis	54	-
Chapter 3. Particular aspects for solving the panel-knife impact model in Explicit Dynamics	56	15
3.1. Introduction	56	15
3.2. Mechanisms for stabbing fabric	59	16
3.3. Stab resistance of materials	61	17
3.4. Analysis of the dynamic strength mechanism of the fabric	63	17
3.5. Defining materials in Explicit Dynamics	65	18
3.6. Defining connections	66	19
3.7. Geometric model	67	19
3.8. Analysis of the simulation results	71	21
3.9. Conclusions and model validation aspects	82	30
Chapter 4. Materials and test methods for assessing the stabbing and puncture behaviour of panels	84	31
4.1. Introduction	84	31
4.2. Importance of testing for bladed weapon resistant materials (knives, spikes)	87	31
4.3. Test classification criteria for assessing stabbing and puncture protection	88	32
4.4.Materials and methods for testing stab and puncture protection panels	90	33
4.4.1. Materials for stab-resistant and puncture-resistant panels, developed by the author	90	33
4.4.2. Auxiliary materials for stabbing and puncture testing	95	35
4.5. Blank weapons threats, used in stabbing and pricking tests	97	37
4.6. Laboratory panel technology	99	38
4.7. Test campaign to assess the behaviour of the panels in the event of puncture and stabbing	101	38
4.7.1. INCAS testing procedure	103	38
4.7.2.Test procedure on Instron 9340 (INCAS) machine	105	40
4.7.3. Measured parameters and repeatability of Instron 9340 tests	111	41

4.7.4 Test procedure and test facility at CCIACBRNE	113	42
4.8. Photographing samples in detail	121	45
4.9. Sample preparation for the scanning electron microscope (SEM)	124	45
4.10. Conclusions on stabbing and puncture testing	126	45
Chapter 5. Experimental data on stabbing and puncture resistance for the tested panels	128	46
5.1. Stab and spike testing	128	46
5.2. Characteristics studied in the stabbing and puncture process	130	46
5.3. Experimental results on the Instron CEAST 9340 impact machine	132	50
5.3.1 Parameter analysis of force, energy and velocity curves determined as a function of time for S1 knife tests	132	50
5.3.1.1. Introduction	132	50
5.3.1.2 Influence of the number of layers on the force, velocity and energy curves as a function of time	133	50
5.3.1.3 Influence of impact energy on force, energy and velocity curves over time	142	55
5.3.1.4 Influence of the number of layers in the panel, when spiked, on the force, velocity and energy curves as a function of time	145	57
5.3.2. Influence of impact energy for spike tests	149	59
5.4. Influence of the weapon on the force-time, energy-time and velocity-time curves	152	60
5.5. Evaluation of hybrid panels	158	62
5.6. Stabbing and puncture damage mechanisms	163	64
5.6.1. Introduction	163	64
5.6.2. Analysis of stabbing destruction processes	164	65
5.6.3. Analysis of the S1 knife stab failure mechanisms for the panels made, based on images obtained with the scanning electron microscope	165	65
5.6.4. Analysis of puncture damage processes	174	69
5.6.5. Analysis of yarn and fibre failure processes under spike impact using SEM images for SRM509 fabric panels	178	70
5.7 Summary of experimental results, obtained on the Instron 9340 drop-test machine	184	72
5.7.1. Summary of results obtained in S_1 knife tests	184	72
5.7.2. Conclusions drawn for the tests performed on the Instron 9340 drop-test machine	187	73
5.8. Tests on the CBRNE installation	195	79
5.9. Conclusions for experimental data	203	81
Chapter 6. Conclusions	205	82
6.1 Importance of the theme	205	82
6.2. Final conclusions on the stab resistance of the tested panels	206	83
6.3 Personal contributions	207	84
6.4. Research directions initiated by this study	209	86
List of the author's scientific works	210	87
References	212	89

Chapter 1
Current Status on the Structure, Testing and Evaluation of Material Characteristics at Impact with Edged Weapons

1.1. Introduction

The anti-personnel threat is the intention to take the enemy out of the fight.

The knife is a tool particularly used for cutting. It has as its component parts a handle and a blade. The blade is usually made of metallic materials, may have serrations and may vary in the shape of the edge. Knives have been used as tools in kitchens, workshops, surgery, slaughterhouses or as weapons, since ancient times.

Armour is an equipment for personal protection for people working in hazardous areas. It is a defensive weapon, used for personal protection in hazardous situations. There are several varieties of armour, including accessories for the head, body, arms, legs or even vehicles.

Armour has been used throughout history, first made of leather and bone, followed by bronze and steel, and now modern materials such as aramid fibers and composites.

1.2. A Short History of Edged and Pointed Weapons and Armours

Knives have been used throughout the ages, as weapons for combat, tools in various situations, in construction, as utensils for survival, in food preparation since prehistoric times, as a vital tool in survival, it became a basic tool that allowed the development of technology, military, culture, science, etc..

Armour has historically been used for both human and animal protection, and even for vehicle protection, once the need arose in the modern era. Since the Second World War (1939-1945), the use of armoured fighting vehicles has become a standard in the field.

What's worth noting is that armour has evolved along with weapons. As soon as the protective elements appeared, so did the weapons that tried to overcome them. And even though in this race, weapons are often more advanced, the creators of weapons are not left behind and sometimes come out ahead, though not for long.

Protective packages or equipment are made up of components, the largest in terms of surface area being the front and back panels of the wearer, and can be classified according to the protection provided: bulletproof, stab-resistant, or a combination of bulletproof and stab-resistant. Some vests may be fitted with neck, shoulder and lower abdominal protection.

The ratio of offensive to defensive weapons has, perhaps, been the most active factor in the evolution of both categories, and in general there has been, at least for the modern era, a certain advance of the offensive element. Thus, it can be said that: the knife appeared first and then the shield, the cannon first and then the fortification system, the bullet first and much later the bullet-proof vest, or the air force first and only later the anti-aircraft artillery, the examples could be continued.

1.3. Stab Protection Materials

In general, ballistic and sharps protective clothing, also called personal armor, can be worn by police, military and other civilians, such as: journalists, security guards, to protect themselves from ballistic threats and knives, etc. [Lewis E., 2021].

The main mechanical properties of fibres are: breaking load or toughness, elongation at break percentage, breaking work, initial modulus, modulus of elasticity, work factor, elastic recovery, fatigue limit, shear strength, friction coefficient, heat retention resistance, flammability, etc. [El Messiry M. 2020].

Examples of fibres also used for personal protection are:

- inorganic: carbon, ceramic, glass, metallic,
- organic: acrylic, aramid, elastane, polyamide, polyester, polyethylene, vinyl.

Personal protective equipment refers to any equipment designed to protect against one or more hazards that could endanger health at work with certain performance as shown in Fig. 1.1.

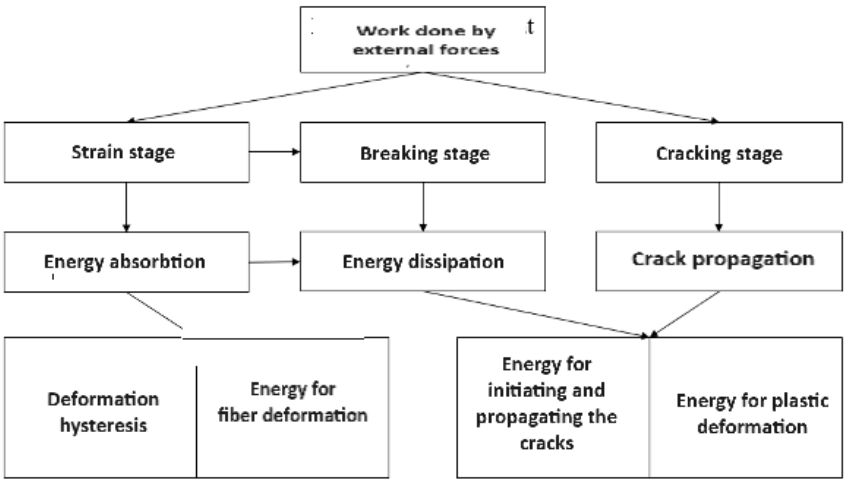

Fig. 1.1. Selection of personal protective equipment

Fibres with high specific strengths and high specific modulus, such as boron fibres, glass fibres, especially E-, S- or R-glass, carbon fibres and aramid fibres, are used to make high-performance composite materials.

Aramid materials have experienced a spectacular development in the manufacture of composites because they have remarkable properties: corrosion stability, absorbs vibrations, therefore shock absorbing, good specific tensile strength, excellent shock and fatigue resistance, zero thermal expansion, good chemical resistance to fuels, low density, flame retardant (does not melt); - low smoke release.

1.4. High Performance Fibres Used in Personal Protection

The mechanical properties of fibres depend on their molecular structure, which can be arranged in crystalline or amorphous forms. The molecules are arranged mainly along the axis of the fibres and are linked with intermolecular bonds. Technical fibres possess a high level of strength and modulus with a low density and they are able to withstand high temperatures. They have chemical resistance, abrasion resistance, fatigue resistance, heat resistance and cut resistance.

High performance fibres are characterised by high strength (3-7 GPa) and Young's modulus (50-400 GPa). Their properties make them ideal for fabric manufacture, ballistic

applications and clothing providing mechanical and chemical protection etc. These properties are achieved through strong continuous isomorphism and ultra-high molecular weight, with a linear fibre strand of covalently bonded carbon atoms and hydrogen bonds. They are used to obtain advanced fabrics for special technical functions, such as: heat resistant armour, chemical resistance protective fabrics, cut resistance gloves, impact energy absorbing hardboard, electromagnetic plates, shielding, flame retardant vests, radiation shield vests, stab resistant vests, bullet proof vests, etc.

1.5 Test Methods for Stab Resistance Assessment

Given the risk that a stab-proof vest has to face, the test methods can be classified into levels:

- preliminary tests on small-sized test panels and classical testing machines;
- tests on standards-compliant panels;
- prototype trials;
- product trials.

To improve stab resistance but, at the same time to reduce the weight of the stab-resistant coating, researchers [Xia, 2019] prepared stab-resistant composites by coating (lining) the aramid fabric with boron carbide (B4C)/epoxy resin. It was shown that when the particle diameter is 2.5 μm, the mass fraction 49%, and the mixing temperature is 30 °C, the particle dispersion is most uniform. Then, the B4C dispersion was mixed with the epoxy resin and the aramid fabric was coated with it, after which, stiffness, pull-out, breakage and quasi-static puncture tests were performed on the treated material. The aramid fabric was cut to a size of 150 mm x 150 mm. In order to test the effects of B4C fillers on the flexibility of coated composites, coated composite specimens were evaluated by the cantilever beam method, with the coated and uncoated side as the bottom side, respectively. The tests were in accordance with Standard GB/T18318-2001. In the punching process, a triangle zone is generated around the cut edge, which has a significant influence on the stab resistance performance.

Cutting tests were also performed by [Wang L., 2021] according to International Standard ISO 13997. A cutting edge with a specified load and a certain speed (2.5±0.5 mm/s) was allowed to cut the samples. In the cut, the normal load and the tangential force, resulting from the sliding motion of the blade, were involved. For each applied load, the horizontal sliding distance of the blade from initial contact to cutting point is recorded. Five identical tests were performed and average values of the sliding distance were calculated.

The resulting load versus displacement curve can be used to determine the shear strength property of the specimen [ASTM F1790-04, 2003].

The use of the technology, allowed designers [Johnson A., 2013] to reduce conventional design restrictions for the manufacture and assembly of protective panels, using additive fabrication.

This provided the designers with a technology to achieve innovative and geometrically complex functional fabric assemblies. Armor designed from polymeric material, fabricated with additives, such as scales, begins to address some of the problems associated with body armor, including:

- use of the layer-by-layer production approach to incorporate cooling channels into a complex armouring assembly, thereby seeking to enhance thermal comfort and operational performance;

- Incorporating body scanning to create custom armour specific to the user's needs, reducing potential injuries sustained as a result of wearing the wrong armour.

In order to facilitate testing, a suitably designed impact platform, resistant to knife and cutting/sharp objects as defined by [HOSDB Body Armor Standard, Publication 39/07/C] was required.

The support material, used for this series of experiments, was a type of clay that is typically used during ballistic tests to replicate the body armor of the human body [Johnson A., 2010], [Croft J., 2007c)].

For each planar thickness, there were three specimens, each manufactured with a size of 80 x 80 mm and showing the impact location in the centre of its upper face. Prior to testing, two centrally located impact zones were identified on the hinged test specimens, each impact location being tested twice. These locations are shown in Fig. 1.2.

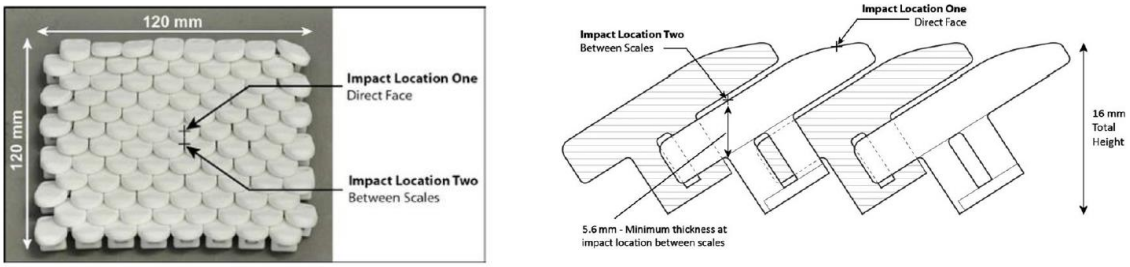

a) Two impact areas b) Cross section

Fig. 1.2. Test sample [Johnson A. 2012]

The first impact site was identified as being directly on the upper face of a scale, where the material was thickest. The second location was between the scales, where there was less material. At the location between scales, the hinged textile samples were designed to have a minimum thickness of 5.6 mm.

The primary objective of this experiment was to evaluate the stab resistance performance of single-thickness test specimens made of two common polymeric materials.

In composite designs with fabrics and fibres, it has been observed that little research has been done on the basic elements in the structural design of the panels.

By mimicking the natural, it could be a new way of making composites with improved mechanical properties and flexibility. By studying biological armour structures, interconnected pyramid structures could be introduced to make a new type of armour.

The interconnected pyramidal structures could significantly dissipate impact energy and produce improved robustness. However, while biological armour can provide inspiration for good design, these complex structures are difficult to produce using conventional manufacturing methods. One possible solution to this problem is additive manufacturing [Bingham G. A., 2007], with laser-sintering (LS) technology, which allows designers to fabricate a part without the restrictions imposed by traditional manufacturing methods. The

effects of material on element design, i.e. angle and thickness, were experimentally investigated and analyzed.

The impact energy dissipation mechanism, characteristic of materials, was analysed using a computer simulation. The stab resistance tests of the reinforcement materials used in this study were used according to the national standard GA 68-2008 (China, 2008). The test platform was composed of an impactor hammer, a double-bladed knife, test materials and backing material [Gong Z., 2019]. The total mass of the impactor and knife was 2.4 kg. It was released vertically from 1 m above the test material in free fall on the test material. This produced an impact energy of 24 J. Three types of materials were used for LS manufacture: PA 4300 PA/GF, PA 3200 and PA 4300, with different polyamide compositions. The PA/GF material was a composite comprising 60% polyamide and 40% glass fibre [Johnson A., 2012].

The experiment plates were made to the dimensions of 60 mm x 60 mm. For the single-layer samples, the sample thicknesses were 12 mm, 11 mm, 10 mm, 9 mm and 8 mm. For specimens with multiple layers, the sample thickness was 1 mm and the total sample thickness was 12 mm. Each stab resistance experiment was repeated three [Gong Z., 2019].

The researchers [Johnson A., 2012a] acquired two common materials: Dura Form and Dura Form EX. The main body of each specimen measured 60 mm x 60 mm and ranged in thickness from 1.0 mm to 15.0 mm in 1 mm increments. Three specimens were manufactured according to thickness. In total, 180 specimens were tested in four material groups, with 45 tests per group. The backing materials were used for one test, with the backing material being changed for each one. All stab tests were performed using an instrumented drop tower (Instron 9250 HV). The total mass of the drop weight assembly, including the blade chuck, was calibrated to 6.50 kg. Roma Clay Plastiline® No. 1 is used as the support material for all tests. The tests were performed with an impact energy [HOSDB KR1-E1] of 24 J and in an ambient temperature range of 21°C +/-6 and a relative humidity range of 30-70%, [Croft J., 2007c)].

Test specimens, which had no full blade penetration through the underside or a blade penetration level of 7.00 mm or less, are identified as providing a successful level of stab protection within the [UKHOSDB] standards [JohnsonA., 2017], [Johnson A., 2014].

As the particle diameter decreased and the mass fraction increased, more B4C particles were dispersed between the wires, the load and elongation of the coated composites increased as the particle diameter of B_4C decreased and the mass fraction of B4C increased.

With particle diameter of 2.5 μm and mass fraction of 40%, tensile load and elongation of coated composites increased by 227% and 237%, respectively, compared to uncoated samples. With decreasing particle size B_4C and increasing their mass fraction, more particles were observed between the fibers, which improved the yarn elongation, and more fibers were involved in the load pick-up zone. Thus, the strength of the coated composites was improved. With the diameter of B4C particles decreasing, more particles were also observed uniformly covering the fabric surface, which is beneficial for the stabbing resistance. When the particle diameter was 2.5 μm, the particles not only covered the fabric surface, but also diffused between yarns and fibres. So, the blade energy would also be consumed by its interaction with the hard particles [Xia M., 2019].

Some researchers have found three characteristics of the stabbing process:

- the blade acts normally on the material, the material deforms primarily due to normal force;

- the blade slides horizontally on the deformed material so that it is cut continuously;

- the fabric is cut/peeled/deformed as the blade passes through the fabric.

There are four stages from initial contact to completion of the cutting mechanism. First, the straight blade with normal loads made contact with the fabric and a dent was left on the fabric surface. The action of the blade on the fabric developed a compressive, transverse deformation on the fabric. At this stage, no cutting takes place. The mechanical work done by the external force was converted into elastic deformation energy, stored in the fabric. Secondly, due to the horizontal sliding movement of the blade at slow speed, the contact between the fabric and the blade resulted in the cutting of the fabric. Yarns in the vicinity of the blade were centrally stressed; if the blade was sharp, the yarn was easily cut to form a split. Third, once the yarn surface had a crack, the elastic potential energy stored in the yarn would be released rapidly, resulting in a slippage of the yarn within the knitted loop. The knitted fabric continued to be subjected to loads, and the break propagated. Fourth, the fabric was cut. The modes of breakage of plain knitted fabric could be divided into four stages, which include: compression deformation, crack generation, crack propagation and tearing [Wang L., 2021].

Since the fabric has formed a tear, the subsequent cutting process is mainly characterised as propagation of the tear until the fabric is cut. The mathematical models for the three stages have the following equations:

$$\Delta W_e = \Delta U_\epsilon \tag{1.1.}$$

$$\Delta U_\varepsilon + \Delta W_l = 2\alpha(\Delta s) + \Delta U_p \tag{1.2.}$$

$$\Delta W_e' + \Delta W_l' = 2\alpha(\Delta s) + \Delta U_p' \tag{1.3.}$$

εe ε lppwhere: -ΔW and ΔW = mechanical work done by external forces; ΔU - fabric deformation energy; -ΔW and ΔU = primary energy values inside the fabric due to yarn buckling; α(Δs) = new surface energy, -ΔU and ΔU = plastic deformation energy.

The contact area between the blade and yarn in the cut is increased, which may reveal that the slant direction of the fabric has better cut resistance [Wang L., 2021]. When the blade presses on the fiber, the initial contact is characterized as transverse compressive strain. After that, as long as the cutting stress of the fiber exceeds the breaking limit, cracks, cuts or local tears occur. Eventually, the fibre was cut due to crack propagation. [JBMayo Jr] and [ED Wetzel] evaluated the cutting deformation of a single fibre acting on the contact area between the blade and the fibre.

Johnson A. et al. [Johnson, 2017] say that the test specimens ranged from 1 to 10 mm thick, increasing in 1 mm increments, and were fabricated by laser deposition of PA2200 polymer. The tests demonstrated that a sample thickness of at least 8 mm was required to consistently achieve an acceptable level of penetration resistance. The results of this experiment revealed that 20 out of 21 flat layers with a thickness of 8 mm failed to achieve a stab resistance within the acceptable range as in [Croft J., 2007c], but also fractured into two or more pieces. When fabricated from a 50:50 blend of pure and recycled PA2200, the first thickness group to consistently demonstrate knife penetration resistance within acceptable limits for the 6 mm thick specimens.

The 5 mm thick group of flat samples performed close to the penetration limit of 7.0 mm. Therefore, the 6 mm thick sample group was the first to achieve a consistent level of knife penetration resistance, for all samples suggested that a wider range of sample thicknesses should be tested, particularly around 5-6 mm thickness. By doing so, there was an opportunity to determine a clearer transition between acceptable and unacceptable stab resistance thickness.

1.6 Research Directions for This Study

The aim of this research is to characterize some author's structured panels in terms of stab and puncture resistance, with materials that have recently appeared on the protective equipment market. The study will include a documentation, a proposal for laboratory technology of some panels, simulations by the finite element method and experimental tests on two impact test installations, investigations of failure mechanisms.

As main results, they will be established:

-influence of panel quality (3 materials will be tested);

-influence of panel thickness on blank threat impact characteristics for two types of tests (on smaller panels on drop-test machine and on larger panels on NIJ compliant facility);

-influence of the shape of the threat (knife and spike);

-determination of parameters of interest for assessing the quality of protection (maximum force, absorbed energy, force-time curves, displacement-time curves, depth of penetration into the support material);

-the study of failure mechanisms for tested materials.

The objectives of this research study are:

- analysis of a state-of-the-art documentation on stab-proof panels made of composites with fibre reinforcement, commenting both theoretical and experimental results; this documentation was the basis for the formulation of research directions for the evaluation of the behaviour of the author's panels in impact with a blank weapon,
- design of a two-stage test methodology: a preliminary stage of ranking materials on drop tests and a stage of testing under almost NIJ conditions,
- making protective panels based on aramid fibre fabrics,
- modeling and simulation of the impact of the blank weapon-panel at macro level (panel made of layers with equivalent mechanical characteristics, taken from the literature), with the aim of limiting the number of tests, as they are relatively expensive,
- carrying out a test method in a specialised laboratory, resulting in a useful study to highlight the impact response of the panels,
- investigations of panel failure mechanisms using macro photographs, SEM images (micro, fibre level),
- recommendations on the classification of the panels developed for protection levels according to the standards.

Chapter 3. Particular Aspects for Solving the Panel-Knife Impact Model in Explicit Dynamics

3.1.Introduction

Numerical modelling is useful in many disciplines, including the design and optimisation of impact protection materials. „Divide-and-conquer/solve" algorithms are used in finite element analysis, where the problem is broken down into many interconnected mini-problems and solved in an iterative manner. Each iteration generates incremental deformation/strain in the elements, resulting in deformation and/or yielding according to the material constitutive equation [Saleh M., 2017]. Numerical modeling allows for comprehensive solution of dynamic and complex scenarios, such as ballistic blade hit, with relatively lower cost and time [Saleh M., 2017). Highly complex and hierarchical geometries, such as those in textile materials, can be modeled at different scales (micro-scale, meso-scale and macro-scale), in two-dimensional (2D) and three-dimensional (3D) domains.

Boundary conditions can easily be introduced. Material behaviour can be simulated with a constitutive material model, which defines the stress-strain relationship, while failure criteria can be prespecified using an initiation algorithm.

The geometry and trajectory of the weapon (knife, spike) can be varied. Contact between fibres/yarn/fabric can be defined, using failure algorithms that include friction between elements. One of the main advantages of numerical simulation is its ability to produce informative results, such as stress-strain behaviour, contact forces, destruction patterns and residual velocity. It is a useful approach to capture the stages of the failure, energy absorption process that would otherwise be impossible to determine. However, the numerical modelling process needs to be used carefully and validated, as inappropriate inputs and problem definition may generate misleading results [Lemaitre J., 2005].

The scenarios of the penetration mechanism into the textile are:

- hitting with a sharp blade (knife) at high speed (arrow),
- penetration of the sharp blade at low speed,
- cutting with a sharp blade in parallel movements with the cutting surface.

The puncture force on the yarn assembly has the following components: compressive strength force, friction force between fibers (due to compaction), fiber cutting force, friction force between fibers and impactor [El Messiry M., 2013]. The sketch of blade penetration through the fibre assembly (Fig. 3.1) shows that the compacted fibre structure under the puncture pressure increases the fibre density until the thickness is almost constant.

Total penetration energy $E_{perforare}$ is given as follows:

$$E_{perforation} = E_{cutting} + E_{friction} + E_{tractoin} + E_{compresion} \quad (3.1.)$$

$$E_{fiber} = \sum\left(E_{friction} + E_{tracton} + E_{compresion}\right) \quad (3.2.)$$

$$E_{perforation} = E_{cutting} + E_{fiber} \quad (3.3.)$$

The energy of the applied forces is to overcome the friction between the fibres during compaction and between the perforator surface and the fibres, during perforator penetration.

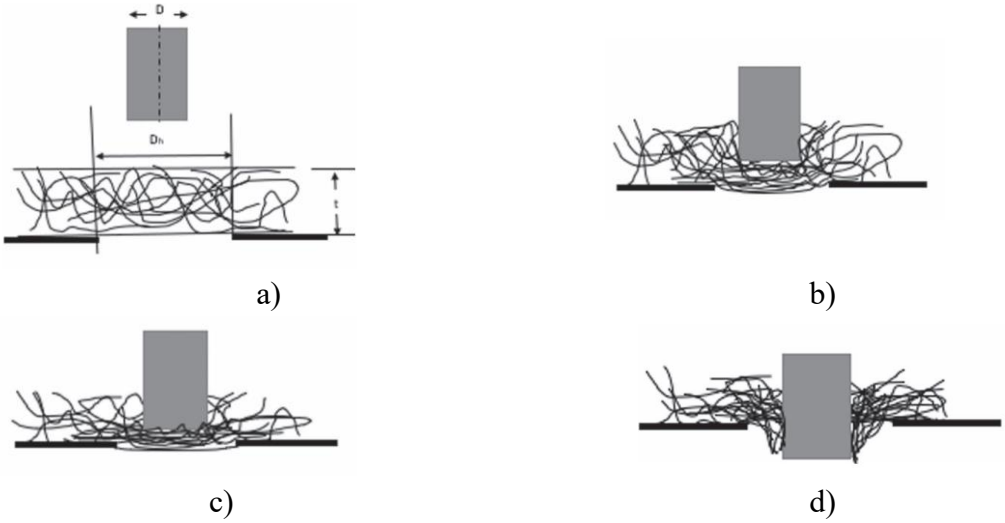

Fig. 3.1. Blade penetration through fibrous material [El Messiry M., 2013]

3.2. Mechanisms of Stabbing Fabric

In some situations, the fabric is cut with a knife or other sharp tools, and the mechanism of failure, in this case, will be different from that of knife penetration. The stabbing mechanism has several scenarios: when the knife penetrates vertically, when the knife moves horizontally relative to the panel, etc.

In general, the factors that influence the cutting force of the fabric are: the force required to cut the fibres and yarns, the architecture of the fabric, the thickness of the fabric, the density of the fabric, the sharpness of the knife, the geometry of the cutting edges (angle of the cutting edge of the knife, angle at the tip of the knife, etc.), angle of penetration of the knife relative to the plane of the panel, striking velocity (velocity before touching the panel), friction properties between yarns/layers and between yarns/layers and the knife, fabric tear strength and cutting direction.

Different mechanisms occur when a knife penetrates a fabric: pushing of threads, shear cutting of yarns due to sheared transverse pressure on the fibres, and tearing of yarns when they are tensioned to break [Jing L., 2011], [Heuse O., 1982]. Fiber shear by transverse movement of the blade at varying blade and fiber angles [Heuse O., 1982], [Johnson A., 1991] should be highlighted. It is revealed that, based on blade tension normalization, inorganic fibers demonstrate higher shear strength than organic fibers.

During the stabing process, the fibre will be deflected under the blade load, then the blade begins to penetrate through the fibre with increasing force, until the cross-section of the fibre is reduced to its limit and shear failure occurs. The cutting force of the fibres depends on their mechanical properties. Fiber cross-section shear can have four distinct zones: indentation zone, deformation of the material under pressure at the blade tip; shear zone, shearing of the material by the sharp edge of the blade; shear-tension zone; and shear-rupture zone [Mayo J. B.,, 2014], [Ding H., 2017].

The roundness of the tip affects the indentation area and develops local transverse compressive pressure on the blade tip. The larger diameter reduces the local stress applied on the blade tip and more force is needed to create the indentation zone [Ding H., 2017].

The stabbing force on fibres decreases with increasing blade sharpness (angle at the tip). Dyneema fibre has the highest cutting strength, while Zylon fibre offers the lowest strength, also due to its lower friction coefficient between the cutting blade and the Zylon fibre. Fibre cutting is a mixture of shearing and tensioning of the fibre under the applied cutting force. [Heuse O., 1982]. Fibre failure is due to either tensile or shear stress, or a combined mechanism. The mechanism of fabric perforation is different from that of a fibrous mat. The morphology of the fabric demonstrates the interlacing of the threads and the pores between them, to be smaller and to have a better protection. The behaviour of the fabric under the perforating tool, depends on the tip configuration, fabric and weave design: woven, knitted, triaxial, non-woven or combined structure.

3.3. Stab Resistance of Materials

The stabbing or cutting of fabric with a sharp blade has the following scenarios: cutting, quasi-static and dynamic perforation. The cutting tip of the knife is oriented towards the weave of the yarns or between yarns, so the resistance force will be different. During penetration of the knife tip through a material, the fibers that come into contact with the knife edge have high tension and tend to be stretched and bent in the direction of the weapon feed and will move in the direction of the knife edge passage. The fabric will be deformed under the force of the knife, the tendency being lessened if the yarns start to shear.

Yarn cutting force plays a key role in predicting fabric protection performance. Thread breakage under the cutting blade should be carefully analyzed [Shin, 2016]. Thread breakage is based on the structure of the thread, either disc-shaped or filament threads. Continuous multifilament yarns have a high density of organization, thus, almost all filaments will participate in the cutting force resistance of the yarn. It has been reported that the cutting force of Zylon threads has a higher value than that of Kevlar and Spectra type yarns at default values of cutting angles, blade sharpness and pretension loads [Shin H.S., 2006] Vectran HT and NT show higher cutting resistance than Aramid yarns.

3.4. Analysis of the Dynamic Strength Mechanism of the Fabric

The total energy required to penetrate a fabric is based heavily on: the energy lost to cut the yarn, the fibers twists around the edge of the blade, the energy to overcome the friction between the blade surface and the surrounding fabric surfaces. Flexible stab-resistant fabrics have been widely used for military and civilian purposes. Efforts have been made to build softer, lighter, better protective armour using high-performance fibres. Recently, research on protection against impact by sharp blade or spike has been studied [Choi, 2011], [El Messiry M., 2016], [Mahbub R. F., 2015], [Wang Q. S., 2016]. Penetration resistance is an essential parameter for estimating the properties of fabrics intended for protection. In addition, a soft vest should provide users comfort, light weight and cost-effectiveness [Mahbub R. F., 2015]. However, a thorough understanding of the design of stab-resistant protective systems to minimize weaknesses such as weight, shape and uncomfortable features should be exposed.

During the blade penetration time interval, the cutting force will increase until full penetration and then gradually decrease [Jing L., 2011].

The stabbing of the fabric with the sharp blade of mass (m) moving at speed (V) will start when its tip touches the surface of the fabric; since the fabric has sufficient elasticity, it starts to bend under the dynamic force.

On impact, the faster propagating longitudinal waves help spread the impact energy through the yarns. Investigation of the dynamic modulus of yarns has shown that it is based on the twist factor and fibres' orientations [Křemenáková D., 2012], [El Messiry M., 2016]. The dynamic elastic moduli of the fabric depend on the yarn arrangement in the fabric. It has been specified that the gathering of fibres into yarns leads to a decrease in the level of the sonic modulus, it represents 0.5 to 0.6 of the fibre modulus, while the weaving of the yarn into the fabric reduces the sonic modulus of the fabric to about 0.017 to 0.25 of that of the fibres. The correlation between sound velocity through the fabric, fiber architecture, fabric anisotropy, strength, stiffness, elasticity, resilience, and fatigue properties was tested [Bilisik K., 2012].

An alternative is to get information using a numerical model. Two approaches can be distinguished. The numerical model is able to directly determine the residual strength and permanent indentation [Lopresto V., 2012] versus impact energy. It is the simplest case, as it is possible to easily optimize the composite structure to allow for damage tolerance. The main drawback of this approach is that it is limited to the impact types identified by the numerical model. This is able to fully simulate impact damage, especially with permanent indentation, and residual strength after impact. The main advantage of this approach is that it is valid for a wide range of impact and residual loads. But this model can be complex and unreliable. Numerical simulation of impact failure is still challenging and is the subject of much research [Lopresto V., 2012], [Gonzalez E. V., 2012], [Rivallant S., 2013], [Tan W., 2015].

3.5. Defining Materials in Explicit Dynamics

Constitutive models are needed to analyse material behaviour under different loading conditions and environments, including variables such as temperature and pressure. These models involve elaborate mathematical descriptions of the mechanical response of the material to various types of stresses, such as elasticity, plasticity and viscosity, and are crucial in predicting this response in static or dynamic situations.

In numerical simulations with Explicit Dynamics, temperature variation is not taken into account when determining elastic properties. Thus, for each property, a single value is used instead of taking into account the change with temperature. The fixed value is then used by the solver in the numerical solution [Jiang T. 2006], [Múgica J. I., (2016)].

The equation of state is a complex mathematical expression that characterises the hydrodynamic behaviour of solid materials under conditions of deformation at high velocities. This situation occurs when the hydrodynamic pressure applied to the material exceeds its yield limit, according to the resources presented in [ANSYS Explicit Dynamics Analysis Guide, 2021]. The linear equation of state was used.

Bilinear models with hardening are often used in studies with large deformations. The yield limit and tangent modulus are the two parameters on the distinctive curve of this model; it has two straight segments, each with a distinct slope. The modulus of elasticity of the

material, E, is represented by the slope of the first segment, which shows the elastic response of the material to stress. The tangent modulus, which characterises the plastic behaviour of the material after exceeding the yield strength, is given by the slope of the second segment. Two values are required to use this model: the yield strength and the material-specific tangent modulus [ANSYS Explicit Dynamics Analysis Guide, 2021].

3.6. Defining Connections

The contact between the panel layers is with friction. The value of the friction coefficient is 0.35. The contact between the panel and the knife is also with friction. The value of the friction coefficient is 0.35.

The layers were embedded on 2 parallel side faces, the other two parallel faces remained free (Fig. 3.2). The pebble symbolizes the fixing on the side in the far plane, but the same embedding (fixing) is on the opposite side.

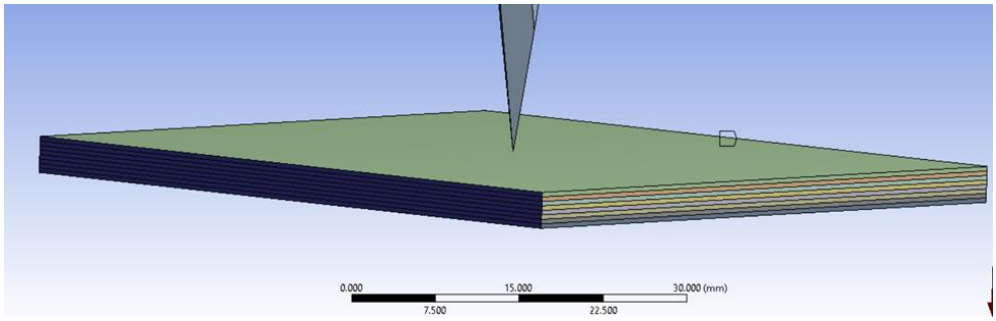

Fig. 3.2. How to embed the panel layers

This specific arrangement, in which the layers are embedded on two parallel side faces of the panel, with the other two faces left free, is important to properly simulate how the layers are fixed in real panels. This condition can influence how the panel interacts with the knife; it has a significant impact on its behaviour under the specific stresses of the experiment. This arrangement more closely reflects the actual conditions of the experiment on the CBRNE facility, allowing relevant data to be obtained and the results to be interpreted more realistically.

3.7. Geometric Model

In this paper the problem of numerical modelling of Twaron SRM509 aramid fabric was posed. This fabric is a special material used in the manufacture of stab-proof vests. This study aims to create a numerical model, which is possible to solve using the commercial software Ansys.

Figure 3.3 shows the knife, which is a key element of the model. Its geometry strongly influences the striking behaviour of this weapon. Its design results in a high concentrated load and therefore produces the highest energy density on the blade; at the same time, the thickness of the blade body prevents buckling. The geometric design of the knife is made according to the NIJ Standard [NIJ Standard 0115.00] (Fig. 3.3). In Fig. 3.4 and Fig. 3.5, details of the knife tip used in the simulation are given. The geometrical model of the simulated model consisting of layers and knife is given in Fig. 3.4c).

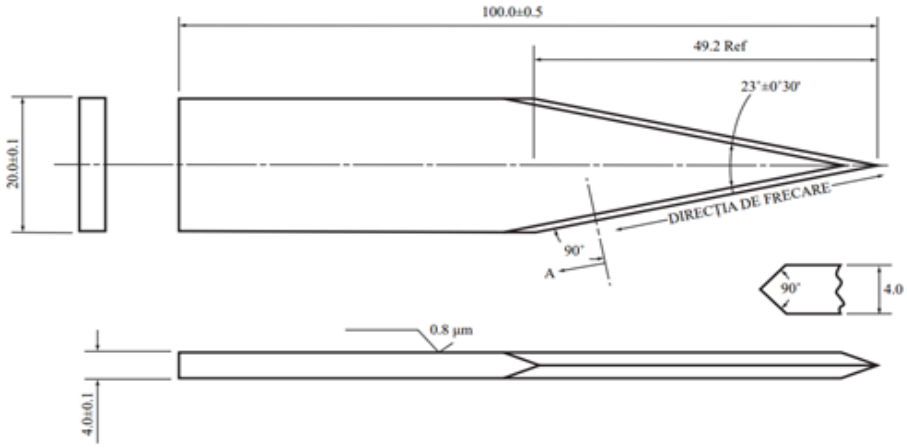

Fig 3.3. Test knife S1 according to NIJ-0115.00

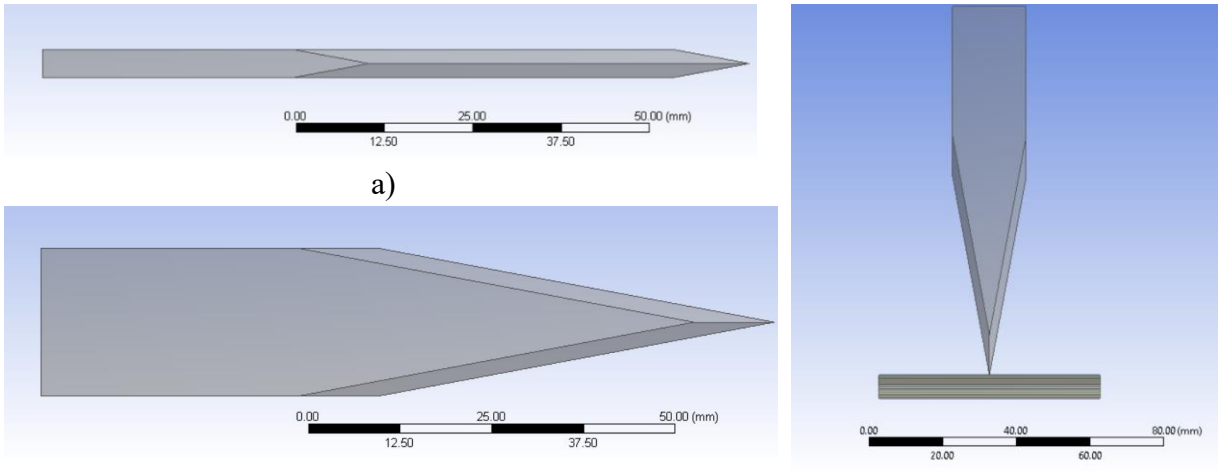

a)

b) c)

Fig. 3.4. Knife geometry

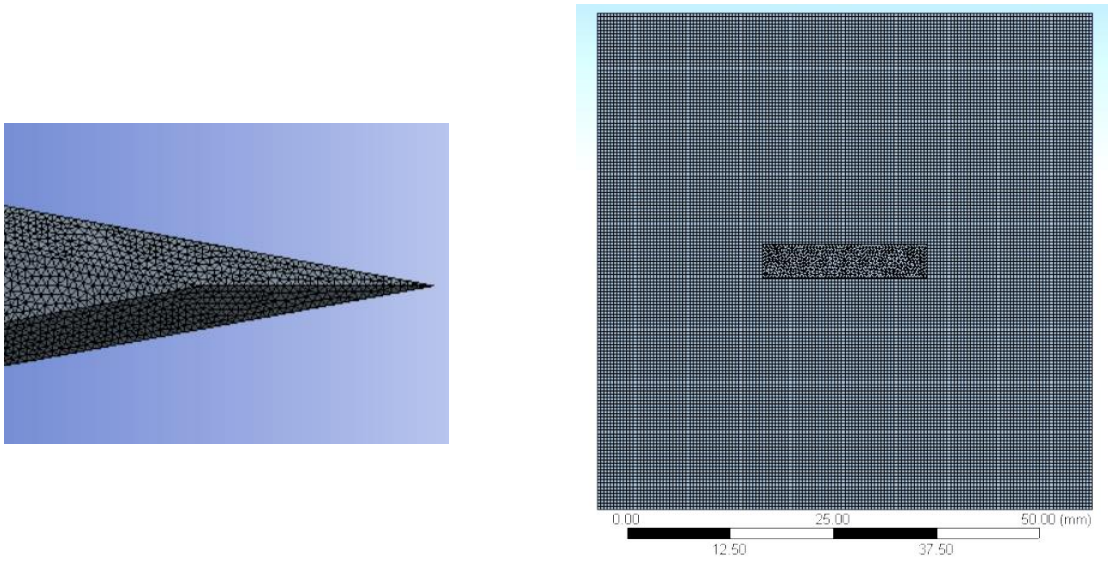

Fig. 3.5. Discretization of the knife tip detail and a top view of the model

In Fig. 3.5 details of the knife-edge discretization network and a top view of the model are given. The finer the discretization, the more plausible the simulation results.

Table 3.5 gives the material properties of the layers and the knife. The knife is considered rigid in this simulation.

3.8. Analysis of simulation results

Each image in the simulation has its own colour scale for the equivalent (or von Mises) stress distribution, these are given in MPa.

Table 3.1. Material properties used for model components

Ownership	**Values for layer**	**Values for knife**	**Unit**
Density	1440	7850	kg m^-3
Young's module	40000	$2{,}07 \times 10^{11}$	MPa
Poisson Coefficient	0,35	0,30	-
Volume module	$4{,}4444 \times 10^{10}$	$1{,}725 \times 10^{11}$	Pa
Shear modulus	$1{,}4815 \times 10^{10}$	$7{,}9615 \times 10^{10}$	Pa
Temperature	22	22	°C
Model with bilinear isotropic reinforcement			
Initial flow limit	250	Perfect rigid body	MPa
Tangent module	1000		MPa
Plastic Deformation at Break (EPS)	0,04		-

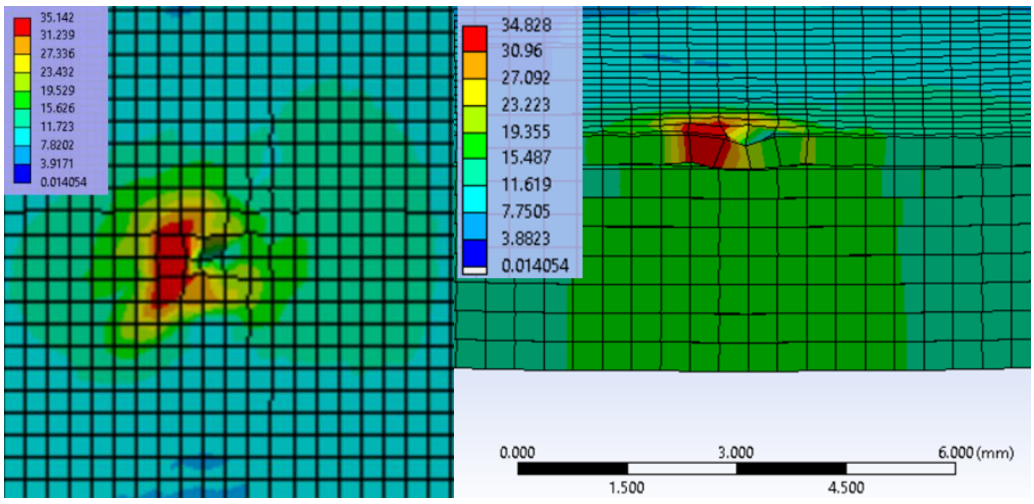

top view

vertical section through a plane containing the side cutting edges of the knife

Fig. 3.6. Distribution of von Mises stress (in MPa) at time instant, $t = 1{,}5 \times 10^{-4}\ s$ for the 8-layer panel

The first moment of the simulation, shows only a compression of layer 1, with the presence of a stress concentrator zone (Fig. 3.6). The von Mises stress value is 34 MPa. At time instant, $t = 7{,}5 \times 10^{-4}$ s, 3 layers are already cut, layer 4 is slightly compressed (Fig. 3.12). At this time, the von Mises stress value is 206 MPa. The cut is not symmetrical and neither is the distribution of the von Mises stress. At $t = 1{,}5 \times 10^{-3}$ s, 6 layers are cut. The von Mises stress value is 233 MPa (Fig. 3.13). The presence of stress concentrators is on the cut edges. The last moment of the simulation records the cutting of all layers. The von Mises stress value is 127 MPa (Fig. 3.7).

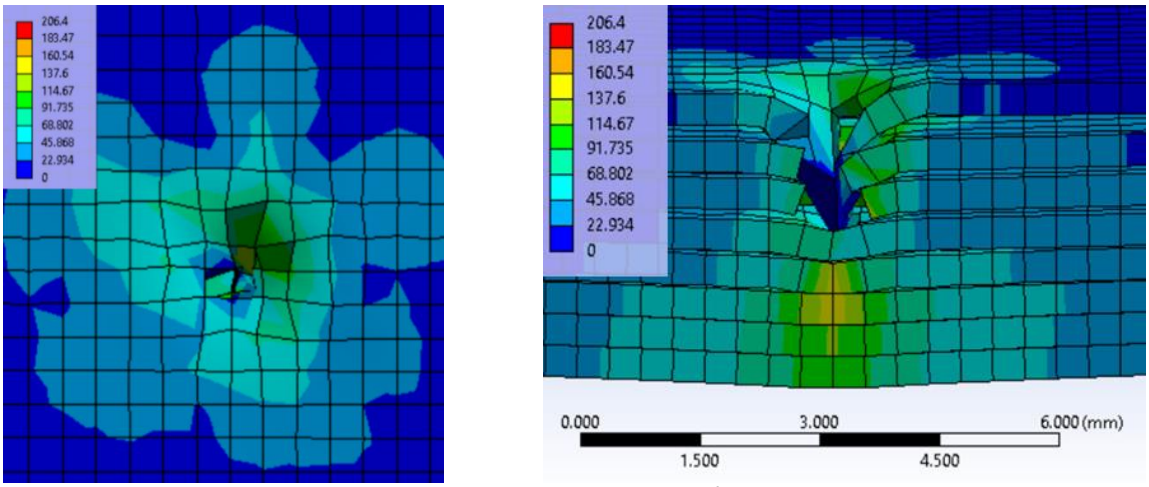

a) $t = 7{,}5 \times 10^{-4}\ s$,

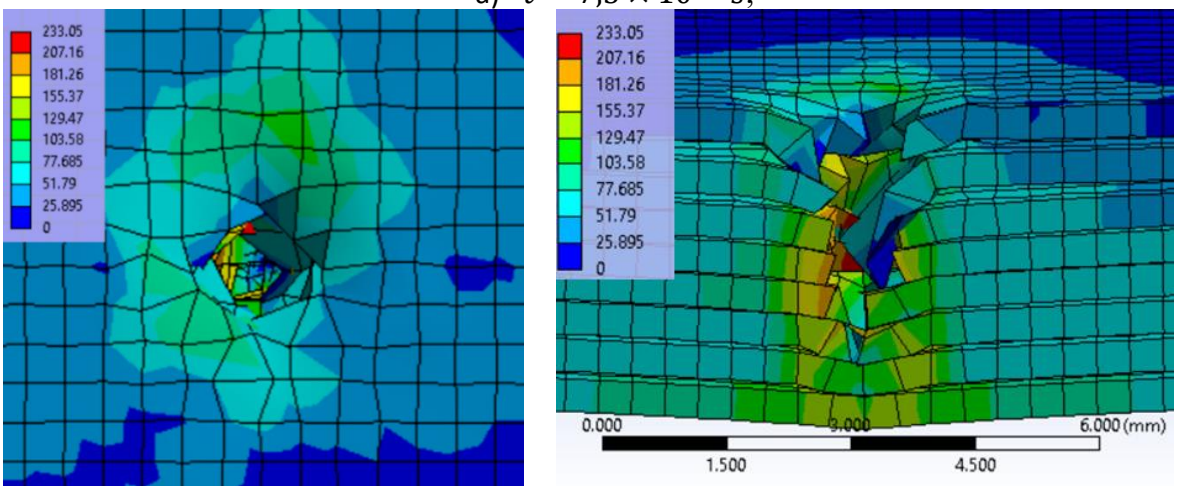

b) $t = 1{,}5 \times 10^{-3}\ s$for the 8-layer panel

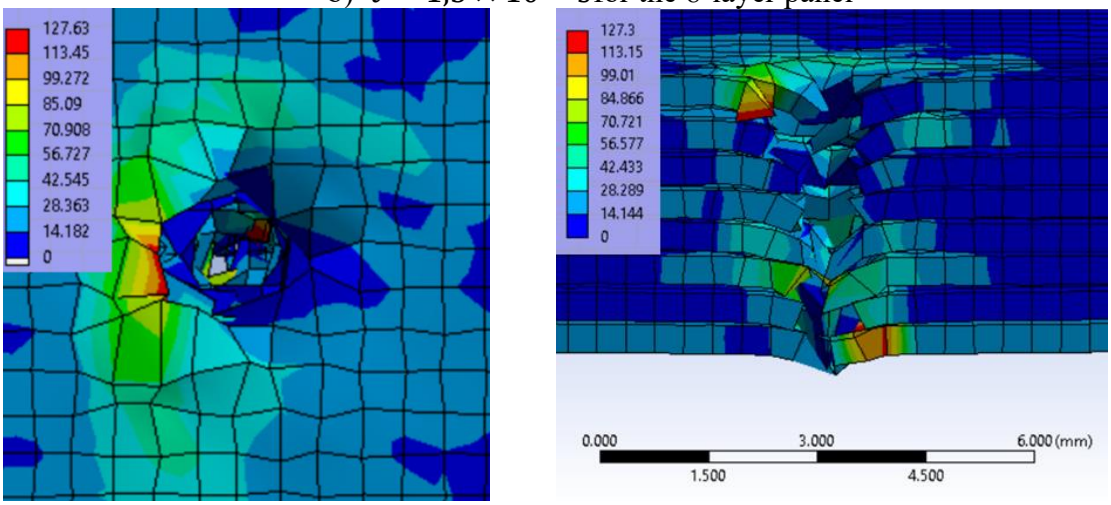

c) time moment $t = 3 \times 10^{-3}\ s$

Fig. 3.7. Distribution of equivalent stress (in MPa) at different times for the 8-layer panel: in the left column are top views of the face of the first layer and in the right column are sections through the plane of the cutting edges of the knife S1

Using the "Path" function in Explicit Dynamics, the distribution of the von Mises stress on a line in the section passing through the knife edges was determined. At the first

time point of the simulation, the wires show a similar stress distribution, layer 1 shows a slight increase in stress, which is normal because this layer makes contact with the knife first. The von Mises stress value on this line for all 8 layers is below 25 MPa.

In Fig. 3.8, the distribution of the von Mises stress on the 8 layers of the 8-layer panel for the moment of time is given, $t = 4{,}5 \times 10^{-4}\ s$. At this time, the von Mises stress value is recorded on layer 4. The lowest von Mises stress value is recorded by layer 3, suggesting that this layer has been penetrated by the knife. In Fig. 3.9 is given the distribution of the von Mises stress on the 8 layers of the 8-layer panel for the moment in time, $t = 1{,}65 \times 10^{-3}\ s$. When the von Mises stress value decreases to zero, it shows that the layer is cut. This time records the cutting of the first four layers. The maximum value of the equivalent stress is recorded on layer 8.

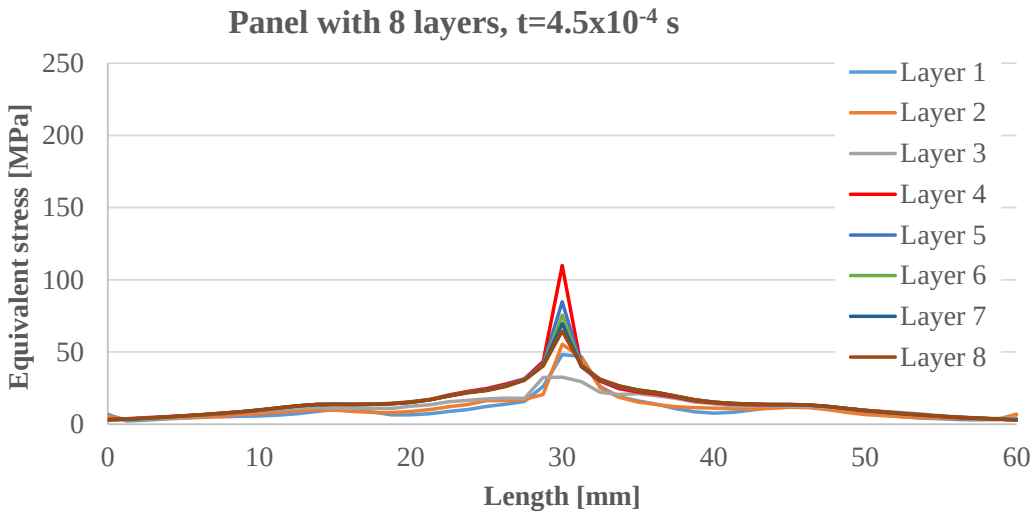

Fig. 3.8. The equivalent stress distribution on a line for each layer for the 8-layer panel, at time moment $t = 4{,}5 \times 10^{-4}\ s$.

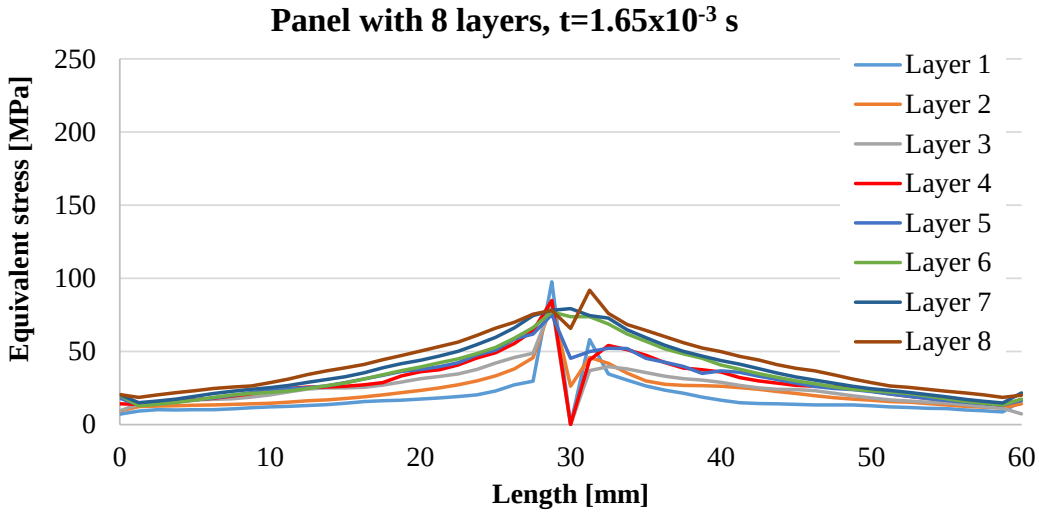

Fig. 3.9. The equivalent stress (in MPa) for each layer, in the plane containing the knife cutting edges, for the 8-layer panel, at time moment $t = 1{,}65 \times 10^{-3}\ s$

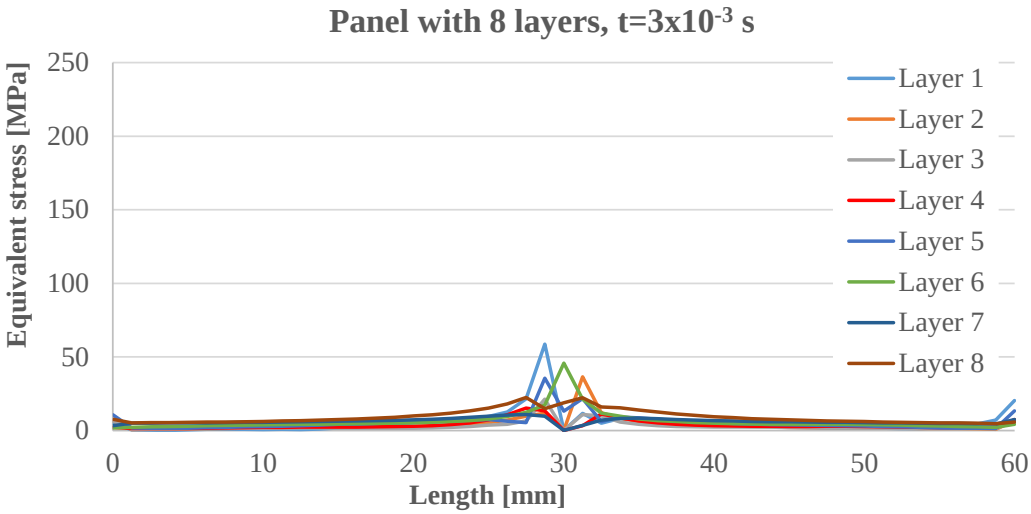

Fig. 3.10. The von Mises stress on a line for each layer for the 8-layer sample at time instant, $t = 3 \times 10^{-3}\ s$.

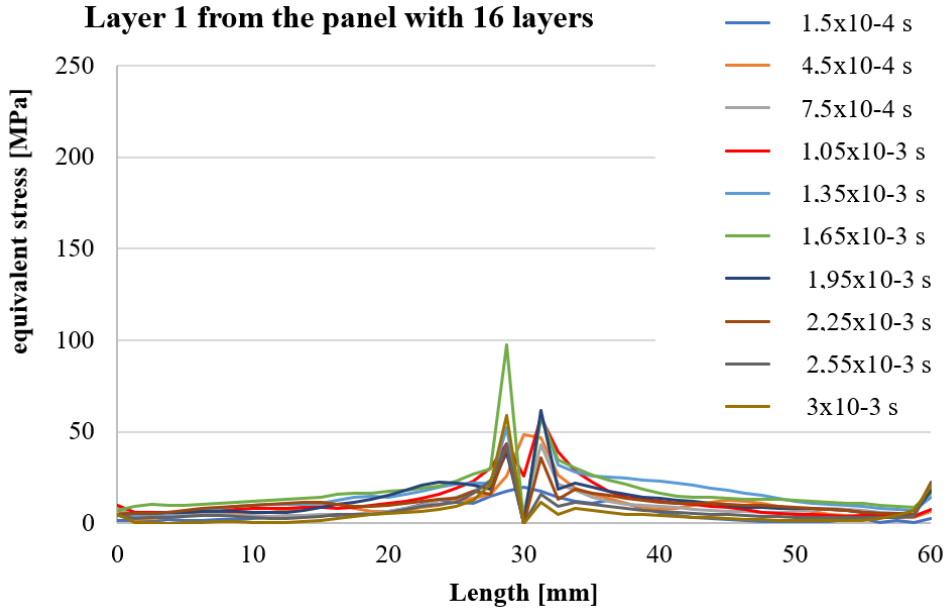

Fig. 3.11. Distribution of equivalent stress on layer 1 from the panel with 8 layers, at different time moments during the stabbing with knife-edge

Figure 3.11 gives the von Mises stress distribution for the 8-layer panel for layer 1 at different times. This plot is intended to follow the evolution of the von Mises stress during the simulation of the knife cutting of the layers. The highest value, recorded during the knife cutting simulation, is about 100 MPa at the time instant, $t = 1{,}65 \times 10^{-3}\ s$.

Figure 3.12 presents the equivalent stress distribution at different times during the stabbing of the 8-layer knife-edge panel. First moment of impact, $t = 1.5 \times 10^{-4}\ s$, shows that the first layer has been broken. The break was between time t=0 and $t = 1.5 \times 10^{-4}$ s. The von Mises stress distribution is over a narrow area with a propagation through the thickness. The maximum value of the von Mises stress is 175 MPa on the whole panel and 167 MPa on the analysed half. Momentum $t = 9 \times 10^{-4}\ s$ shows that five wires were

broken. The von Mises stress value is 206 MPa on the analysed model section and 219 MPa on the whole simulated model. On the front view, a stress concentrator is also present on layer 1. The layer breakage and the von Mises stress distribution is not symmetric. At $t = 1{,}35 \times 10^{-3}$, six layers are broken. Layer 7 is not completely broken, it will be broken at the next time. At this time the von Mises stress value is 182 MPa.

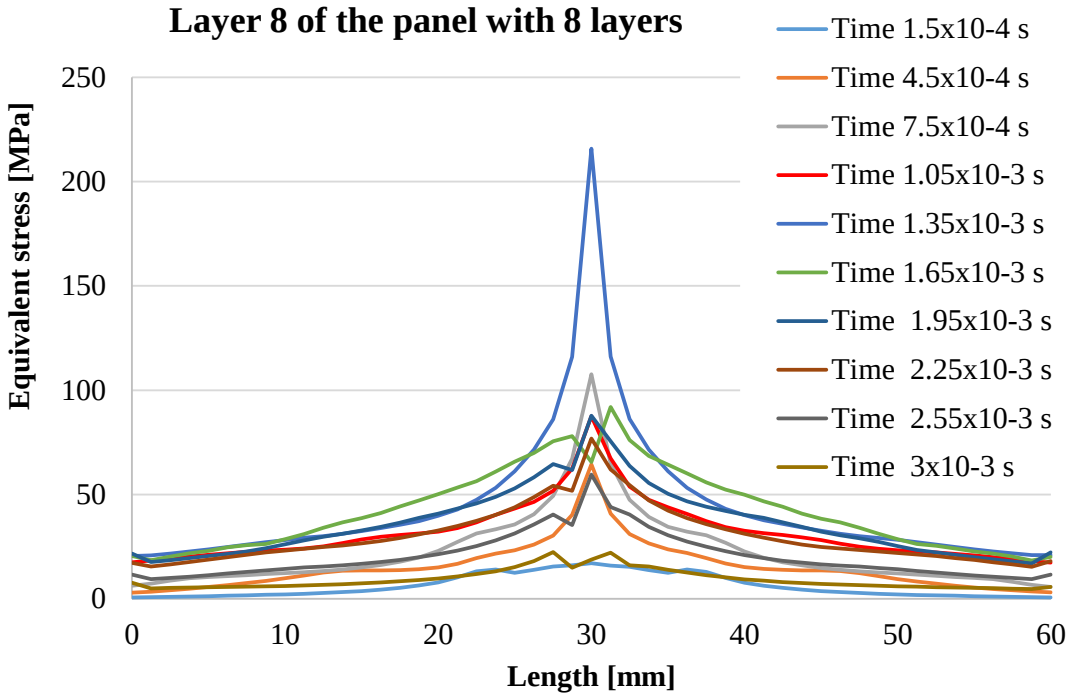

Fig. 3.12. Distribution of the von Mises stress at different time points during the cutting of layer 8, knife-edge, of the 8-layer panel.

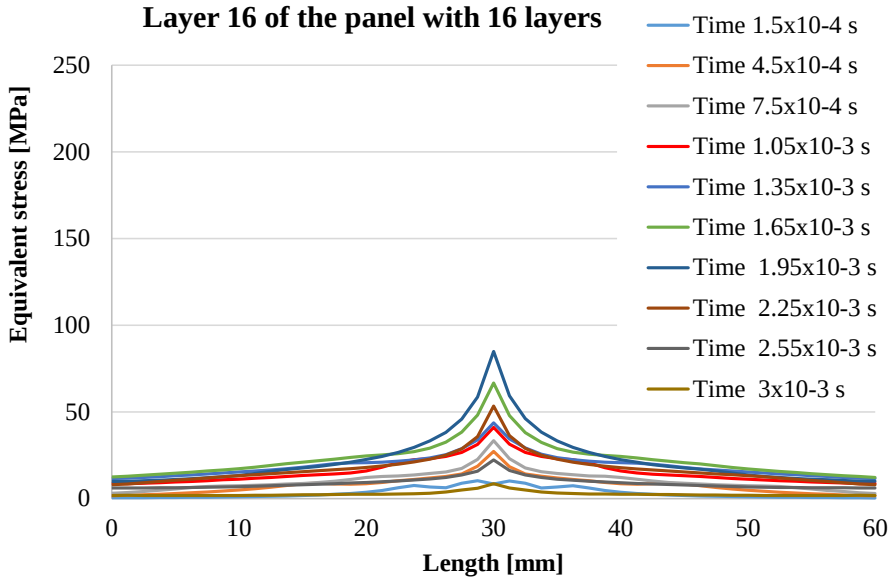

Fig. 3.13. Equivalent stress distributions (in MPa) on the main section of layer 16 from the panel with 16 layers, at different time moments during simulation

Figure 3.13 presents the equivalent stress distributions on the main section of layer 16 from the panel with 16 layers, at different time moments during simulation. One may notice that this layer is not broken and it is tensioned bellow the yield limit. This results was obtained also on panel with 16 layers tested on the instalation from Research Centre and Inovation for CBRNE Defence and Ecology.

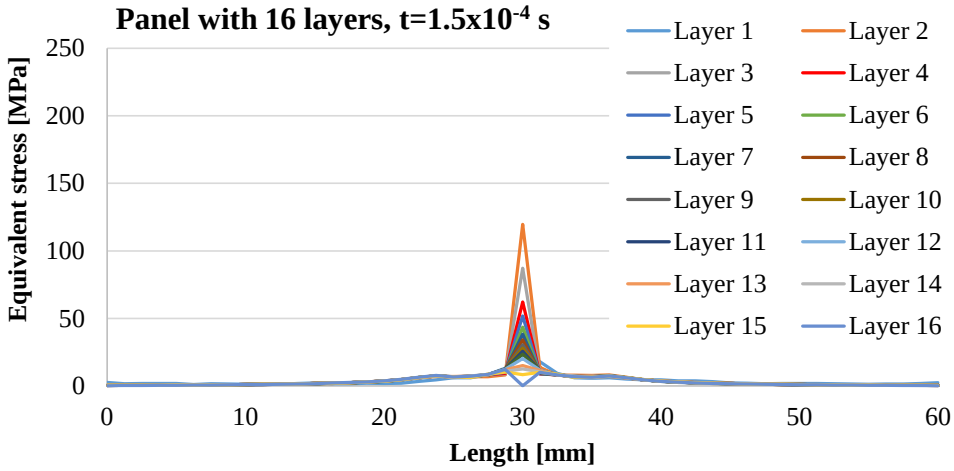

Fig. 3.14 The equivalent stress distributions on each layer, for the 16-layer panel, at time moment $t = 1.5 \times 10^{-4}\ s$

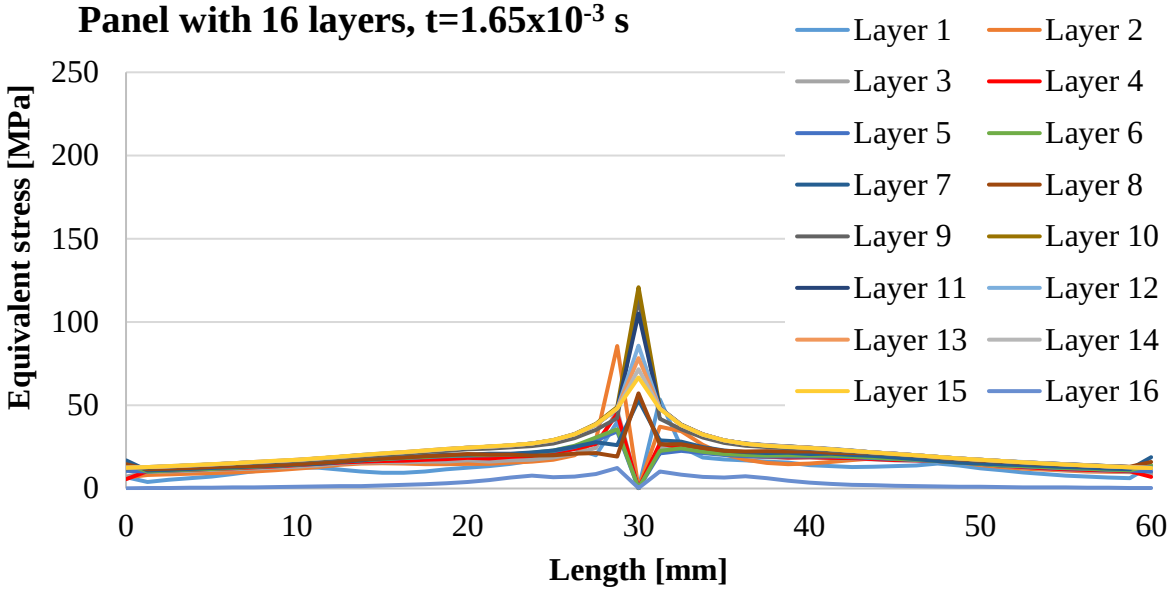

Fig. 3.15. The equivalent stress for each layer, for the 16-layer panel, at timemoment $\mathrm{t} = 1{,}65 \times 10^{-3}$ s

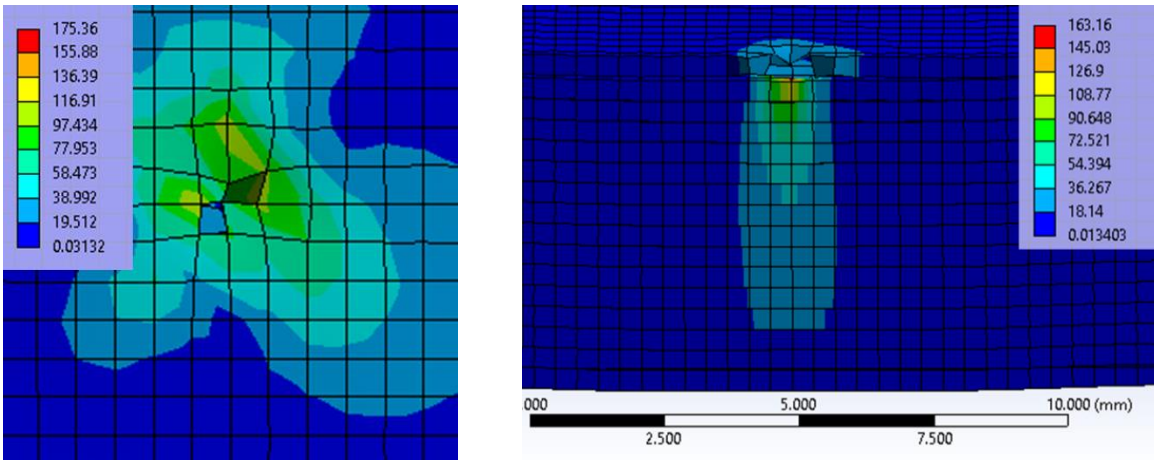

a) point in time $t = 1.5 \times 10^{-4}$ s,

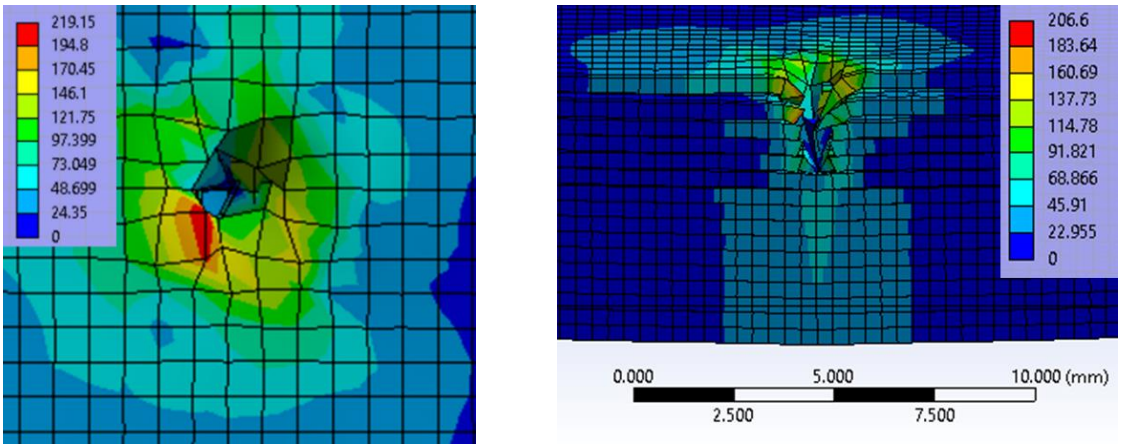

b) point in time $t = 9 \times 10^{-4}\ s$ for the 16-layer panel

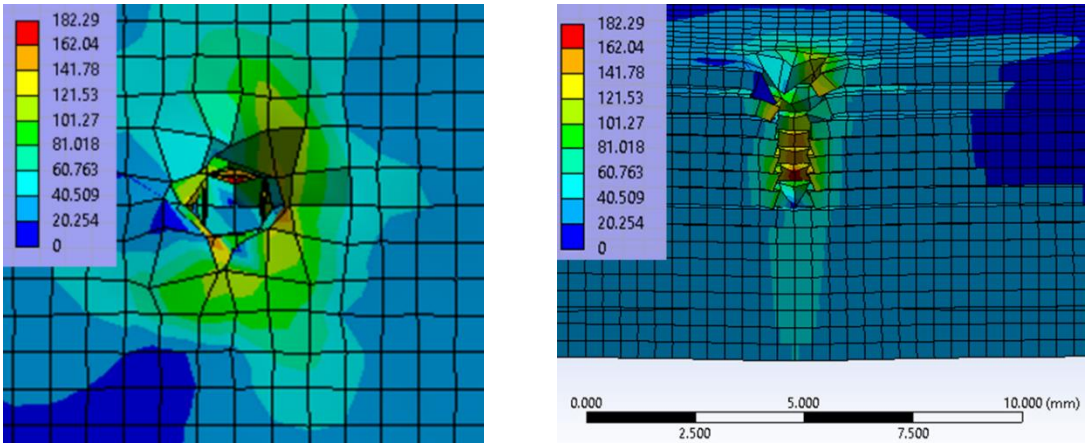

c) time $t = 1{,}35 \times 10^{-3}$

Fig. 3.16. Distribution of von Mises stress at time for Distribution of von Mises stress (in MPa) at different times for the 8-layer panel: in the left column are top views of the face of the first layer and in the right column are sections through the plane of the cutting edges of the S1-type knife

The last moment of the simulation, $t = 3 \times 10^{-3}$ s, records 8 broken layers, layers that were broken at the time point, $t = 2{,}1 \times 10^{-3}$ sbut also a knife rebound (Fig. 3.16). The von Mises stress at this time point records a value of 64 MPa.

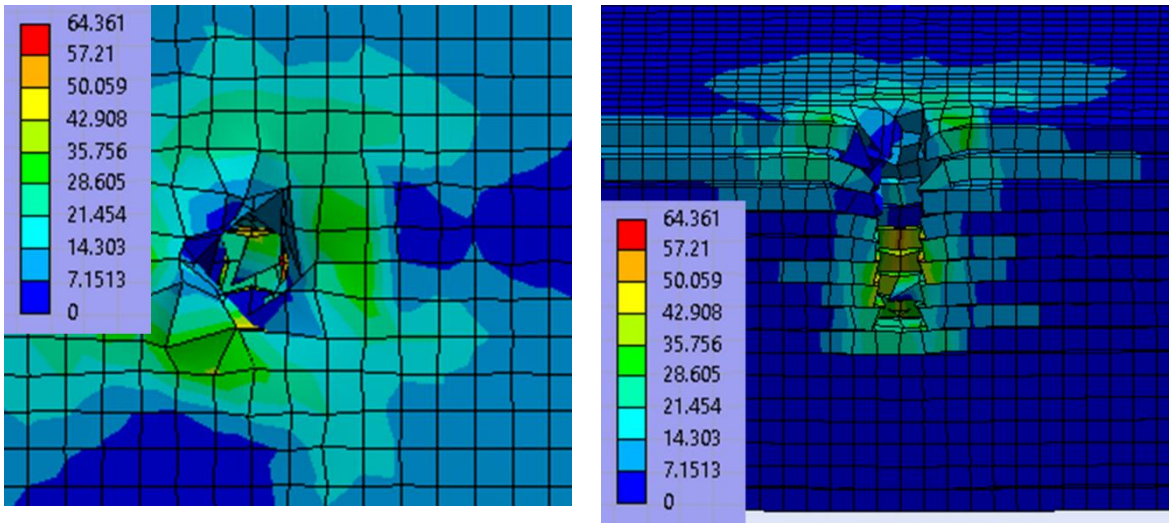

a) top view b) vertical section

Fig. 3.17. Distribution of equivalent stress (in MPa), at time $t = 3 \times 10^{-3}\ s$, for the 16-layer panel

In Fig. 3.17 is given the equivalent stress for the 16-layer panel, on one line for each layer, at the first time of the simulation. At this first time, the last three layers have the lowest von Mises stress value. In Fig. 3.17, there is given the equivalent stress on a line, for each layer for the 16-layer sample at the time instant, $t = 1{,}65 \times 10^{-3}$ s. At this time instant, $t = 1{,}65 \times 10^{-3}$ s, there have been already cut 6 cut layers. The maximum stress value is around 125 MPa.

In Fig. 3.18 is given the von Mises stress on a line for each layer for the 16-layer sample at the time instant, $t = 3 \times 10^{-3}$ s. This time of the simulation records a relaxation of the stress distribution. In Fig. 3.30 is given the von Mises stress distribution for the 16-layer sample at different time points during the cutting of the layers by the knife. The plot shows that layer 8 was broken after time , $t = 1{,}65 \times 10^{-3}$ s.

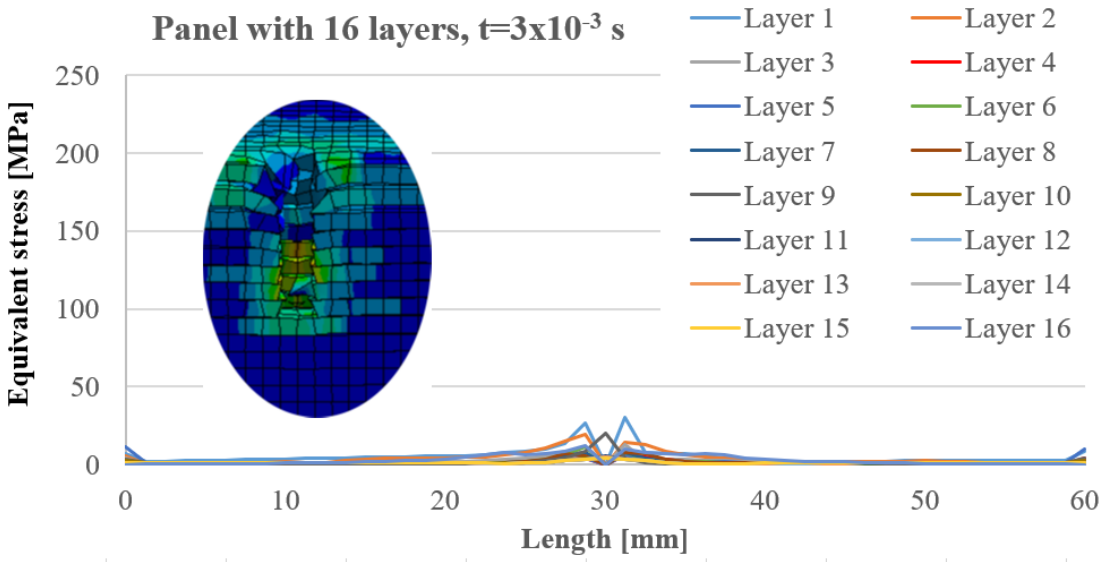

Fig. 3.18. The von Mises stress on a line for each layer for the 16-layer sample at time instant, $t = 3 \times 10^{-3}$ s

3.9. Conclusions and Model Validation Aspects

The validation of the simulated numerical model is done by a qualitative criterion (Fig. 3.19, Fig. 3.20) and by numerical evaluation of the broken layers. The 16-layer model has 8 layers cut and the 8-layer model shows cutting of all layers. This validation is essential to ensure that the model is able to provide accurate results and remain useful in practical applications.

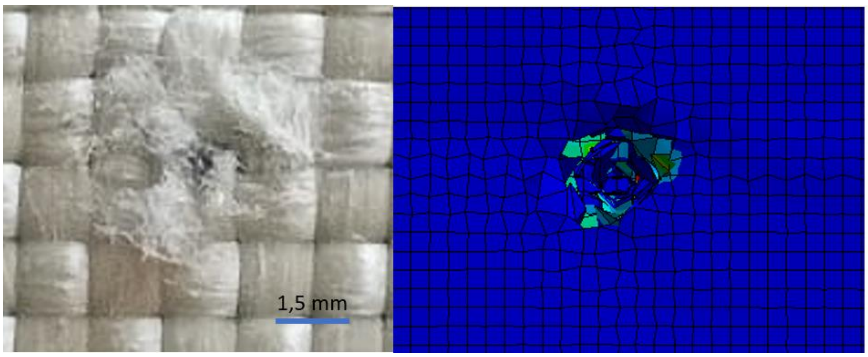

Fig. 3.19. Model validation Physical material destruction on the left side and material destruction on ANSYS simulation on the right side

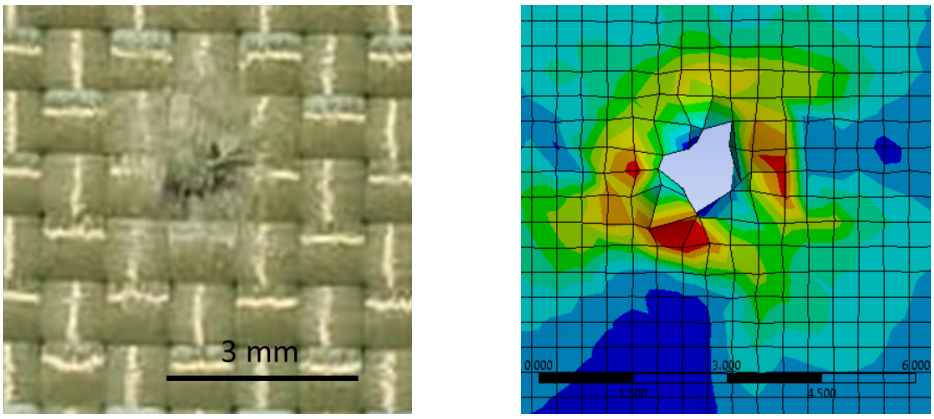

a) experimental b) numerical

Fig. 3.20. Validation of the destruction mode of layer 1 of the 16-layer panel

Chapter 4
Materials and Test Methods for Assessing the Stabbing and Puncture Behaviour of Panels

4.1. Introduction

The testing program is an applied research effort that determines the technology needs of justice system agencies, establishes minimum performance standards for specific devices, tests commercially available equipment against these standards, and disseminates standards and test results to interested institutions nationally and internationally.

Croft J. and Longhurst D., revised in 2007 the British standard, originally developed in 1993 by the Home Office Scientific Development Branch (HOSDB), developed in 3 parts, including general requirements, personal protection, ballistic protection and stab and puncture protection. Part 3 of the standard allows procurement units and specialist staff to choose equipment according to three levels of protection against stab and stab threats [Croft J, 2007a], [Croft J., 2007a]. All of the above levels of protection, described in Part 2 of the standard, can be combined with ballistic vests to provide dual protection against stabbing and against being struck by certain ballistic blows.

Dixon and Croft's 2007 document [Dixon, 2007] on the quality framework aims to standardise procedures on risk assessment and raise awareness of procurement/threat levels and health and safety issues when selecting, purchasing and using bulletproof or stab-resistant vests.

Stab-resistant vest testing is crucial for the safety and protection of users, for compliance with quality and safety standards and for the continuous development of this essential equipment in various fields.

There are several international and national standards governing the testing and certification of stab-resistant vests, designed to ensure that this personal protective equipment is safe and effective under certain test conditions.

The classification of a protective panel (armour) providing two or more levels of protection at different locations on the panel shall be that of minimum protection provided at any location on the panel.

A stab-proof vest system must provide protection against penetrating injuries from knives, edged weapons and sharp-edged weapons, while ensuring that the wearer's movement is not unduly restricted. The protected area provides coverage for vital organs, in particular: heart, liver, spine, kidneys and spleen.

4.2. Importance of Testing for Materials Resistant to Bladed Weapons (Knives, Spikes)

Tissue damage examinations are required in cases of stabbing or puncture. These involve testing knives or other weapons to determine if they could have caused damage to the evidentiary clothing. Currently, a coroner performs these tests by manually performing the stabbing action. A biomechanical performance test was conducted to assess how a number of human factors contribute to the creation of textile stab damage. Studies of sharp force fatalities and clinical penetrating injuries have reported the chest and abdomen as the most

common target locations for stab wounds. The location of cut-type injuries recorded during the test was found to correlate with the location of stab wounds sustained in actual stabbing cases [Croft J., 2007c].

Sloan et al. [Sloan K, 2020] studied the variability of the human factor contributing to stabbing action, 40 participants performed stabbing actions with 3 weapons, with blades (utility knife, hunting knife and a machete), in front of and behind the target (a dummy). The type of weapon has a different impact on the actions. The machete was used in the fastest action, recording a maximum speed of 9.6 m/s. The tests performed fall within the range of striking velocities of 3-4 m/s, which is in line with the literature. Most of the stabbing scenarios are dynamic and the positions of victims and assailants are often unknown. The largest variable was the individual. Standardizing the simulation of experiments using mechanical or robotic systems would be advantageous to eliminate the natural variation that is inherent in human stabbing performance.

4.3. Test classification Criteria for the Assessment of Stabbing and Puncture Protection

An interesting paper, published by [Johnson A.A., 2017], presents tests performed on relatively small (50 mm x 50 mm) samples cut from a vest to compare stab resistance with an attack blade. The sample is placed directly on a ballistic plasticine box and is not clamped in the ring system as on the Instron CEAST 9340 machine on which the tests for this study were performed. On such a small sample, the reaction may be different from the reaction of a front panel from a real vest. Although the tests are customized for this study, the work is meritorious because it highlights weapons with higher trauma/penetration risk. The results demonstrated that Stanley Tools 1992 cutting blades were at least three times more powerful in stab penetration than the HOSDB P1/B blade when tested against certified KR1 body armor specimens. Therefore, there is a significantly higher threat value imposed by the more readily available and affordable utility blade.

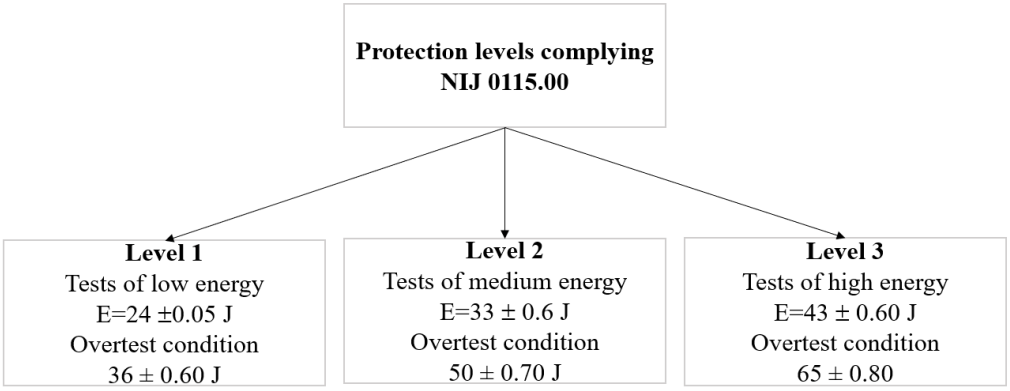

Fig. 4.1. Test energy levels for stab and puncture protection [NIJ Standard-0115.00]

The first energy level is called "E1". Under these conditions, a maximum blade or tip penetration of 7 mm is allowed, determined by research indicating that internal organ damage would be extremely unlikely.

A classification of the tests performed by the researchers can be seen as follows:

- tests that can rank stab and/or puncture resistance, without mimicking as much as possible conditions similar to real attack, such as drop-test machines, where impact energy, speed, weapon can be observed, but do not realistically mimic the grip or resilience of panels;
- tests according to accepted standards for stab resistance assessment under conditions closer to reality.

The following materials were purchased:

- Twaron SRM509 and Twaron CT736CMP materials, Tesa professional spray glue tubes (Spray glue extra strong).
- auxiliary materials: black rubber sheets, sponge sheets of two different sizes; polyart marker paper;
-Sample preparation materials: holding clamps, cutters with spare blades, protective foils for samples;
- materials for white weapons: 4 HSS-CO8%4X20X200 steel bars, 2 with 4 mm x 40 mm section and 2 with 4 mm diameter,
- auxiliary materials: pencil, ruler, permanent markers, tripod, camera.

The third stage consisted of preparing the materials and samples to be tested.

Another stage is to draw up the test plan. Two types of tests have been done: tests that are closer to the realistic ones on the CCIACBRNE facility, resembling the real thing, and tests that help us to prioritize materials, on the Instron CEAST 9340 testing machine at INCAS, which underlines the importance of testing for materials resistant to bladed weapons (knives and spikes).

The tests were performed on 3 types of material: Twaron CT736CMP, Twaron SRM 509 and Twaron SRM 509 bonded.

The operations to make the panel are: marking the size of samples on the fabric, cutting of sheets (130 mm x 130 mm panels were used in tests on Instron 9340 drop-test machine INCAS and 400 mm x400 mm panels were used for testing on CCIACBRNE facility. The assemlying of the panels involved several steps, namely: determining the number of layers, weighing and measuring the thickness of each one.

For Twaron SRM bonded panels, additional operations were required, such as:

- each sheet was sprayed with a Tesa® Extra Strong 60022 synthetic rubber adhesive, with adhesive film formation for permanent bonding of materials;
- the layers of material were laid side by side and bonded together;
- pressing them with a weight of 0.75 kg under a plate for 24 hours;
- samples are placed in envelopes and left to undergo the natural aging process for 48 h.

4.4. Materials and Methods Used in Testing of Stab and Puncture Protection Panels

4.4.1. Materials for Stab-Resistant and Puncture-Resistant Panels, Developed by the Author

The materials used in this research are supplied by Teijin Limited [Catalog Teijin Ballistics Material Handbook QMB1.1-20181001EN], [Catalog Teijin Ballistics Material Handbook,

38-14-05/2012]. Teijin Aramid has also developed Twaron® SRM, which is a unique material offering superior protection against a wide range of weapons. Twaron® SRM incorporates Twaron® CT microfilament fabric with a polymer matrix coating and embedded silicon carbide abrasive particles (Fig. 4.5). The coating absorbs and dampens the thrust of the blade or needle as if it were a stiffer body, and the impact energy is then absorbed by the high impact strength and toughness of the para-aramid threads in the fabric underneath. Thanks to the special matrix, the material is quite flexible.

Hockauf has tested the CT736CMP for ballistic applications. This fabric which has only been mentioned in a few recent articles on ScienceDirect (Elsevier) is shown in Fig. 4.4 [Hockauf M., 2007].

Huang et al. [Huang C., 2021] tested Twaron® CT612 fabric panels, at low-speed impact, neither with a knife nor a spike, but with a spherical indenter. Low velocity drop-weight impact experiments of single Twaron® CT612 fabric at an impact energy of 15 J, 20 J, 30 J are performed. The experimental results reaffirm that Twaron® is an impact rate sensitive material and that higher impact energy resulted in higher breaking load, higher breaking strain, higher energy absorption and shorter fabric contact time.

Research conducted by Kędzierski P. (he used CT709) confirmed that embroidered structures, in combination with woven structures, can significantly improve the properties of protective fabric used in personnel protection [Kędzierski P., 2022].

The SRM509 coded bonded panels, are panels made by the author, by bonding with a relatively elastic (flexible) adhesive the layers of SRM509.

The adhesive is a sprayable tesa® Extra Strong 60022 brand synthetic rubber film-forming adhesive for permanent bonding of plastics, textiles, cardboard, foam rubber, insulation, vinyl, leather, synthetic leather, rubber, metal and wood. The adhesive resists moisture and temperatures up to 100°C in the short term and 80°C in the long term. For bonding SRM509 fabric sheets, the surface was cleaned with a moderate air jet to remove dust.

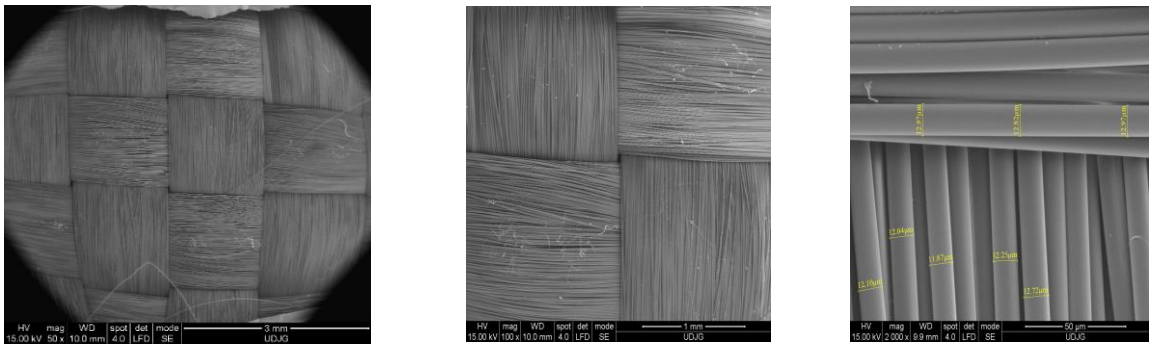

a) b) c)

Fig. 4.2. SEM images of CT736 material (a) and (b) fabric (c) fibre size

CT736 and CT737, 1680 dtex, type 2000 [Teijin. Ballistic Materials Manual, QMB1.1 20181001EN] used in this study is a 410 g/m^2 ballistic fabric - CT736: basket 2x2 weave flat or 1/1 type fabric. CT 737 is a 2x2 Z twill weave, for better drapeability in difficult shaped pieces: state-of-the-art ballistic helmets, mine boots. Twaron® CT736 is a fabric successfully used for the production of modern state-of-the-art ballistic helmets or ballistic applications.

This style of fabric is available impregnated with pure PVB or phenolic PVB. In addition to protection against ballistic impact, protection against sharp weapons attacks has become an increasing priority. In more and more countries, police officers are facing the threat of a wide range of bladed weapons.

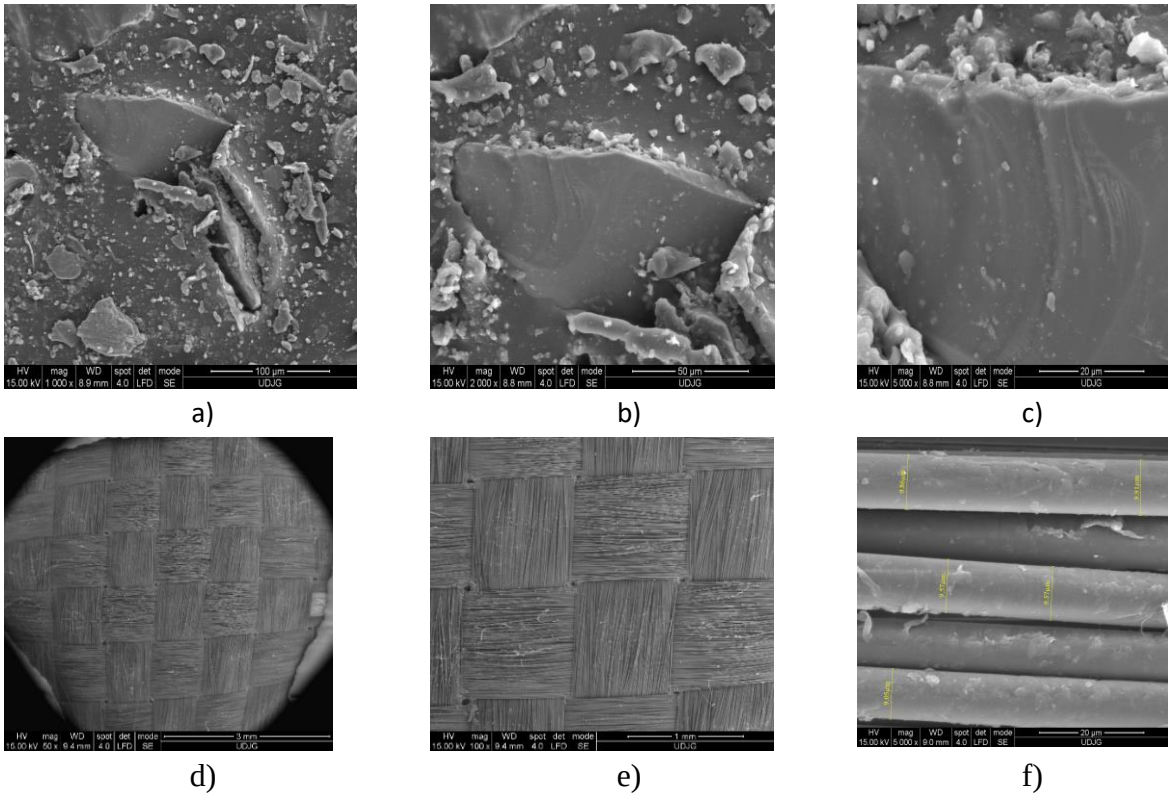

a) b) c)

d) e) f)

Fig. 4.3. SEM images of SRM509 fabric a), b) and c) silicon carbide fabric face, d), e), fabric back represented by the fabric, f) fiber size

Teijin Aramid has also developed Twaron® SRM, a unique material that offers superior protection against a wide range of weapons. Twaron® SRM incorporates Twaron® CT microfilament fabric with a functional silicon carbide coating that is embedded in a matrix. The coating absorbs and dampens the thrust of the blade or needle as if it were a stiffer foil, and the impact energy is then also absorbed by the high impact strength and toughness of the para-aramid threads in the fabric underneath. Thanks to the special matrix, the material is flexible.

4.4.2. Auxiliary Materials for Stabbing And Puncture Tests

The same auxiliary materials were used for both sets of tests, the one on the Instron CEAST 9340 drop-test machine and the one performed on the CBRNE facility.

For the support material [NIJ 0115.00, 2000] the configuration in Fig. 4.4. Taking into account these recommendations and the supply possibilities, we [illegible] following materials for the support package of the test panel shown in Table 4.1.

4 layers of neoprene sponge

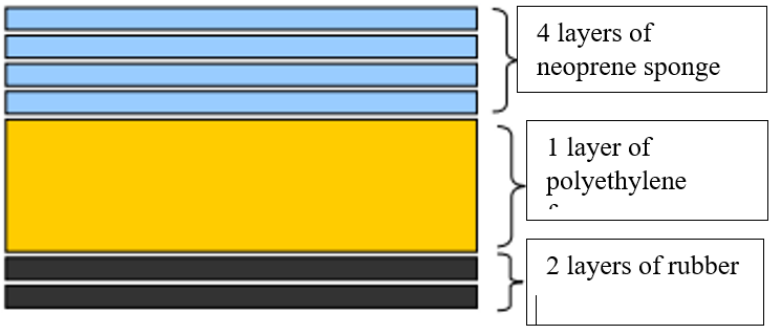

Fig. 4.4 Backing material of sponge and rubber layers [NIJ 0115.01, 2020]

Table 4.1. Characteristics of the components of the backing material used in this thesis

Component material	**Specifications**	**Supplier from Romania**
Sponge	25 kg/m^3, type HR, pressure resistance 2000 kPa, 8 mm thick	Intex Conect SRL Giurgiu
Soft sponge	35 kg/m^3 density, type HR, pressure resistance 2500 kPa, 30 mm	Intex Conect SRL, Giurgiu
SBR rubber technical plate -	6mm thick, smooth, black, 1400mm wide Hardness 65±5°Shore A, 6mm thick	SC Arte Rubber Distribution SRL

The test paper is a special paper that does not fade after the test and therefore the cut length is realistically judged by the cut length in the paper. In the panel and sponge plates, the material backing/relaxation effect screens the actual cut length. In this work, a single paper witness was used, placed between the back of the panel and the first 8 mm sponge plate.

The standard [NIJ 0115.01, 2020] recommends a single sheet of polyart paper, placed between the sample and the backing material for measuring knife penetration. The quality of the paper is characterised by: surface density of 140g/m^{2,} thickness of 0.178 mm. PolyArt paper was used in this work, from Antalis SA Bucharest, who delivered the paper cut to 130 mm x 130 mm and 400 mm x 400 mm, dimensions of the samples tested in this work. PolyArt is a synthetic "paper" made of HDPE (high density polyethylene), treated on both sides, durable, water and mechanical resistant. Polyart paper is only useful for determining penetration depth when using knife blades. It is not effective for spike testing because spikes do not leave a well-defined mark in the test paper. The penetration depth of the spikes is measured directly with a ruler with a millimetre scale.

If panel perforation/penetration occurs, the paper retains the penetration dimension (as length), which can be used to determine the penetration depth [Tien D.T., 2010]. Tien et al. [Tien D.T., 2010] used a different arrangement of backing materials. It is among the few papers that tested two weapons (S1 knife and spike), as recommended in [NIJ 0115.01, 2020], but only at one energy level, 24 J.

In this thesis, tests were performed at three energy levels, at values recommended in NIJ, both for material hierarchy tests and those performed on larger panels, with clamping recommended in [NIJ 0115.00, 2000] for the tests done on installation of CCIACBRNE. The

test specimen backing material is replaced when it can no longer be used because it has been cut/punched in previous blows [NIJ 0115.00, 2020].

4.5. Blank Weapons Used in Stabbing and Puncture Tests

From the threats listed by [NIJ 0115.00, 2000] two of the three recommended threats were chosen for reasons of time and expense of the relatively expensive protective materials, the S1 knife blade and the spike, executed according to the drawing in Fig. 4.5. and following the geometry given in [NIJ 0115.00, 2000].

For this study, flat bars and a round bar made of B01 steel (high speed tool steel, hardness 52...55 HRC) were purchased from Proma Machinery SRL. The bar had initial dimensions of 20 mm x 4 mm x 200 mm, code B014/20x04, and the round bars had a diameter of 4 mm, code B012/04. The processing was carried out at the Faculty of Engineering of "Dunărea de Jos" University.

B01 BS4659 is a steel for cold working tooling. The material is composed of a combination of manganese, chromium and tungsten. B01 tool steel offers characteristics including good surface hardness after tempering, dimensional stability in hardening and machinability. It is equivalent to AISI 01, GB 9CrWMn, JIS SKS3, ASTM A681, DIN 17350, BS ISO 4957:2018 [https://www.smithmetal.com/bo1-tool-steel.htm]. B01 HSS-Co 8% brand steel has the following characteristics: dimensional stability, good machinability, good durability, excellent wear resistance and for use as cutting blades, very good and constant surface hardness on the heat-treated surface. It is usually hardened in oil. Typical applications include: tools, punches, punching tools, active components of dies and stamps.

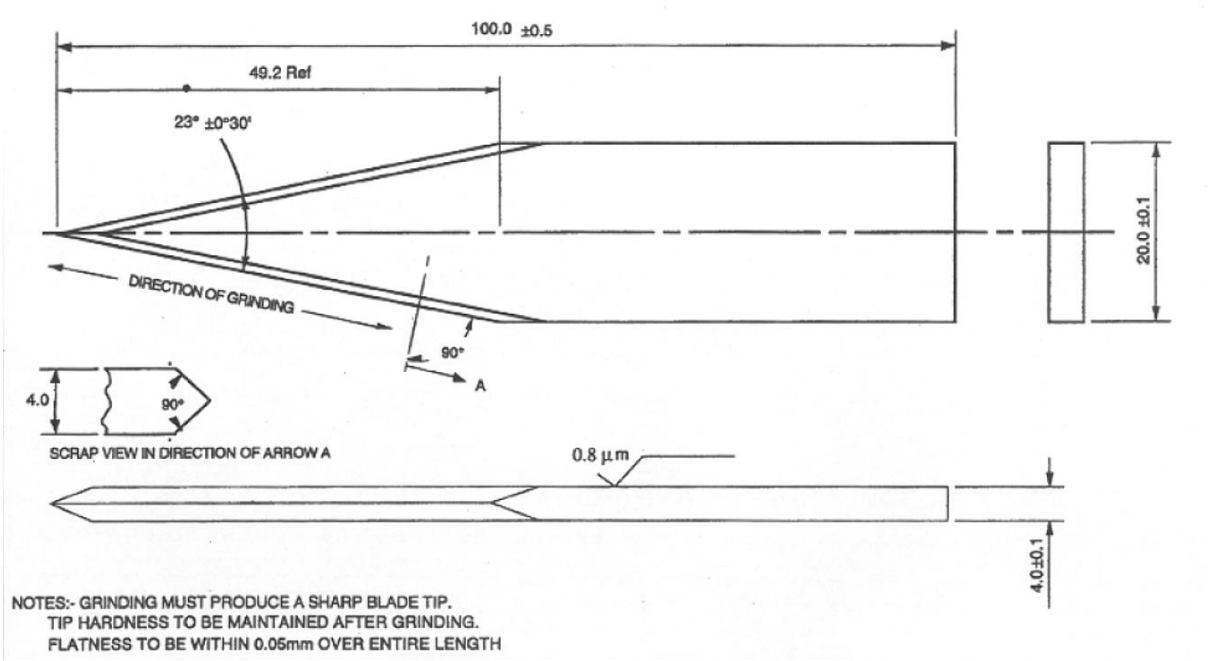

a) Dimensions in millimeters

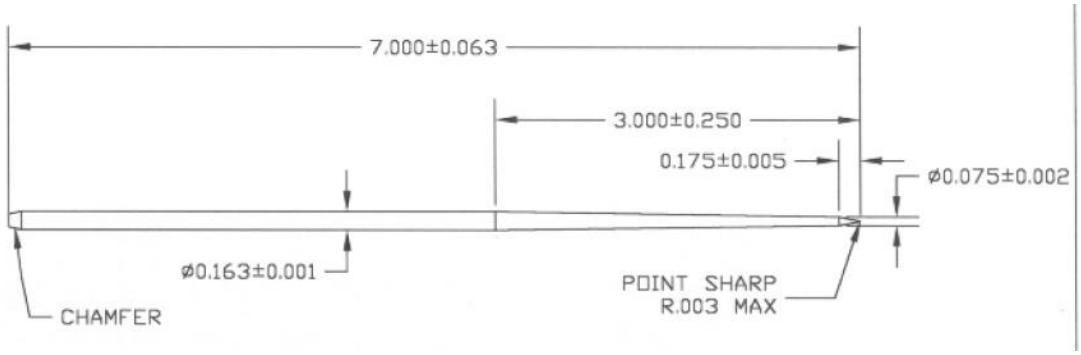

b) dimensions in inch

Fig. 4.5. Dimensions of blank weapons tested according to NIJ 0115.00.
Knife (a) and stab-bullet (b)

4.6. Panel Technology in Laboratory Conditions

From a roll of Twaron SRM509 measuring 1.64 m, squares measuring 400 mm x 400 mm were measured and cut. These squares were then divided into smaller squares, each measuring 130 mm x 130 mm, because the Instron 934 sample testing machine at the National Institute for Aerospace Research and Development "Elie Carafoli" - INCAS Bucharest, on which part of the tests were carried out, could not accommodate larger samples. We did the same with the Twaron CT 736CMP material plates, from which we made only nine packages (16, 24 and 32 layers).

After being cut to size, the sheets were grouped into bundles of 16 layers, 24 layers, 32 layers and 40 layers respectively. Some sample packs were made by gluing, layer by layer, using professional Tesa spray (Fig.4.6). The samples were individually placed in protective foils with the appropriate identification labels.

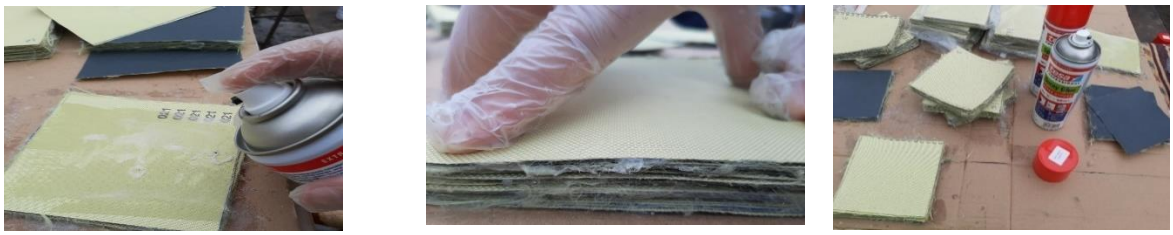

a) b) c)

Fig. 4.6. Layer-by-layer bonding of sheets, using Tesa professional spray. a) spraying the 130 mm x130 mm sample, b) bonding the sheetes, c) the panels

4.7. Test Campaign to Evaluate the Behaviour of the Panels Developed for Puncture And Stabbing

4.7.1. INCAS Testing Procedure

The following test plans are given for a single material. These test plans in Fig. 4.7 and 4.8 have been followed for panels made of SRM509 and bonded SRM509. For CT736, only several tests (3 tests each for E_N =24 J) and 3 panels with 16, 24, and 32 layers were performed.

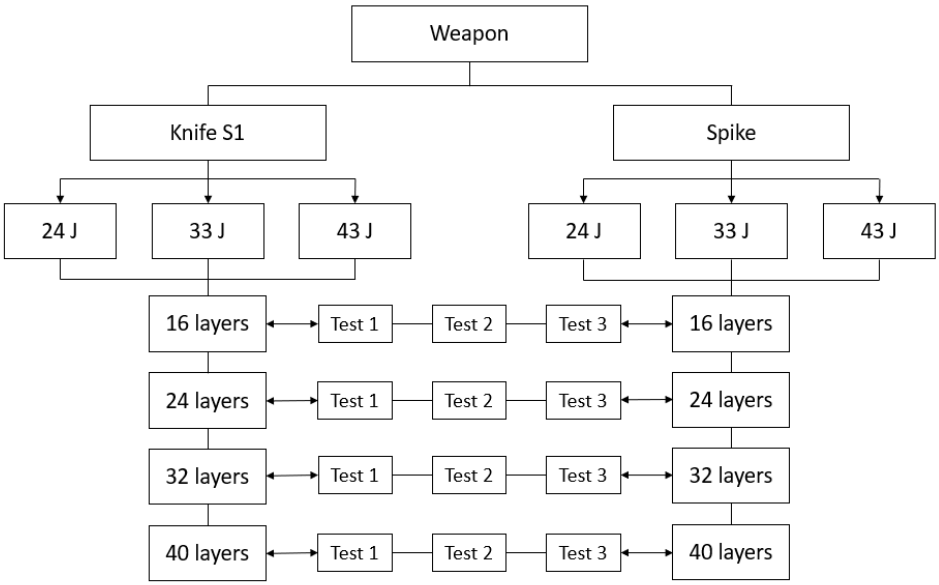

Fig. 4.7. Test plan for the Instron 9340 drop-test machine at the National Institute for Aerospace Research and Development "Elie Carafoli" - INCAS Bucharest

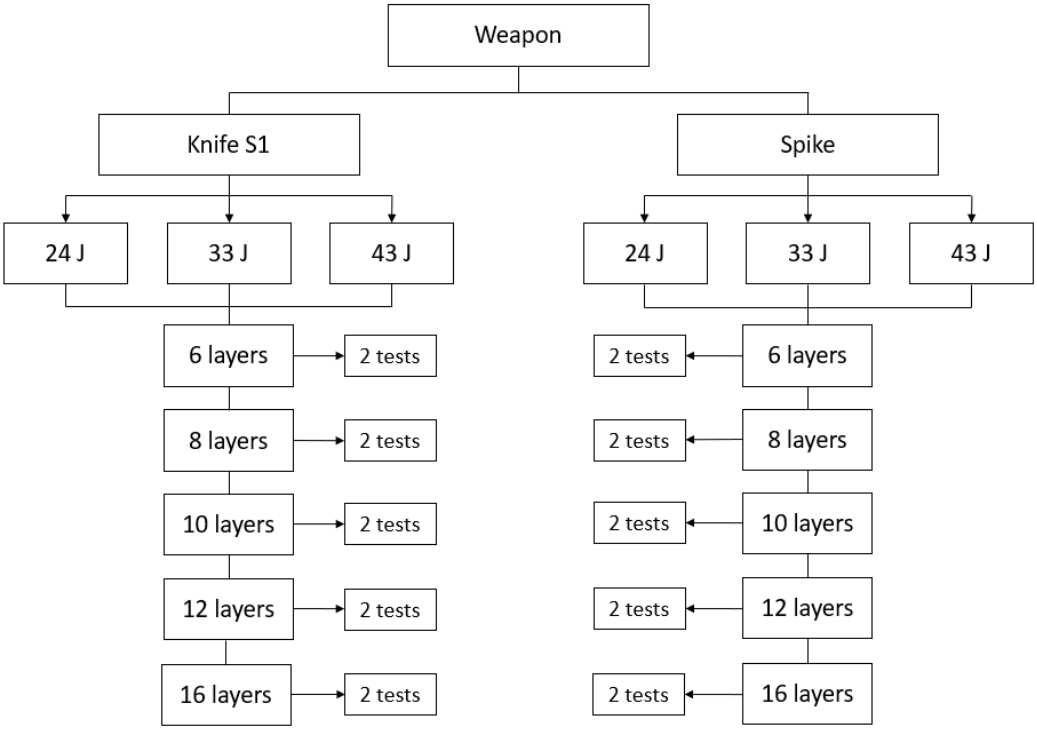

Fig. 4.8. Test plan for the test facility at CCIACBRNE Bucharest

The batch of sample packs prepared for testing on the Instron 9340 machine was:

- S1 knife tests = 72 Twaron SRM509 samples + 9 Twaron CT 736CMP samples,
- Spike tests = 72 Twaron SRM509 samples.

Total samples performed with Instron 9340 at INCAS Bucharest = 153 tests.

One group, of hit energy tests, will consist of three sized armour samples.

Samples were taken at three levels for each energy: 24 J, 33J, 43J, as listed in NIJ Standard-0115.00.

For the CT 736 material, 3 tests for 24J energy and 3 layer numbers and tests were performed.

The production of the packages was according to NIJ Standard-0115.00. At the bottom the 2 layers of rubber were placed, over them followed the layers of sponges, then the polyart or marker paper, over these the run sample was placed with the label inscribed with the sample details as shown in Fig.4.9.

Fig. 4.9. Preparing samples for testing on the Instron 9340 machine

4.7.2. Test procedure on Instron CEAST 9340 (INCAS) machine

The following test plans are given for a single material. These test plans have been followed for SRM and bonded SRM fabric panels.

The test procedure on the Instron 9340 includes the following operations:

- checking the quality of the material and the number of layers,
- check test parameters (sample number, 1, 2 or 3, energy level),
- check the labels of the set of 3 samples (front, back, paper) to have the same information: material, number of layers, mass, thickness, energy, threat, test number, date,
- checking the backing material as order of components (paper, sponge, number of sheets, paper, thin sponge 8mm x 3, thick sponge 30 mm and rubber 2 pieces x6 mm ,

- weighing the sample and recording it in the table,

- measurement of sample thickness; measure in four points, tabulate, calculate mean and standard deviation,

- a single layer of polyart paper is placed between the armour and the top layer of the composite backing material to provide a possible means of measuring knife penetration in blade stabbing tests. If full penetration of the armour occurs, the witness paper will be cut or pierced. The dimensions of the cut can be used to determine the penetration depth, on;y for knife action, as shown in Fig. 4.10b,

- label - where the material designation (name, number or other description) is found; which serves to uniquely identify a specific armor configuration based on the details of the protective panel construction (i.e. number of layers of one or more types of stab resistant material, sample mass, sample thickness, impact energy, cut or track on the panel left by the weapon, front or back, test number, date the tests were done, and the name of the operator of the materials to be tested as presented,

a) b) c)

Fig. 4.10. Laying of layers for backing material: a) side view: 2 layers of 2x6 mm rubber at the bottom, 1 sponge of size 30 mm (middle) and 3 three layers of thin sponges of size 8mm (top), b) polyart paper, c) Fixture fixtures for Instron CEAST 9340 INCAS testing machine knife (a) and spike (b)

- Check the weapon (blade or tip) for signs of abrasion from previous tests. If there is, the blade is ground again and the angle at the tip and the angle of the cutting edge are checked,

- machine adjustment - setting the machine parameters of interest: force, displacement, speed, energy and determining the form of recording the results,

- The attachment of the arms to the impactor of the machine is done with a bolt-nut system as shown in Fig. .4.10 (c),

- mounting the sample in its holder: panel package with backing material,

- tightening the ring pack to 0.8 MPa,

- closing the door because otherwise the test machine will not start,

- conducting the test,

- removing the test sample from the machine and checking the cut,

- labelling the witness paper and labelling the panel,

- perform three consecutive tests and check if the results are close (force-time curve and energy-time curve),

- checking the records in the computer memory,

- checking the test list and switching off the machine, removing the machine from the power supply,

- measuring the dimensions of the knife cut-out and the hole for the pipette,

- placing the samples, individually, in protective foil with identification labels.

After completion of the tests, the database with the results obtained was created (as can be seen in Appendix 5 with experimental data). Data processing was done by calculating the means of the measured parameters were calculated and the standard deviation for each.

4.7.3. Measured parameters and repeatability of Instron CEAST 9340 tests

Repeatability is the degree of agreement between the results of successive measurements of the same measurement when performed under the same measurement conditions. A measurement is repeatable when the variation is less than a predetermined acceptance criterion. The following conditions must be met to establish repeatability: -same observer, -same conditions, -same measuring instrument used under the same conditions, -

same location, -repetition over a short period of time, same objectives [JCGM 100:2008] [Evaluation of measurement data].

Figure 4.11 is an example of experimental data processing for a set of 3 tests performed under the same conditions.

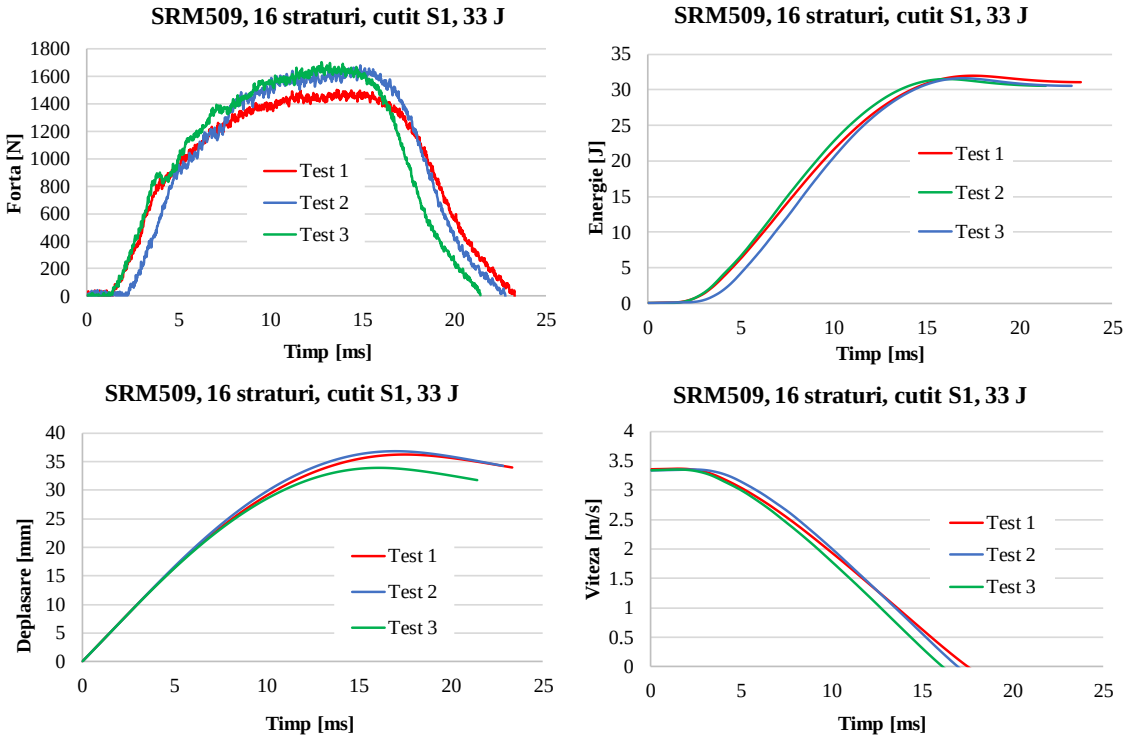

Fig. 4.11. Example of graphs with experimental data obtained from testing with INCAS Instron CEAST 9340 repeatability testing machine

4.7.4. Test Procedure and Test Facility at CCIACBRNE

Although the test plan was initially set up similarly for the drop-test machine and the CBRNE stab-test facility, the difference in sample size and sample gripping systems, and the much different preliminary results for the 16-layer samples, led to the modification of the test plan on the CBRNE stab-test facility.

The second campaign of tests was carried out at CCIACBRNE - Research and Innovation Centre for CBRN Defence and Ecology Bucharest. The facility at CCIACBRNE is shown in Fig. 4.27. The sample packs, for this stage of testing, were made of 400mm x 400mm Twaron SRM509 material plates. The sample packs were made in this case by stacking the plates in 6 layers, 8 layers, 10 layers, 12 layers and 16 layers respectively, resulting in 11 packs. The total number of samples used on the CCIACBRNE facility was 11 panels and 66 tests.

The batch of sample packages prepared for testing at CCIACBRNE, is shown in Table 4.8. below. The total number of tests performed under the CCIACBRNE's stab and puncture test facility is 66 tests.

The tests are carried out using a guide tube assembly as in Fig.4.28. This system has been designed to allow the dropping mass (blank weapon) to fall under the influence of gravity and strike the armour sample at a predetermined impact point. Catch systems, located

on the outside of the tube, prevent the tube from rotating about its axis or falling to the left or right side during the test, ensuring that the knife blade, or the tip of the test spike inside the tube, strikes at the correct and continuous orientation until it stops.

The weapons are clamped into a device with a screw, forming the impactor system or drop table. The knife blade is machined and designed to represent a type of edged weapon used in attacks. The knife blade reproduces a thicker, sharp-pointed commando-style blade and has two cutting edges with a rigid spine as shown in Fig. 4.29a.

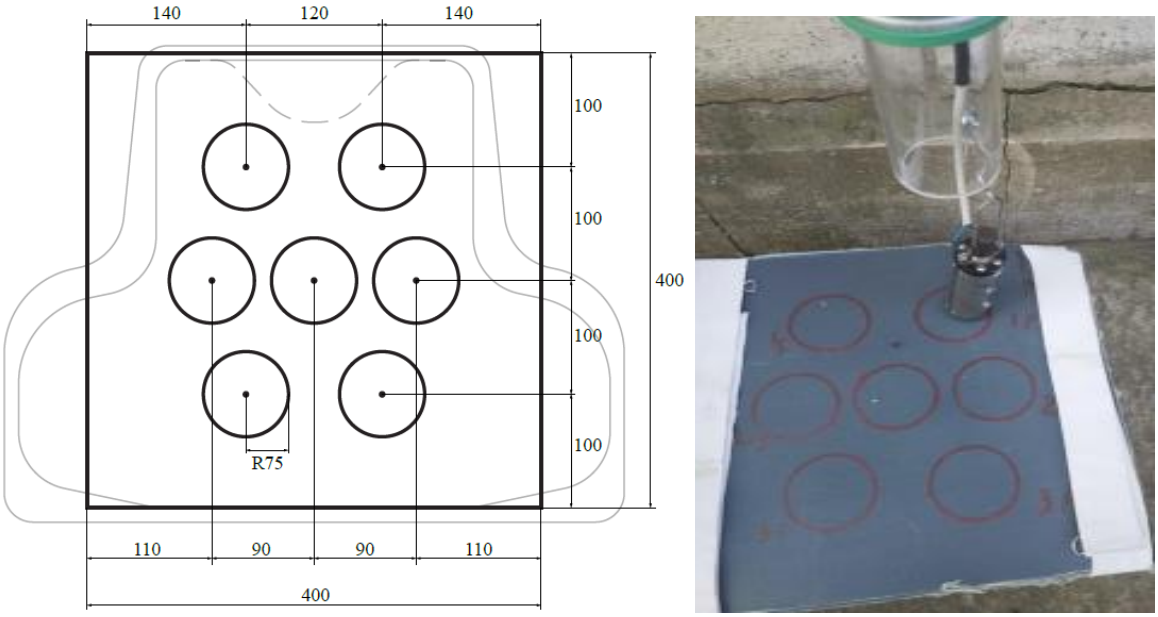

Fig. 4.12. a) Template for the positioning of the strikes on the test panel, on a model of a vest pattern, front and back, with the dimensions of the standard (NIJ 0115.00) after which the template for the positioning of the strikes was made b) Preparation of the electromagnetic test rig with guide tube and clamping of the test specimen with a strap

A template is used to mark the locations of the impact positions intended for stabbing. Fig. 4.12 illustrates a typical template design for a front and rear panel. A single impact can be placed in each impact area shown in Fig. 4.12. The central position shall not be used.
The dropping mass is the device that falls freely under its own weight to hit the armor panel at a specified energy. The body mass consists of an engineered knife blade or tip, a clamping device (Fig. 4.13) to hold the knife blade or tip in position, and the nylon shoe designed to ensure that the knife blade or tip falls vertically within the drop tube apparatus.

A test procedure includes the operations and their order in detail concerning sample verification, mounting the sample in the CBRN facility, adjusting test parameters, etc.

Table 4.2. Drop height of the impactor to have a given energy

E [J]	$h_{(knife\ S1)}$, [m]	$H_{(spike)}$ [m]
24	1.1	1.2
33	1.6	1.7
43	2.0	2.2

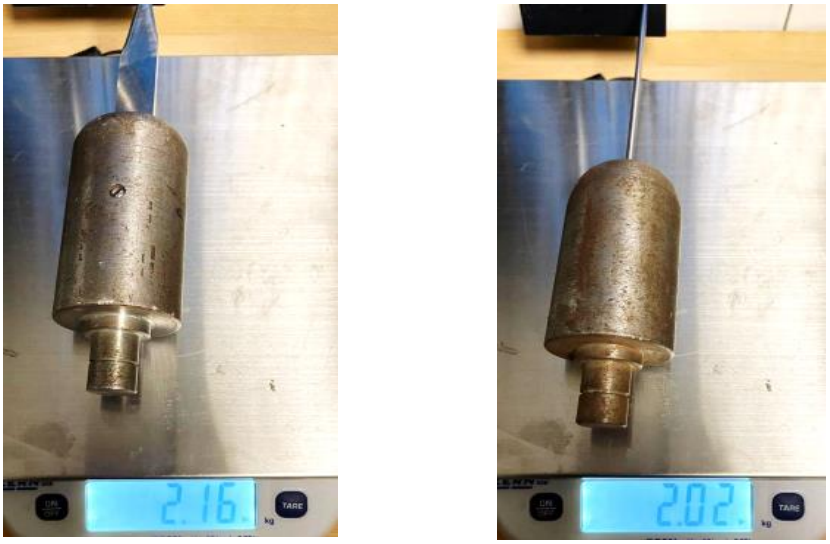

a) b)

Fig. 4.13. Mass of impactor (a) with knife S1, (b) with spike (in kg)

Based on these preliminary tests, the thicknesses of the panels to be tested on this installation were modified. The test panels were made with a number of 6 layers, 8 layers, 10 layers, 12 layers, and 16 layers, respectively, as shown in Fig. 4.36 obtaining a number of 11 panels. The total number of samples, used on the CCIACBRNE facility, was 11 and there were performed 66 tests.

The operations performed before testing and during the tests are:

-removing the packages with identification labels from the individual protective foil,

-weighing and measuring operations of the panel,

-clamping the panel layers,

- calculation of the impactor drop height for each energy (24 J, 33 J and 43 J),

-verification of measured panels and impact positions,

- positioning the panel and the backing material on the plastiline box, tightening the straps over the panel to be tested (Fig.4.12) and mounting the weapon (knife or spike) in the support,

- after mounting the panel and raising the impactor to height, the test perimeter is checked to ensure that no one is in the impact area and that persons operating the plant are placed at a safe distance to avoid an industrial accident,

- pressing the start button represents demagnetization, the electrical current supporting the impactor and the weapon falling through the guide tube until the sample hits,

- measurement of test parameters,

-Introduction of samples in protective foil with identification labels.

4.8. Photographing the Samples

After completion of the two experimental procedures (INCAS and CBRN), the next step was to shoot the samples. Photographs were taken in normal and macro (for details), front and back, of all samples tested.

4.9.Sample Preparation for the Scanning Electron Microscope (SEM)

Another step in the experimental approach was to prepare the samples for electronic scanning. The layers of a panel were cut into 20 mm x 20 mm sizes (Fig.4.40.), then each placed in protective aluminium foil, which also serves to enclose the scanning screen, resulting in an enhanced image. Fig.4.41. highlights aspects of the preparation of the samples for detailed study under the microscope. These were, as specified above, cut to the size of 20 mm x 20 mm, followed by a gilding process of the samples.

4.10. Conclusions on Stabbing and Puncture Testing

The stab resistance of the specimen is evaluated using machined test blades or spikes of uniform size. In these tests, the knife blade or test spike is held in a drop weight (mass) of specified mass. The weight is dropped from various heights into an apparatus that controls the orientation and impact position of the test blade or test spike. The armour is supported on a composite backing material. The measure of the test is the depth of penetration of the blade or barrel through the armour at specified impact energies. The test applicant shall specify the class of protection and the level of protection desired.

Tests on the drop-test machine (here Instron 9430) are only done for the prioritisation of the materials tested and the study of failure mechanisms. Why?

- Because the clamping differs from the NIJ test (the whole package consisting of the panel and ancillary materials are clamped tightly between the clamping rings, so the material response will differ if the clamping is different,
- The surface area of the tested panel is small and therefore does not favour higher elastic deformation as in the case of panels tested after NIJ.

Tests done on larger panels with light webbing fastening, without pressing the whole package, is closer to the behaviour of the vest in reality. That's why test results may differ.

This chapter discusses the selection of materials and the two test plans (campaigns) carried out.

Chapter 5. Experimental Data on Stabbing and Puncture Resistance for the Tested Panels

5.1. Stabbing and Puncture Testing

From the point of view of test results for the assessment of stabbing and puncture resistance, there are several criteria:

- tests for the prioritisation of materials or designed systems,
- tests that simulate reality, but are performed on components or panels,
- prototype tests.

In terms of the standardisation of these tests, there are

- standardized tests according to
  - international (ISO), regional (EN) or national standards (see British and American NIJ tests, but which are also recognised internationally),
  - military standards,
- non-standardised tests, but relevant for the assessment of the quality of materials or protection systems as a whole.

Comparison of force-displacement and force-time plots, and micro and macro analysis of sample failure can lead to a realistic formulation of the damage scenario and could offer solutions for improving the design of such protective systems.

5.2. Characteristics Studied in the Stabbing and Puncture Processes

Since there are two sets of tests, each characterized by the used blank weapon (S1 knife and spike), the characteristics of each, resulting from the tests carried out on the Instron CEAST 9340 machine, are given below, together with the respective symbols (the same used in the tables in the Appendix with experimental data). Their understanding can also be made with the help of the sketches in Fig. 5.1.

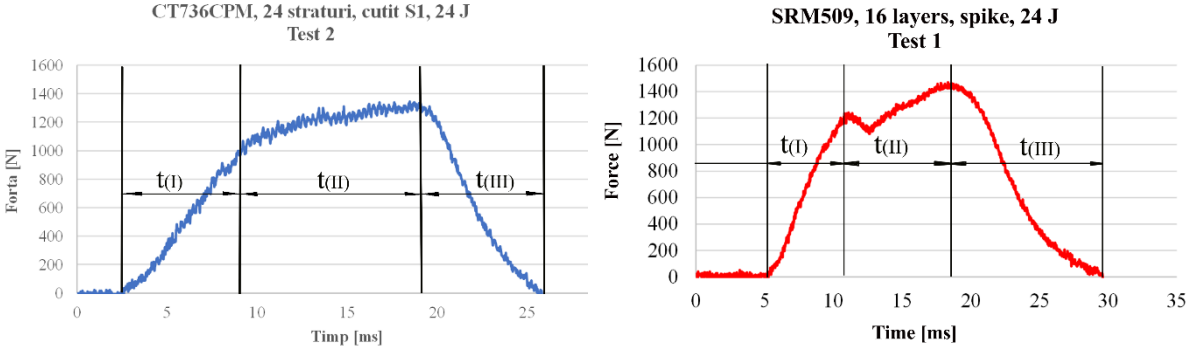

Fig. 5.1. Stabbing (left) and puncture (right) stage durations

Time I: compression zone - the perforation mechanism of fibrous material and layered structure differ from woven or knitted fabrics, therefore, the low compression value of the structure makes a critical change in the packing density, under the perforating blade and the area around it. During the punching process, the fiber stretches and entangles with the punching blade advance. The drag force is the compressive force on the tip of the perforator or cutting blade.

Time II: with the movement of the perforator blade, the fibrous structure becomes more compressed and the fibres more strained to resist perforation. Fibre tension is based on the frictional force with the perforator surface and friction with other surrounding fibres. The movement of the fibres during penetration of the perforator is largely responsible for the difference in the perforation behaviour of the fibrous structure. The puncture force is the result of the friction of the fibres at the contact points between fibres and the compression force on the tip of the punch blade.

Time III - (cutting controlled mechanisms); with further penetration of the perforator, the fibres involved with the perforator tip will begin to crack and/or slip. The total resistance force is the result of the bending force for all fibres involved with the perforator blade and the frictional forces between the fibres contacting the blade surface and the compaction force on the perforator blade tip, for a penetration height "h". Subsequent destruction of adjacent fibres occurs in all directions. If the fibre mat has a high packing density and the fibres are long and tightly packed, the puncture resistance will be the highest, as most of the fibres under the punching blade will be cut.

For S1 knife test

g_p - panel thickness, in mm
F_{max} - maximum force, in N
E_{max} - maximum energy, in J
E_{total} - total energy, in J
δ_{max} - maximum displacement, in mm
δ_{total} - maximum displacement, in mm
H_0 - impact height, in mm
v_0 - nominal impact velocity in m/s
E_N - nominal impact energy, in J
L_f or $L_{față}$- length of cut on panel face, in mm
L_s - length of the cut on the back of the panel, in mm
L_h - cut length on PolyArt paper, in mm
m - mass of the panel, in g
$h_{calculated}$ - depth of penetration of the knife, in mm

For the spike test

Some of the notations are identical to those in the knife tests (H_0, E_N, E_{max}, m, g_p δ_{max}, F_{max}, , E_{total}, v_0).

To characterize the mark left by the spike, the following were introduced:

$d_{maxfață}$ - maximum diameter of the orifice, on panel face, in mm
$d_{maxspate}$ - maximum diameter of the orifice, on the back of the panel, in mm
$d_{max\ paper}$ - maximum diameter on PolyArt paper, in mm

Characteristics determined from tests performed on the CCIACBRNE facility. This facility, although not instrumented, meets NIJ Stantard 0115.01 recommendations for energy levels, clamping system and sample size.

On the force-time diagram (for tests on Instron 9340 machine), both for the knife and the spike, three stages are clearly distinguished:

1. the force increases rapidly apparently after a straight,
2. a slope linking the increase in force of stage I to stage II,
3. the step of decreasing the force to 0 (zero) for the material has linear portions.

The following points can be identified on the force-time graph:

- the initial point of impact, when t_0 =0 and F_0=0, where both values are considered null, but are the last null values in the string of (t, F) pairs.

Figure 5.3 shows a typical force-time curve for a knife-strike test and one for a puncture test, specifying the parameters to be tracked on the recorded plots.

t_0 is the initial moment of impact (the force F oscillates around zero during the distance travelled until it hits the panel, so it is the moment of the last zero value of the force, when it starts to increase),

t_f is when the force F reaches the first zero value after impact, so $F(t_f) = 0$.

- duration of stages
  - stage I has a linear increasing of force over time
$$t_I = t_{FM} - t_0 \tag{5.1}$$
  - stage II ends when the maximum force is reached, F_{max},
$$t_{II} = t_{Fmax} - t_{FM} \tag{5.2}$$
  - stage III comprises a zone where the force acting on the specimen decreases from F_{max} to zero
$$t_{III} = t_f - t_{Fmax} \tag{5.3}$$

5.3. Experimental Results on Instron CEAST 9340 Impact Machine

5.3.1. Parameter Analysis of Force, Energy and Velocity Curves, Determined as a Function of Time, for S1 Knife Tests

5.3.1.1. Introduction

It should be emphasised that these tests, as conducted, are tests to prioritise materials and to determine factors influencing stab or puncture resistance. As will be discussed in the conclusions of this chapter, the response of the tested panels depends very much on their size and the system of attachment of the whole package (test panel, backing material). Particular attention will be paid to highlighting the differences between the results of the two test campaigns.

For objective reasons (price of materials in relation to the funding of the research topic) tests were carried out on the following materials:

- CT736 (16-layer, 24-layer and 32-layer panels, at 24 J impact energy),
- SRM509 (16-layer, 24-layer, 32-layer and 40-layer panels, at impact energy of 24 J, 33 J and 43 J, respectively),
- SRM509 bonded (16-layer, 24-layer, 32-layer and 40-layer panels at impact energies of 24 J, 33 J and 43 J),
- hybrid panels, made of CT736 and SRM509 layers (16-layer, 24-layer and 32-layer panels, at 24 J impact energy), which will be discussed in another subchapter.

5.3.1.2 Influence of the number of layers on the force and energy curves as a function of time

In this abstract of the PhD thesis, only the analysis of force-time curves and panel absorbed energy-time curves are presented.

The influence of the number of layers on the force-time curve can be seen in Figures 5.2, for each energy level tested.

For tests performed at 24 J (Fig. 5.2), two types of force-time curves were obtained: the characteristic shape for CT736, with three distinct slopes, and the specific shape of SRM509 fabric panels, resembling an asymmetric bell. The maximum force recorded increases with increasing number of layers for all tested materials, and the duration of the strike also decreases with increasing number of layers.

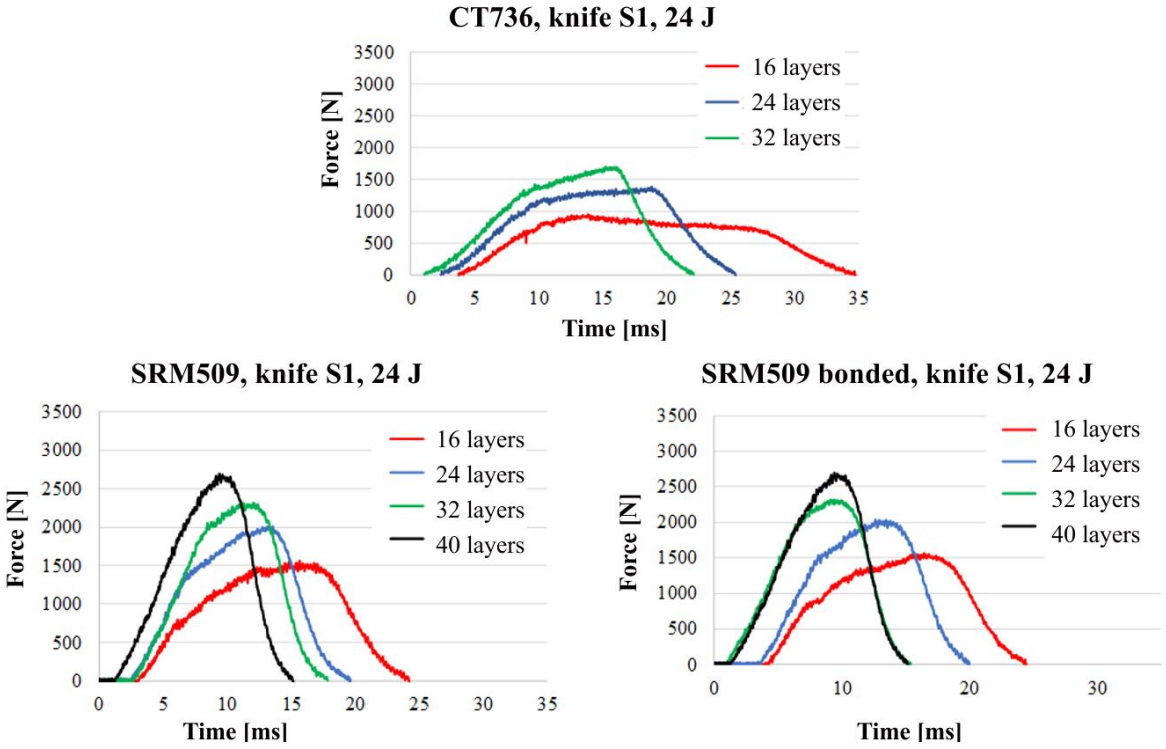

Fig. 5.2. Influence of the number of layers and materials on the force-time curves, for an impact energy of 24 J

The slope of the first stage at 24 J energy increases with the number of layers, regardless of the material, but is more differentiated for CT736 fabric panels. Likewise, the slope of stage 3 is steeper with increasing number of layers. It was observed that for CT736 panels, the orientation of the slope (negative) changed in step 2 for those bundles with a number of plies higher than 16.

From the force-time diagram, it can be seen that the stabbing process time is longer for the panels with less number of layers. Qualitatively analysing these curves (only one of the three tests performed with the same set of parameters, the intermediate value test, considered typical), over the range of layers tested at this energy level, the following observations can be made:

- the maximum measured force, F_{max}, increases with increasing number of layers,
- the duration of the striking process decreases as the number of layers increases,
- for the CT736 panels, the maximum force is positioned at the end of stage II, but for the other SRM509 and bonded SRM509 panels, the force curve is bell-shaped for the 32-layer and 40-layer panels, and for the thinner panels, the curves have a greater degree of asymmetry, with stage II being characterised by a longer duration and an ascending (not necessarily linear) shape,

- abrasive coated fabric panels have close values for F_{max}, at the same number of plies, much higher than those obtained for aramid fabric panels: at 16 plies $F_{max(CT736)(16)}$~900 N, but for SRM509 blank panels, bonded or not, $F_{max(SRM509)(16)} \sim F_{max\ (SRM509\ bonded)\ (16)}$~2700 N,
- SRM509 has steeper slopes than CT736, at the same number of layers. It means that energy is absorbed in a shorter time, which means that the SRM509 material performs better.

In Fig. 5.3 there are given images of the cut obtained on the CT736CMP fabric panels, according to the number of layers. It can be seen that the length of the cut on the panel front decreases with increasing number of layers, and, on the back surface of the last layer, it can be seen that, for 32 plies, the last layer is not pierced. However, the length of the cut on the panel front, $L_{față}$, and the length of the cut on the back of the last layer, L_{spate}, is not relevant for the process because the fabric recovers and, therefore, the measured length includes the relaxation and recoil phenomenon of the yarns/fibres. Therefore, the length of the cut on the witness paper, $L_{hârtie}$, is relevant. This type of paper has negligible recoiling and relaxation processes.

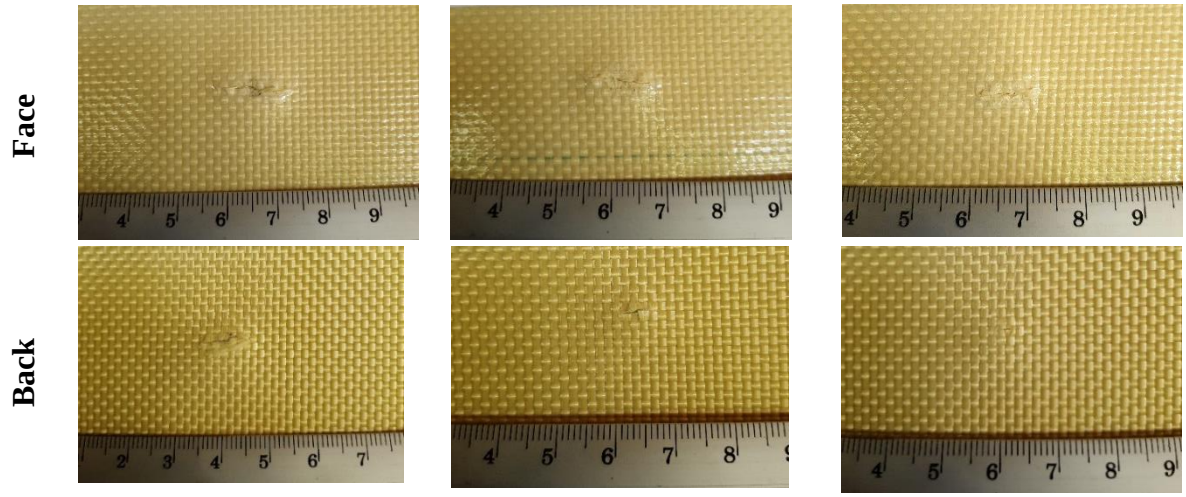

a) 16 layers b) 24 layers c) 32 layers

Fig. 5.3. Photographs of cuts on CT736CMP fabric panels, made with S1 knife, at an energy level of 24 J

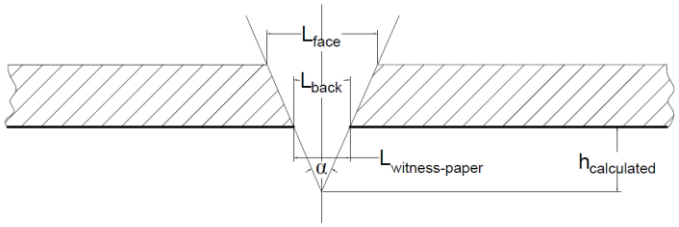

Fig. 5.4. Sketch for calculating the knife penetration height

According to NIJ Standard-0115.00 [NIJ Standard-0115.00], the parameter by which stab resistance is assessed is the calculated height) of the blade that protrudes beyond the last layer. This dimension is calculated taking into account Fig. 5.4 and the following geometrical relationship:

$$\mathrm{tg}\frac{\alpha}{2} = \frac{\frac{L_{paper}}{2}}{h_{calculated}} \rightarrow h_{calculat} = \frac{L_{paper}}{2}\frac{1}{\mathrm{tg}\frac{\alpha}{2}} \tag{5.4}$$

in which $h_{calculated}$ is the measured length of the cut on the witness paper, in mm, α is the angle at the tip of the S1 knife, according to NIJ Standard-0115.00 Stab resistance of personal protective clothing [NIJ Standard-0115.00].

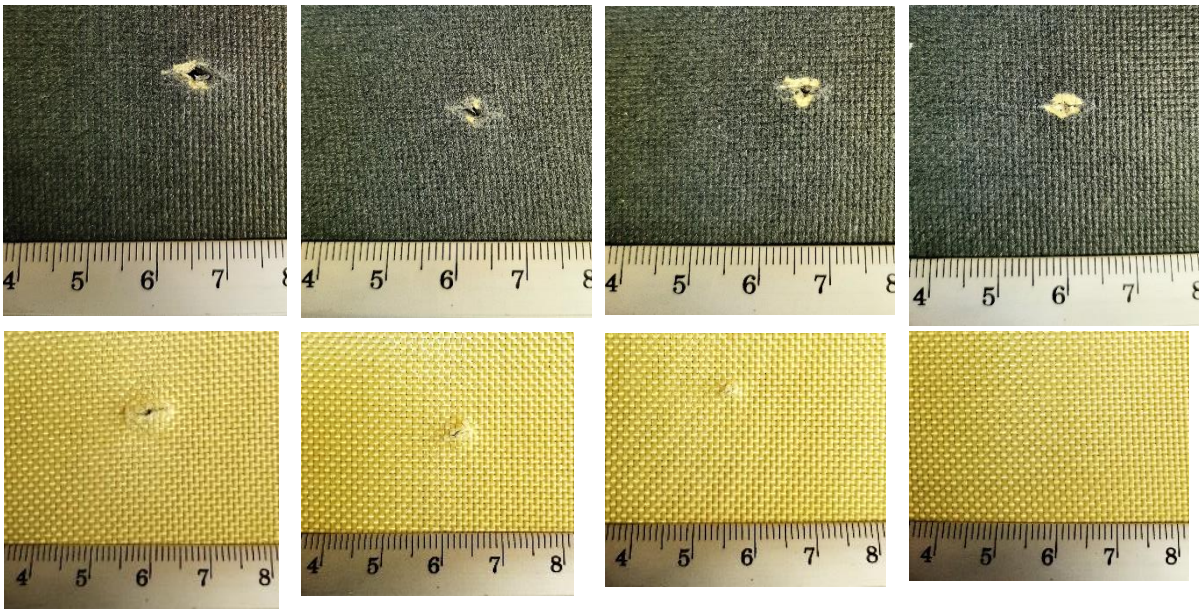

16 layers 24 layers 32 layers 40 layers

Fig. 5.5. Panels made of SRM 509, with different number of layers, tested at energy level 24 J, with S1 knife (top - panel front, bottom - panel back)

For the panels made of SRM 509 fabric, in unbonded (Fig. 5.5) and bonded variants, it can be seen from the photographs that, on the face of the panels, the destroyed area decreases with increasing number of layers. However, the visual difference between two successive panels (as number of layers) is more difficult to differentiate and for bonded panels, this area is ever more difficult to differentiate, except for the 40-layer panel. For both types of panels, the 40-ply panels were not pierced on the back of the panel.

These panels determined specific material characteristics, due to number of layers, energy levels and assembly technology (adhesive bonding):

- the total time of force action is higher for the panel obtained by gluing,
- the order of values for F_{max} is maintained, from 16 layers to 40 layers,
- for SRM509 panels, F_{max} was higher for 16- and 32-layer panels,
- for 24 and 40 ply panels, F_{max} had higher values for the bonded panels, but the difference is less than approx. 10%.

On the back of simple panels, the length of the cut decreases visibly and proportionally to the number of layers. The bonded panels have the ends of the damaged areas similar to those of the unbonded panels. A qualitative conclusion would be that bonding (with the adhesive and technology applied) does not visibly improve the stabbing protective behaviour, at an energy of 33 J.

Figure 5.6 shows typical force-time plots, obtained for the highest tested energy level, 43 J. At this impact energy level, the hierarchy of curves is different for panels formed simply by adding the blank sheets as compared to panels made from the same blank, but bonded. For unbonded SRM509 panels (Fig. 5.7), the maximum force increases with increasing number of layers, but for bonded panels, the time of action of the force decreases with increasing number of layers; the very small increasing slope in time of the 16-layer panel tends to disappear, and for the 40-layer panel, the shape of the graph is bell-shaped, almost symmetrical. For bonded panels, the increase in maximum force with the number of layers in the panel is preserved up to the 32-layer panel, and for the 40-layer panel, the maximum force decreases and the slightly tilted plateau is larger. At the extremes of the range for the number of layers, F_{max} for bonded panels is smaller than that for unbonded panels, but the force action durations are longer.

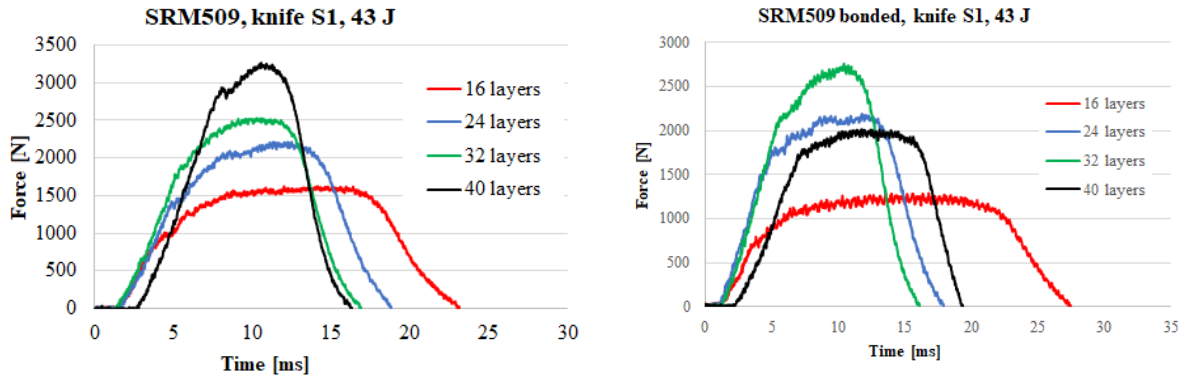

a) b)

Fig. 5.6. Force-time diagrams as a function of the number of layers for a) SRM509, b) SRM509 bonded, at an energy level of 43 J

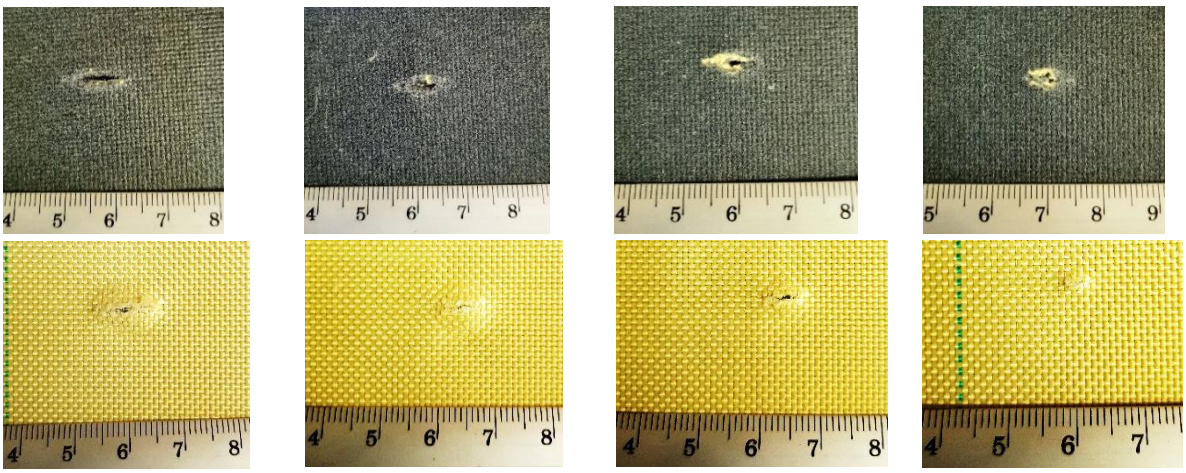

16 layers 24 layers 32 layers 40 layers

Fig. 5.7. Panels made of SRM509, with different number of layers, at energy level 43 J, after S1 knife test (top - panel front, bottom - panel back)

The energy-time plots suggest a better response for materials where the slope of the increase in absorbed energy is greater. Increasing the number of layers of CT736CPM (Fig. 5.8) determined the size of the slope of the absorbed energy evolution, but for SRM509 panels,

bonded or not, the difference between the slopes of these curves is small, a distinct difference being seen only between 16-layer panels and the following ones.

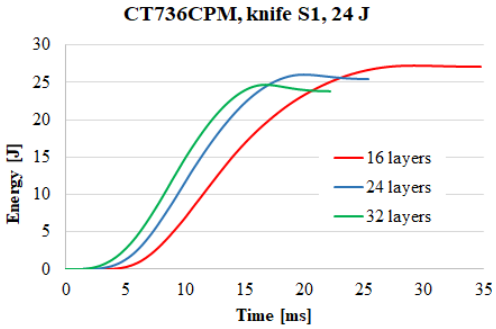

a)

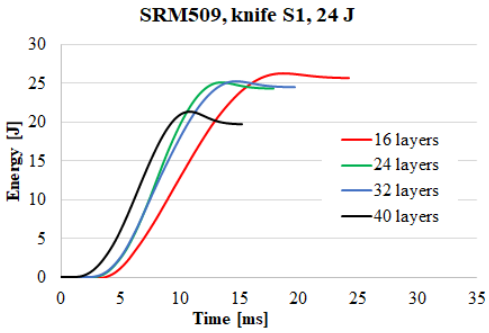

b)

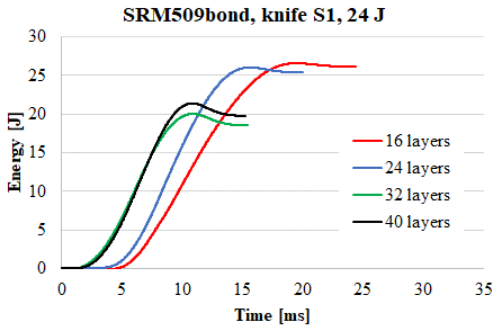

c)

Fig. 5.8. Influence of the number of layers on the energy-time curve, for an impact energy of 24 J

For tests at 43 J, the slopes of absorbed energy increase with increasing number of layers, with the difference being more pronounced for unbonded SRM509 panels (Fig. 5.9).

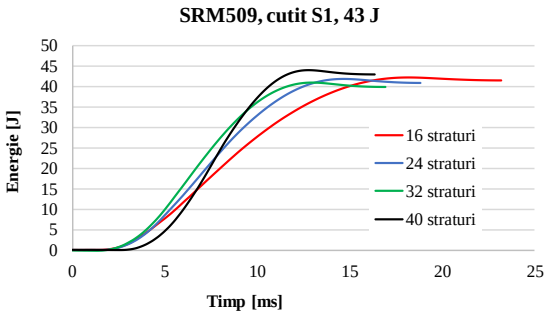

a)

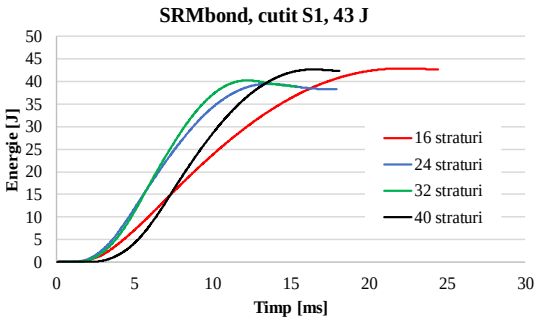

b)

Fig. 5.9. Influence of the number of layers on the energy-time curve, for an impact energy of 43 J

5.3.1.3. Influence of Impact Energy on Force, Energy and Velocity Curves over Time

In this sub-chapter, only panels made from SRM509 blanks will be compared, i.e. panels made by adding layers only (with fixed two edges) and those made by bonding layers with adhesive, coded SRM509 bonded.

Panels with 16 and 24 layers have the maximum force value less dependent on the impact energy. The large difference in the positioning of the force-time curves occurs especially in the bonded SRM509 panels, at 32 layers and 40 layers, as shown in Fig 5.10.

The impact duration decreases with increasing number of layers.

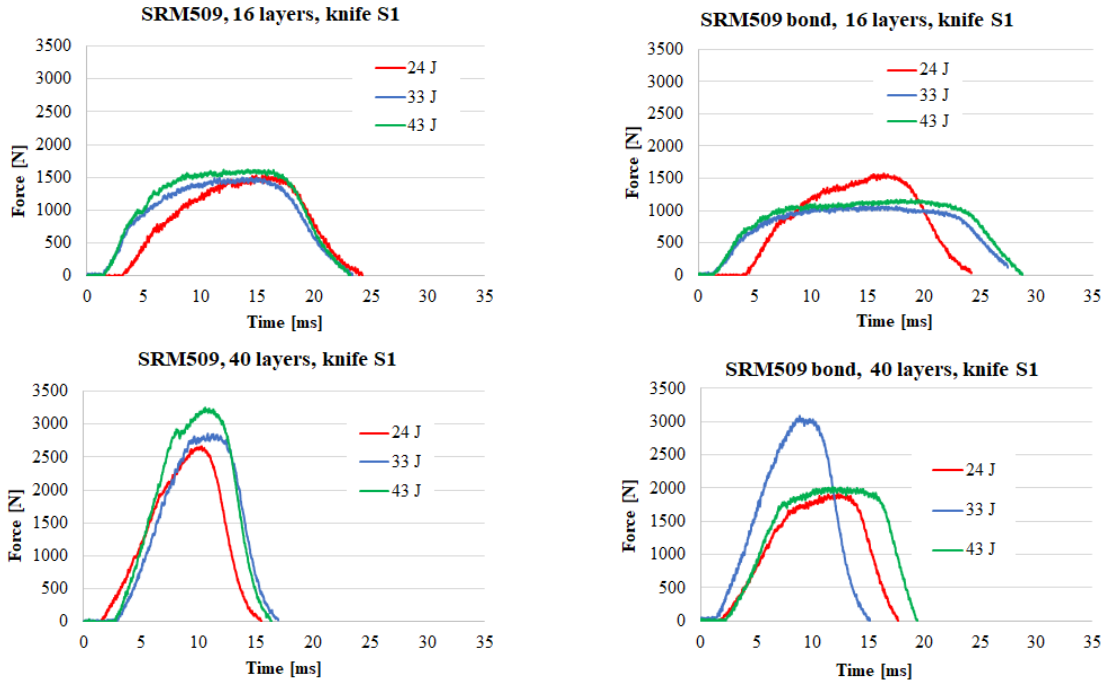

Fig. 5.10. Influence of impact energy on the force-time curve for the two types of panels

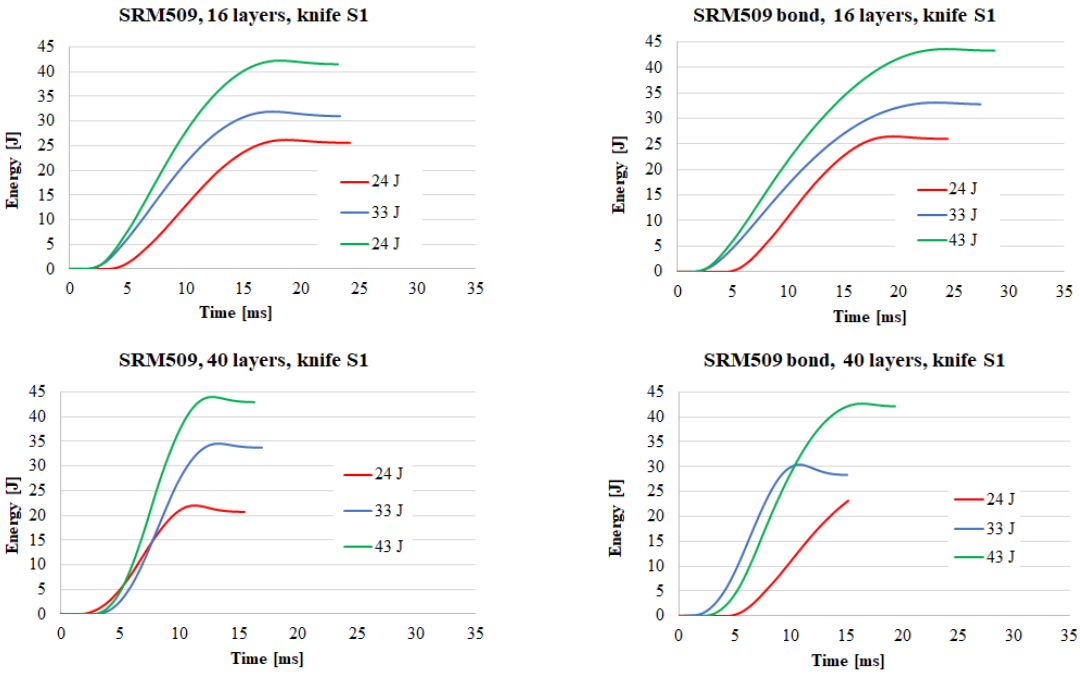

a) SRM509 b) SRM 509 bonded

Fig. 5.11 Absorbed energy – time curves

The maximum force increases substantially with increasing number of layers, from 1500 N to 16 layers, this maximum being characteristic of all impact energy levels, at 3200 N for 40 layers, at maximum energy of 43 J.

With increasing number of layers, F_{max} has distinct values, proportional to the impact energy.

The force curve, characteristic of 16-layer panels, changes in the sense of creating an increasing slope or shortening the duration.

The starting slopes (stage I) differ more for thinner panels (16 layers).

Analysis of the absorbed energy - time plots reveals a higher absorption rate, the higher the impact energy, as shown in Fig. 5.11.

5.3.1.4 Influence of the Number of Layers in the Panel, in spike Tests, on the Force, Velocity and Energy Curves as a Function of Time

The influence of this parameter is discussed on groups of graphs: force - time, energy - time, velocity - time.

The influence of the number of layers on the force-time curve of the spike impact is shown in Fig. 5.12, for each tested energy level. For bonded and unbonded SRM509 panels, the maximum force increases with increasing number of layers. The duration of the striking process decreases with increasing number of layers.

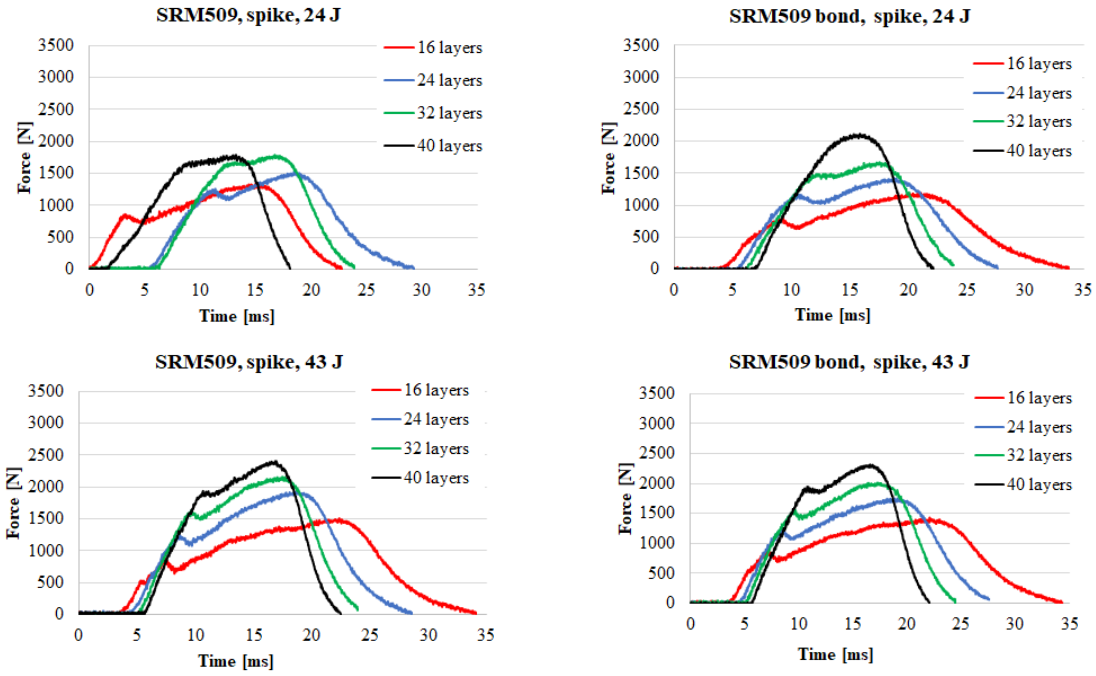

a) b)

Fig. 5. 12. Force-time diagrams, as a function of the number of layers, for a) SRM509, b) bonded SRM509

Figure 5.13 shows panels of SRM509 layers, after spike tests, at an energy of 24 J (top - front of panel, bottom - back of panel). The shape and dimensions of the hole formed by the spike are not much different, the biggest difference being observed on the back of the last panel.

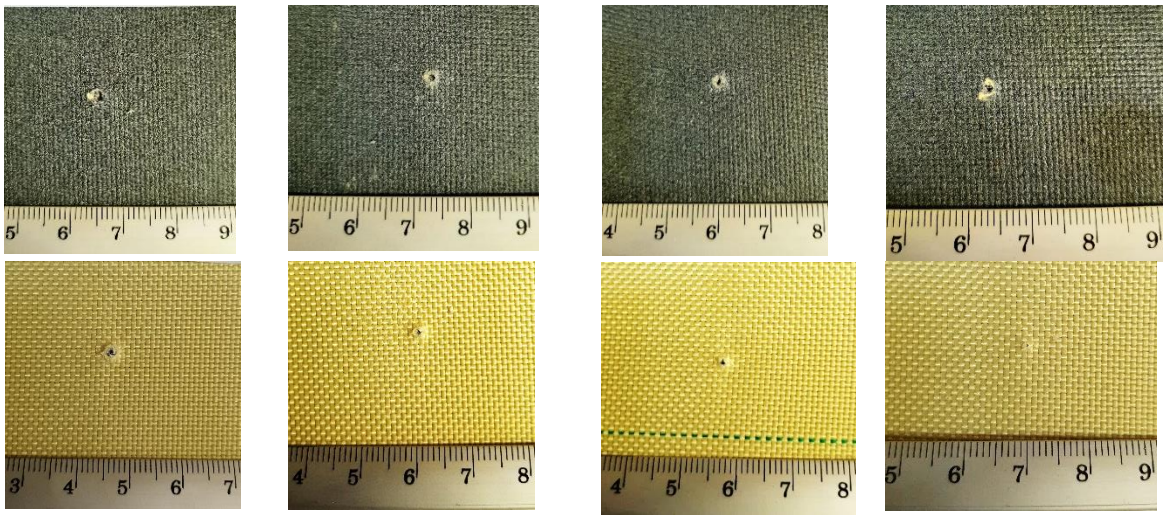

16 layers 24 layers 32 layers 40 layers

Fig. 5.13. Layered panels made of SRM509, after spike tests, at 24 J impact energy (top - front of panel, bottom - back of panel)

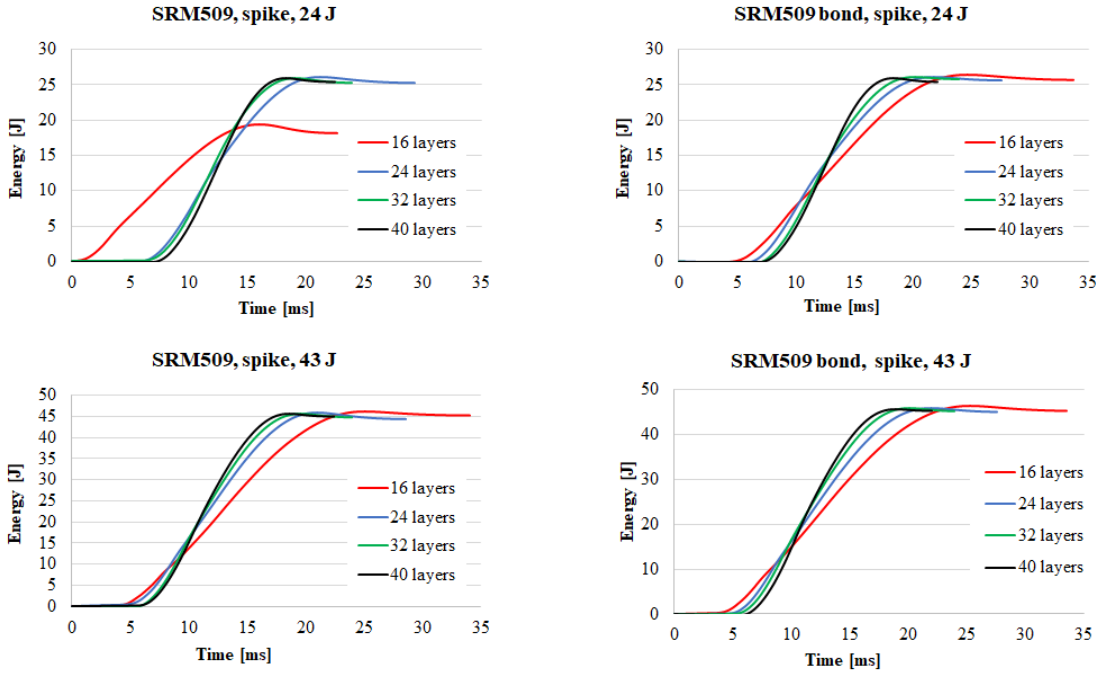

a) non-bonded SRM509 b) bonded SRM509

Fig. 5.14. Influence of the number of layers on energy-time curve for two impact energies

For tests performed at 43 J, the slopes increase with increasing number of layers, the difference is more pronounced for unbonded SRM509 panels. At these impact energy levels, for the panels with the same number of layers, the hierarchy of curves is not different for plainly formed panels as compared to panels made of bonded layers. In Fig. 5.14, the influence of the number of layers on the energy-time curve for all impact energies is shown graphically.

5.3.2. Influence of Impact Energy for Spike Tests

The influence of impact energy on the force-time curve for 16-layer, 24-layer, 32-layer, 40-layer spiked panels is shown in Fig. 5.15. The slopes of the thinner 16-layer panels differ more from the 24-layer, 32-layer and 40-layer panels.

Analysis of the absorbed energy - time graphs reveals a higher absorption rate, the higher the impact energy. The slopes of the curves increase with increasing impact energy.

The slope is smaller for tests at 24 J energy. The other two slopes, that of 33 J and that of 43 J are closer together.

Analysis of the absorbed energy - time plots reveals a higher absorption rate, the higher the impact energy, as shown in Fig. 5.16.

The influence of the number of layers of SRM509 panels, spiked at an impact energy of 43 J (top - front of the panel, bottom - back of the panel), are represented by the photographs in Fig. 5.16. Panels with bonded SRM509 layers are shown photographically in Fig. 5.17.

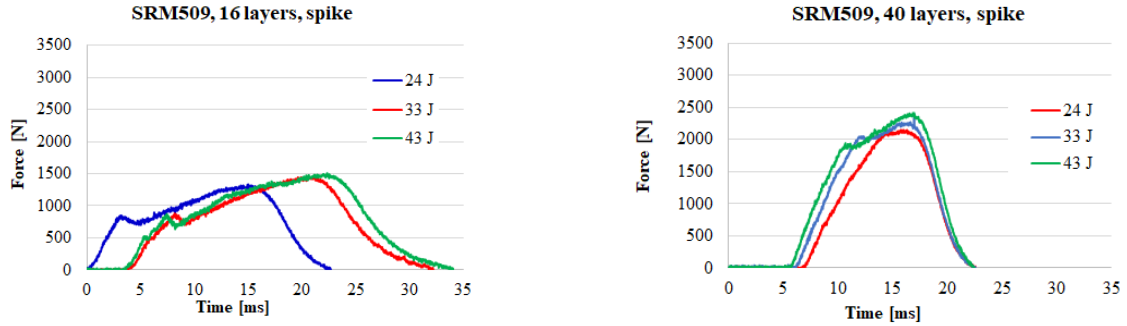

Fig. 5.29. Influence of impact energy on the force-time curve, for 16-layer, 24-layer, 32-layer, 40-layer spiked panels

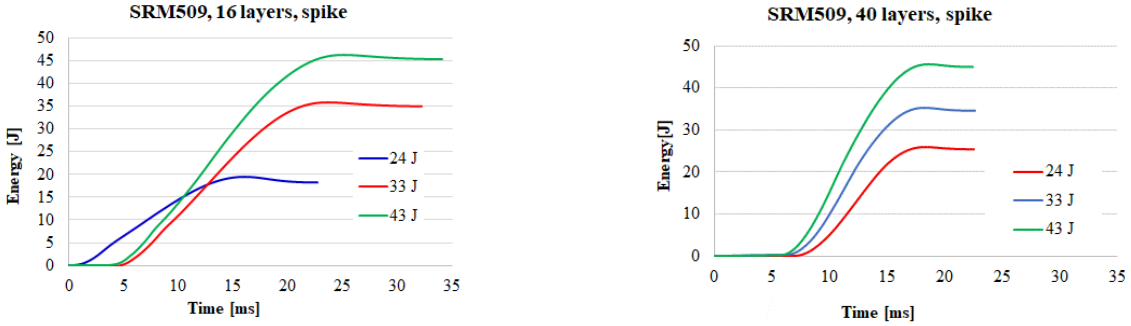

Fig. 5.16. Absorbed energy analysis - time

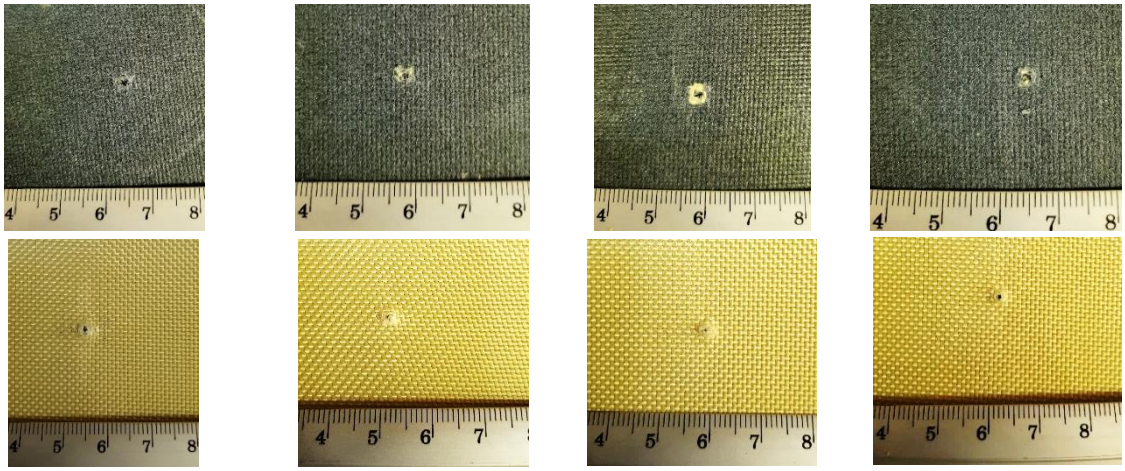

Fig. 5.17. Layered panels made of SRM509, spiked at an impact energy of 43 J (top - front of panel, bottom - back of panel)

5.4. Influence of the Weapon on the Force-Time, Energy-Time and Curves

The following graphs (Figures 5.18-5.21) show, in the left column, information on the S-knife strike and in the right column information on the spike strike, the other parameters (material, striking energy) being kept constant.

- Figure 5.18 shows force-time plots, as a function of the number of layers, for SRM509, at different energy levels (24 J and 43 J), on the left side, the weapon used is the knife and, on the right side, the weapon used for impact is the spike.

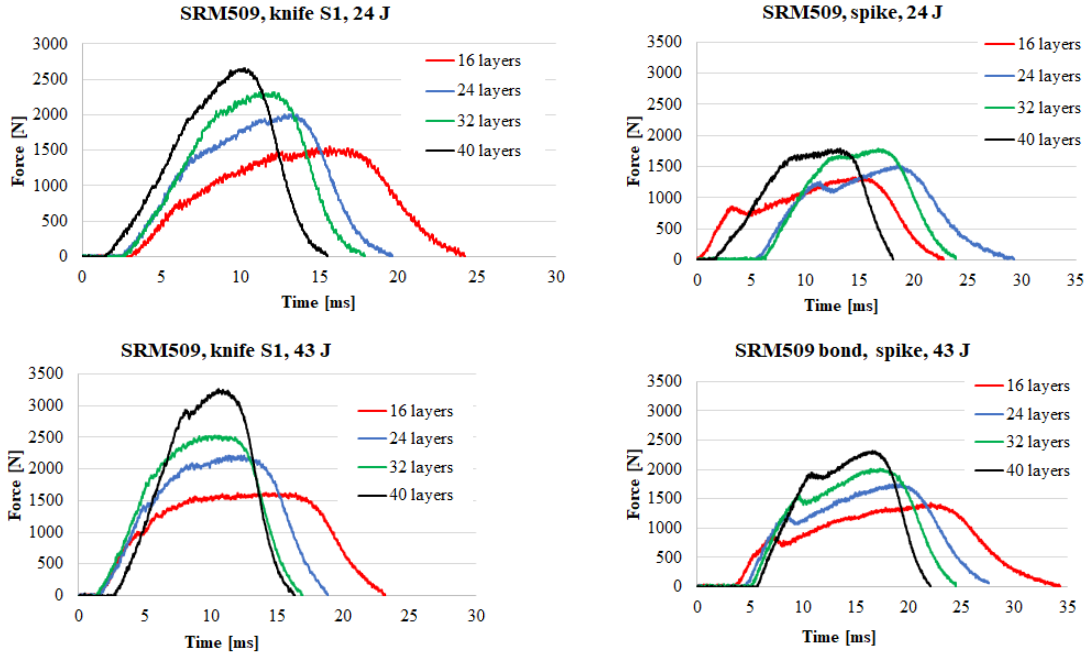

Fig. 5.18 Force-time diagrams as a function of the number of layers for SRM509, at different energy levels (24 J and 43J), left – knife S1, right - spike

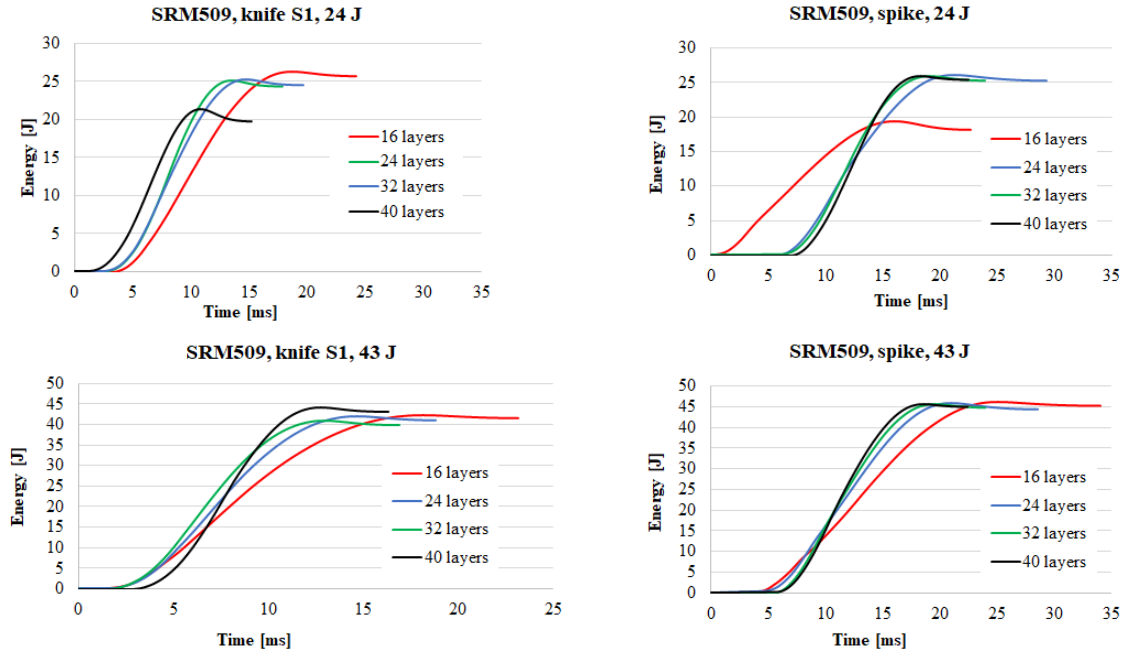

Fig. 5.19. Influence of the number of layers on the energy-time curve, for impact energy of 24 J, 33 J,43 J, on the left the threat is S1 knife and on the right – the spike

On the range of layers tested at this energy level, the following observations can be made:

- the maximum measured force, F_{max} , increases with increasing number of layers,
- curves have a high degree of irregularity,

the duration of the striking process decreases with increasing number of layers.Influence of the number of layers on the energy-time curve, for impact energy of 24 J and 43 J; on the right the threat is knife S1 and on the left spike is given in Fig. 5.19.

There was noticed the following:

- the slopes of the curves are different for both threats,
- 16-layer panels have more different curve slopes than 24-layer panels,
- for 32-layer and 40-layer panels, the slopes of the curves are less different.

The slopes of the velocity plots increase with increasing number of layers, with the difference being larger between 16-layer and 24-layer panels.

In Fig. 5.20, a comparison of the force-time graphs for the same material, bonded SRM509, for the two white weapons tested, knife S1 (left column) and spike (right column), is shown.

The large difference in the positioning of the force-time curves is particularly noticeable in the 32-layer and 40-layer bonded SRM 509 panels, for knife tests. Panels that were tested with a spike have a smaller difference in force-time curve positioning.

On the range of layers tested at this energy level, the following observations can be made:

- impact duration decreases with increasing number of layers,
- the maximum force increases substantially with increasing number of layers, from 1500 N for 16 layers, this maximum being characteristic of all impact energy levels at 3000 N, for 40 layers at 33 J energy.

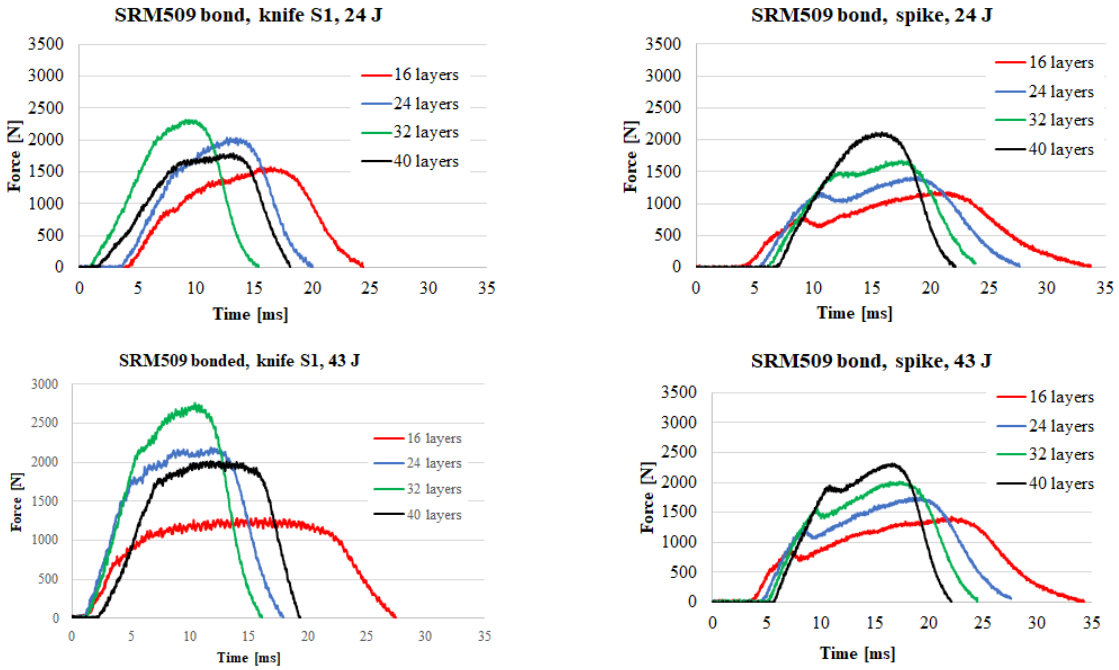

Fig. 5.20. Comparison of force-time graphs for the same material, SRM509 bonded, for the two white weapons tested, S1 knife (left column) and spike (right column)

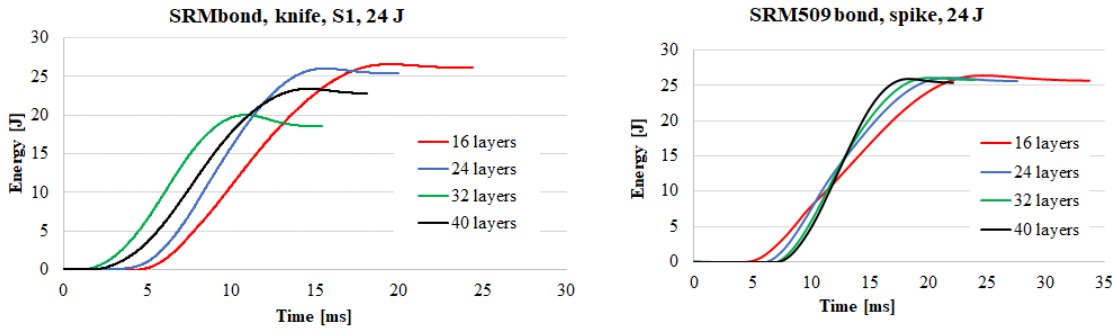

Fig. 5.21. Comparison of energy-time plots for the same material, SRM509 bonded, for the two white weapons tested, knife S1 (left column) and spike (right column)

Analysis of the absorbed energy - time graphs reveals a higher absorption rate, the higher the impact energy. The slopes of the curves increase with increasing impact energy. In Fig. 5.21 there is a comparison of the energy - time plots for the same material, SRM509 bonded, for the two white weapons tested, knife S1 (left column) and spike (right column).

5.5. Evaluation of Hybrid Panels

This sub-chapter presents results and discussion of hybrid panels and their comparison with two aramid fabrics to determine their stab resistance. SRM509 and CT736CMP sheets, were arranged in a combination of them (10 layers SRM509 and 10 layers CT736CMP). 130 mm x 130 mm and 150 mm x 150 mm samples were cut from the fabrics, weighed and measured for thickness. Tests were performed for an impact energy of 24 J (3 m/s). The blade had the geometry recommended in [NIJ Standard-0115.00] as S1 blade.

Table 5.1 shows the tested panels with some characteristics. The SRM509 fabric sheets were laid out successively with the coated surface facing the threat (blade).

Table 5.1. Characteristics of the panels tested for hybrid system highlighting

Material	**Layers**	**Thickness [mm]**	**Mass [g]**	**Areal density [kg/m^2]**	**ΔE [J]**
Twaron CT736CMP (150 mm x 150 mm) (130 mm x 130 mm)	16 20	8.86 11.12	292 165	7.35 9.76	24 24
Twaron SRM509 (150 mm x 150 mm)	16	6.25	286	7.15	24
(130 mm x 130 mm)	20	7.83	166	9.82	24
Hybrid (20 layers) (130 mm x 130 mm) 10 layers (first) Twaron CT736CMP + 10 layers Twaron SRM509	20	10.00	159	9.42	24

The tests were performed on an Instron CEAST 9340 drop test, instrumented impact system. The panel was clamped tightly with a ring clamp, with a pressure of 5 bar (which is not the case in reality, the straps or the vest cover do not reach this value).

Figure 5.22 shows the results of a hybrid panel made of Twaron SRM 509 (first 10 layers) and Twaron CT 736 CMP (next 10 layers, in order of blade impact).

The impact duration is about half the range of uniform panels, i.e. $25x10^{-3}$ s, the shape of the force curve is more similar to that of the panel made of Twaron SRM 509, but the peak force decreases by 400 N. The gradient of the absorbed energy is almost the same as for fabric-coated panels.

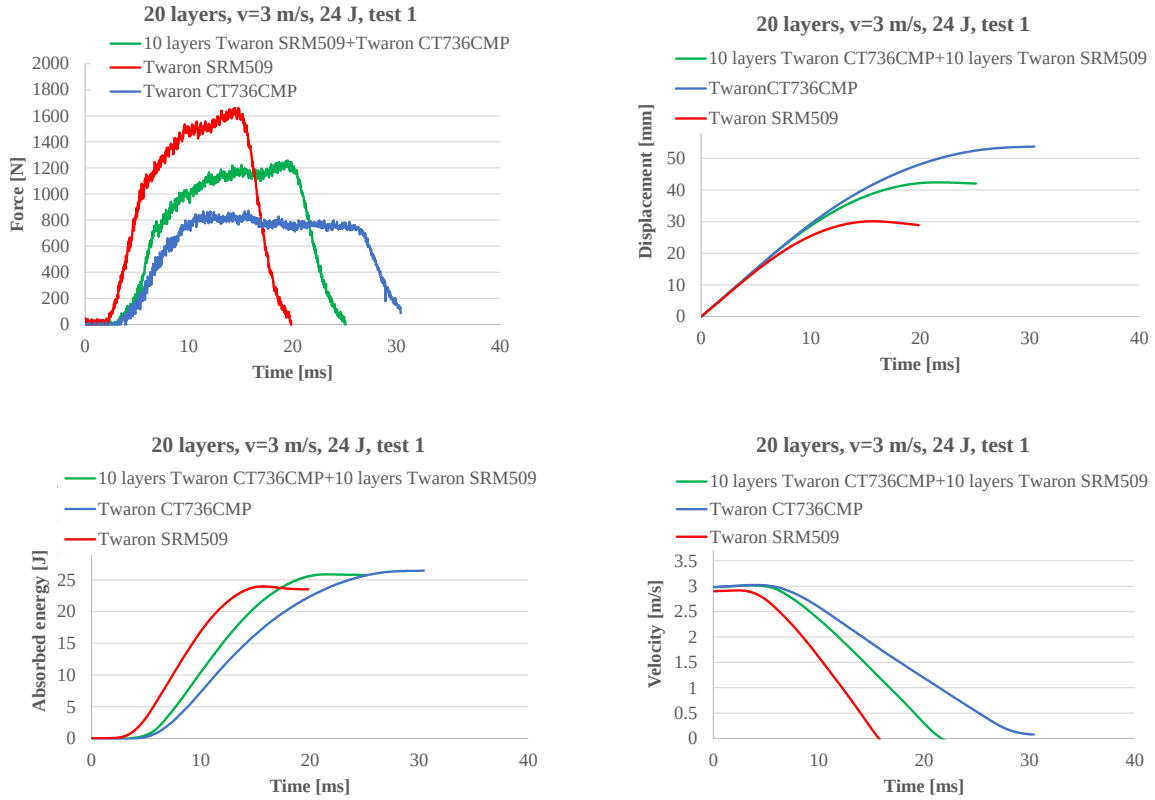

Fig. 5.22. Parameters recorded and calculated for tests with 20-layer panels made of the same fabric and a hybrid panel made of 10 layers of SRM 509 (front) and 10 layers of CT 36 CMP (back).

The conclusion of this analysis is that good stabbing behavior is obtained for panels that have higher gradients over time for all four characteristics discussed here: force, weapon displacement, energy absorbed by the panel, and weapon velocity.

The length of the cut in the hybrid panel also has an intermediate length, a value between panels with layers made of a single fabric. Only the hybrid panel is shown here (Fig. 5.23), with details of the cut on the front of the panel and on the back.

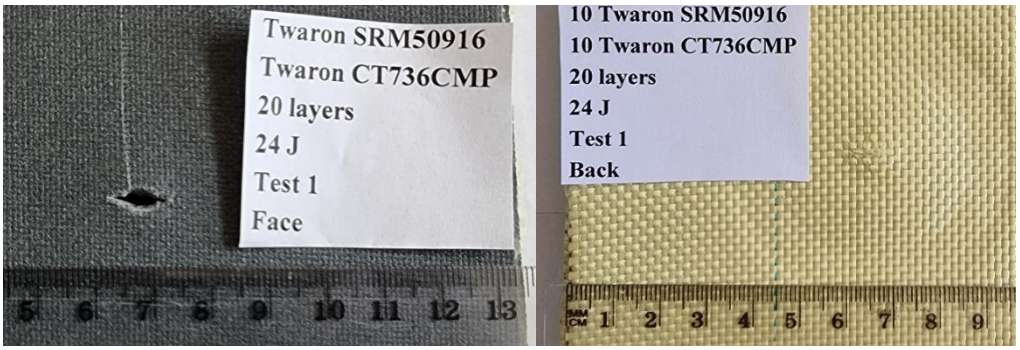

a) b)

Fig. 5.23. Photographs of the hybrid panel (130 mm x 130 mm) with 10 layers of Twaron SRM509 and 10 layers of Twaron CT736 CMP: a) front, b) rear

Even though these tests do not strictly follow standard methods in dealing with threats, the results obtained from tests on a drop test machine indicate that a better response in terms of

stab protection (assessed by the width of the cut for full penetration) will be obtained for panels with a high slope for both absorbed energy and velocity drop during impact and high values of maximum stab force with a ramp shape, not a plateau.

When hybrid panels are used, the results could be intermediate to those of the components, this solution could be recommended for reasons such as weight, the panel presenting the same level of protection.

5.6. Stabbing and puncture damage mechanisms

5.6.1. Introduction

The kinetic energy absorbed by the fabric, $E_{absorbită}$is defined by the following six different components: E_S – yarns shear energy. E_D – deformation energy of all other yarnss. E_T – the energy up to tensile rupture of directly affected yarnss. E_F – energy required to overcome the friction between the fabric layers. E_J – energy required to overcome friction between the blade and the yarns. E_M – energy required to displace the fabric during impact. So, it can be written

$$E_{absorbită} = E_S + E_D + E_T + E_F + E_J + E_M \quad (5.5)$$

In the time after impact, the puncture force value will increase until full penetration and then gradually decrease. To increase the fabric absorption energy, it is expected to evolve each component of the fabric absorption energy, increasing the friction between the blade and the fabric yarnss [Wang L., 2012].

5.6.2 Analysis of stabbing destruction processes

Based on the studied literature and the analysis of macro and SEM photographs taken on the spiked samples, Fig. 5.24 shows synthetically the destruction processes occurring in stabbing with a blade-type weapon. It is worth mentioning that the analysis of the photographs obtained from the tests carried out are for symmetrical blade, type S1 according to [NIJ Standard-0115.00].

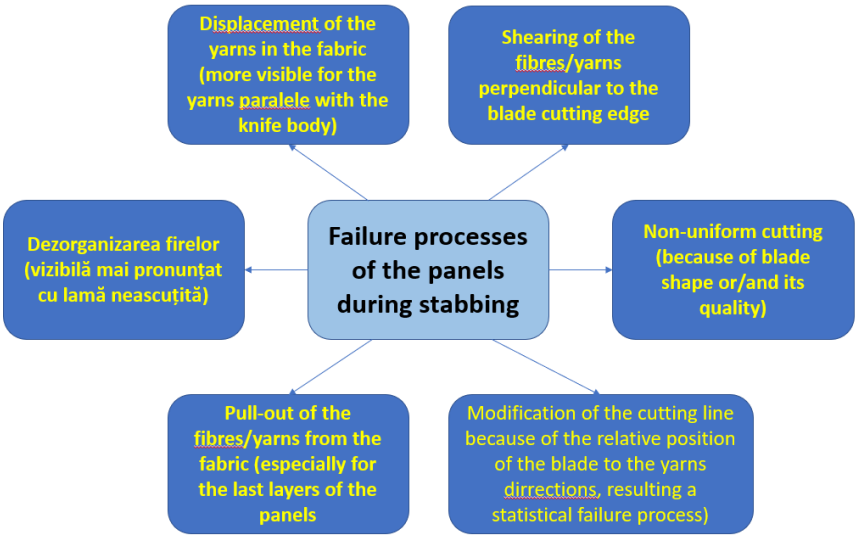

Fig. 5.24. Stabbing destruction processes of panels

5.6.3. Analysis of the S1 knife stab failure mechanisms for the panels made, based on electron microscope scan images

Figure 5.25 shows aspects of the S1 knife cut on layer 1 - face on the 16-layer panel of CT736. The appearance of the cut is still noticeable at low magnifications (x29, see image in a) and b), with details of the wires easily seen at higher magnifications (x100):

a) A - left corner of the cut, B - disorganized yarns during knife penetration and perpendicular yarns cutting, C - polymer film, torn,

b) A - left corner of the cut, B - transition area from the cutting edge of the knife, to the parallelepipedic body of the knife, C - disorganized yarns during knife penetration and perpendicular yarns cutting, D - a few broken fibers from the disorganized yarns (noted with C in this image),

c) A - the polymeric film protecting the fabric, B - part of a cut yarns, with more fibres destroyed by shearing, C - a crack in the film applied to the fabric, D - some broken fibres from the disorganised yarns.

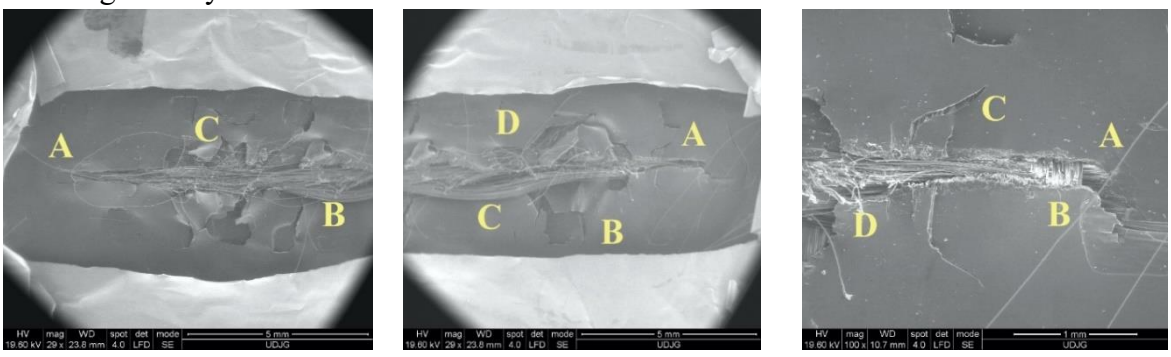

a) b) c)

Fig. 5.25 Aspect of the S1 knife cut on layer 1 of the 16-layer CT736 panel

Figure 5.26 shows details of a broken yarns from the S1 knife cut on the face of layer 1 of the 16-layer CT736 panel at various magnifications to highlight the forms of fibre destruction specific to the sharp edge cutting of the weapon:

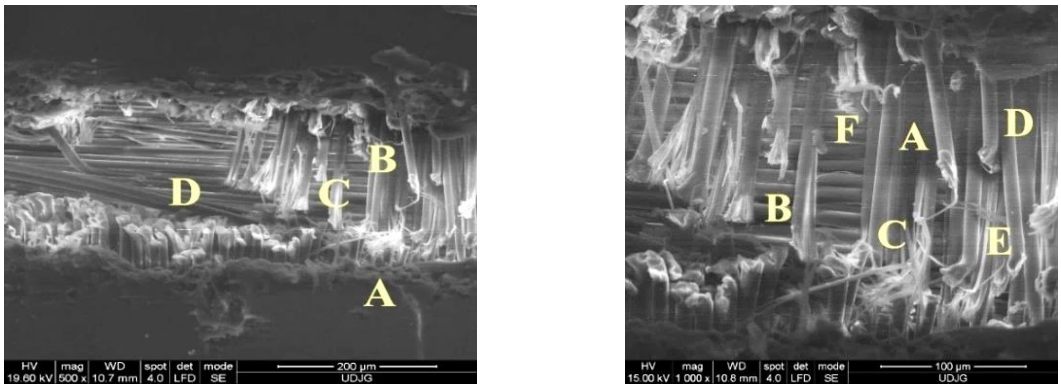

a) b)

Fig. 5.26. SEM images of the S1 knife cut, with an energy of 24 J, on layer 1 - front of the 16-layer CT736 panel.

a) A - aramid fabric protective film, broken, B - fibre broken by a combination of shearing with stretching, C - broken fibres, originally part of D yarn, D - yarn with fibres sheared almost in the same plane,

b) A - fibre broken by a combination of shearing with stretching, B - broken fibre, originally part of the D yarn, C - fibre with fibrillation (cracked along the length of the fibre, D - sheared fibre (of typical shape, obtained when cutting aramid fibre), E - a fibre sheared and with bent end, F - fibre broken and by stretching,

Figure 5.27 shows details of shear-torn fibres from the S1 knife cut, with an energy of 24 J, on the 2 - back layer of the 16-layer CT736 panel: a) disorganisation of the pulling and cutting of the yarns of the fabric, b) end of fibre, predominantly shear-torn, but with detachment of fibrils of different cross-densities, c) fibre torn by stretching

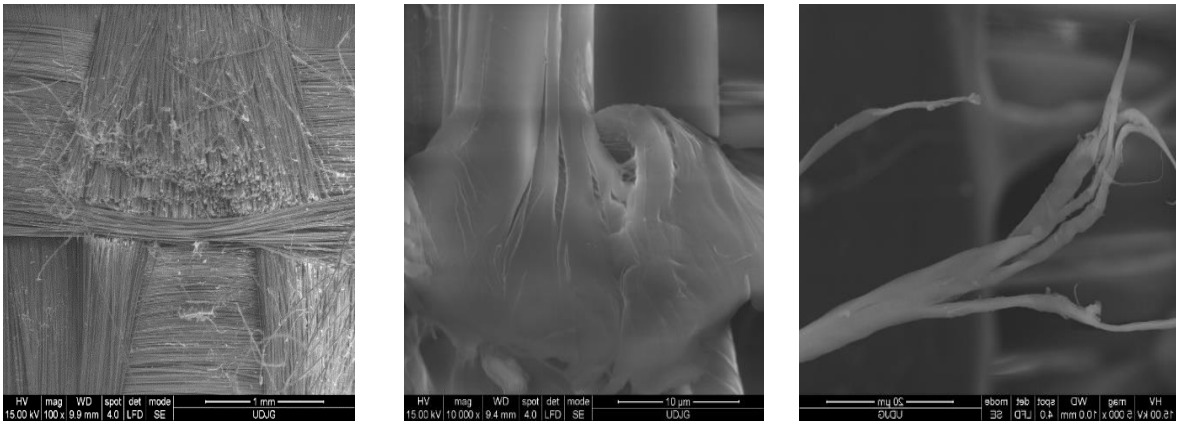

a) b) c)

Fig. 5.27. Details of the shear-broken fibres from the S1 knife cut, with an energy of 24 J, on layer 2 - back of the 16-layer CT736 panel.

Figure 5.28. shows the cut through layer 1 - face, through the 16-layer panel of SRM509, after S1 knife hit with 24 J :

a) a magnification of x30 allowed the precise measurement of the length of the cut, $L_{față}$, on the face of layer 1; the processes that absorbed the impact energy are observed: cutting of the wires, twisting of others and bending, detachment of the coating with abrasive particles

b) detail of image a) at x100 magnification: A - fragment of coating, rotated by knife advance, on which traces of fibres can be seen, B - yarn with stretched, plastically deformed fibres, broken under traction, C - yarn with sheared fibres, D - upper part of the same yarn, displaced by knife advance, E - fragment of coating, F - edge crack of abrasive coating,

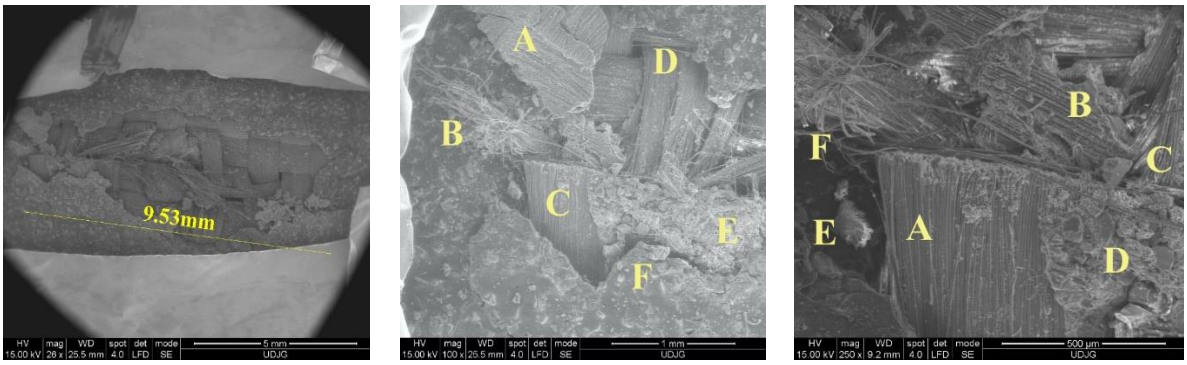

a) b) c)

Fig. 5.28. SEM images of layer 1 - front of the 16-layer panel of SRM509 after S1 stabbing with 24 J

c) a detail of the image in b) for the yarn with fibres sheared almost in the same plane: A - yarn with fibres cut by shearing, the fibres are cut at the same level, B - fragment of the polymeric coating with abrasive, on which traces of the torn yarns can be seen, C - another partially cut yarn, next to the letter is an abrasive particle, partially detached from the coating, D - the abrasive coating, partially detached, E - fragment of the rubber

Figure 5.29 shows details of abrasive particles sheared off at the knife cut with an energy of 24 J on layer 1 - front of the 16-layer panel of SRM 509: a) abrasive particles denoted A1, A2, A3, A4, A5, different from those in the previous image, b) a detail obtained at a magnification of x5000, in which two hard particles can be seen, right at the edge of the cut, so most probably interacted with the knife blade.Brushing, F - a few fibres broken by stretching from a yarn roughly parallel to the cut

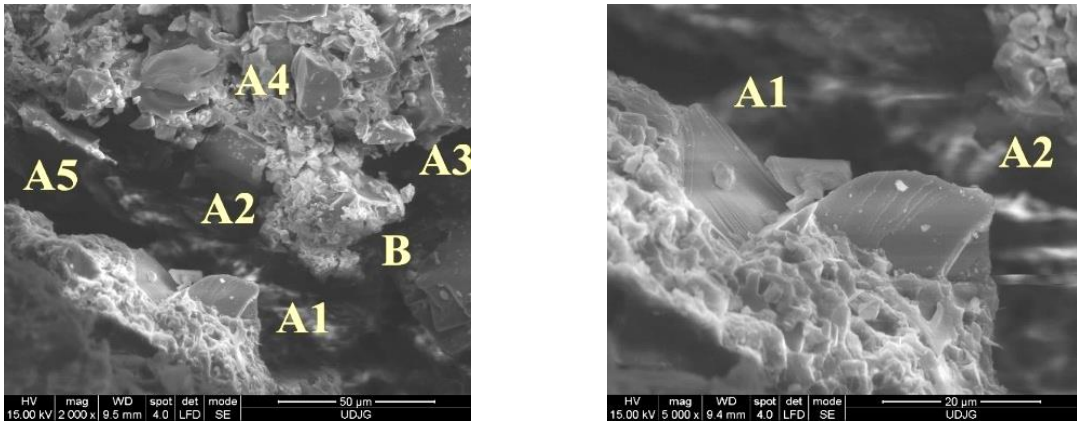

a) c)

Fig. 5.29 Details of abrasive particles sheared off from S1 knife cut, with an energy of 24 J, on layer 1 - front of 16-layer panel of SRM 509

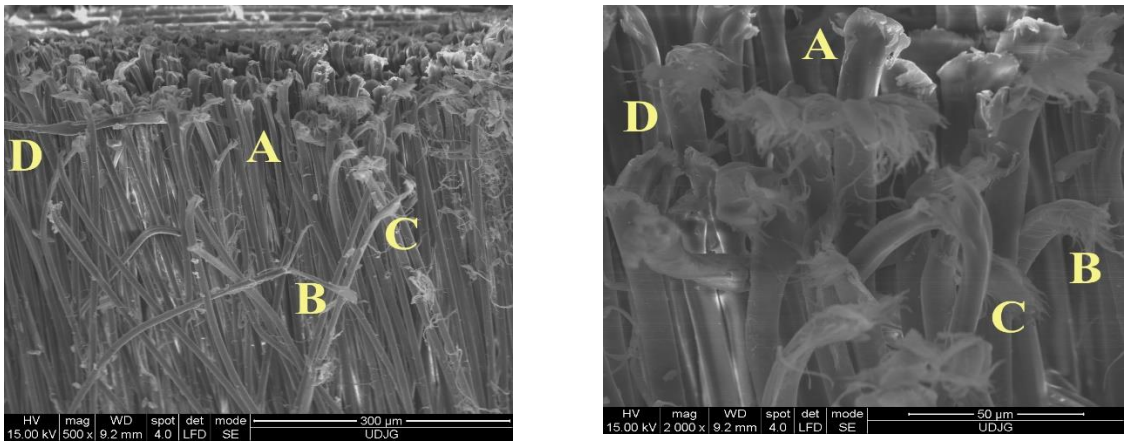

a) b)

Fig. 5.30 Details of shear-broken fibres from the S1 knife cut, with an energy of 24 J, on layer 1 - back of the 16-layer panel of SRM 509

Figure 5.30 shows details of the shear-broken fibres from the S1 knife cut, with an energy of 24 J, on the 1-back layer of the 16-layer panel of SRM 509 :

a) A - sheared fibers, B - fibrillated fiber at the end, fibrils are broken by stretching, C - fiber broken by stretching and shearing, with throttled areas, indicating differences in the degree

of crystallinity and/or micro defects in the fibrils, D - sheared but blade driven fiber, with a flattened area,

b) A - the fiber has been sheared, forming a "nail flower", typical of aramid fibers, B - C-bending the fiber and severed, the cut end of the fiber is like the opening of a flower.

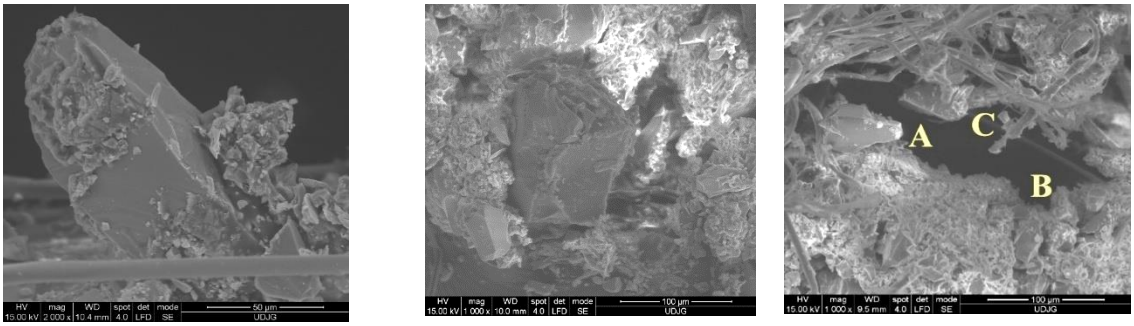

a) b) c)

Fig. 5.31 SEM details of abrasive particles broken by knife cut shear at an energy of 24 J on layer 2 - front of 16-layer panel of SRM 509

Figure 5.31. Shows details of abrasive particles broken by knife cut shear at an energy of 24 J on layer 2 - face of the 16-layer panel of SRM 509

a) and b) the particles are observed with different sizes and shapes, but the particles have sharp edges, which can scratch the knife blade, consuming more of the impact energy through friction compared to the uncoated fabric panel,

c) a detail at a magnification of x5000, with hard, fibrous particles, A -B sheared at stretching by yielding part of the particle, C - sheared at stretching forming a flattened area.

5.6.4. Analysis of puncture damage processes

Based on the studied documentation, but also based on the study carried out at the micro level, using the scanning electron microscope, we realigned the diagram in Fig. 5.65, which suggestively shows the destruction processes of panels made of woven and non-woven fibres/fire.

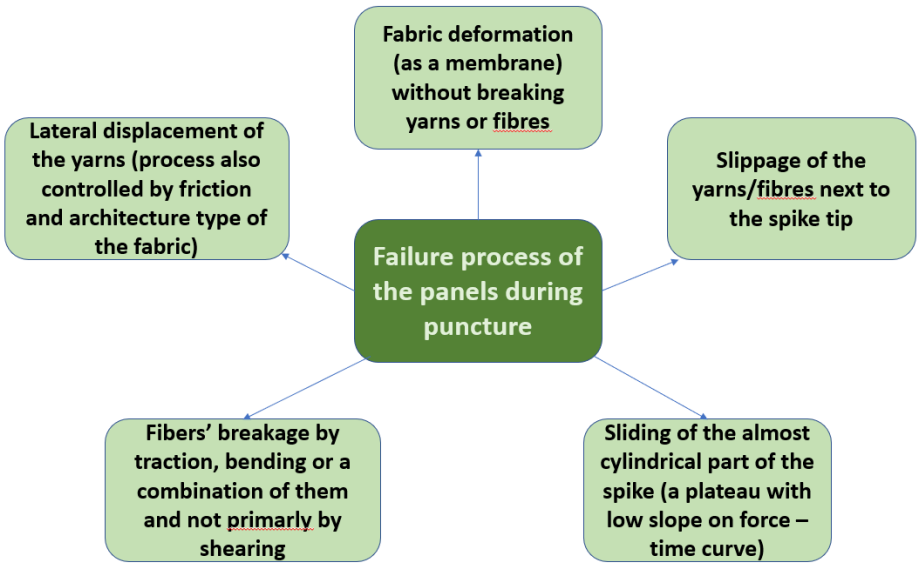

Fig. 5.32. Fabric destruction processes on puncture

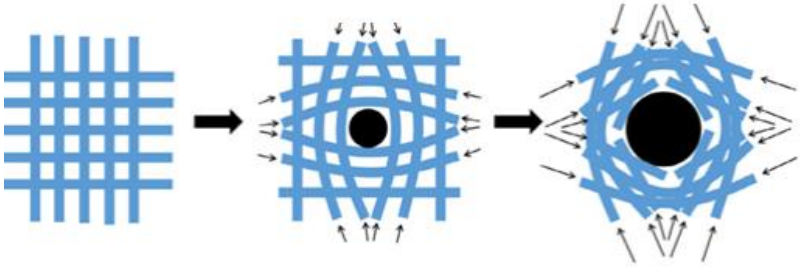

a) b) c)

Fig. 5.33. Schematic penetration diagram for the damage mechanism
a) the fabric b) the force pushes the yarns apart c) the destruction of the fabric [???; ????]

Figure 5.33 shows the failure mechanism of yarn and fabric during quasi-static needling. When the penetration depth of the weapon increased, the yarns near the tip bent, twisted, and the contact pressure and holding force on the yarns increased dramatically. As can be seen in Fig. 5.50c), the wires in the centre break, and the surrounding wires bend noticeably, with some wires being pulled together. The friction between the weave and the fibres had a remarkable effect on the stab resistance property of the fabrics. The contact pressure and friction of the weapon with the fibres had the main function of preventing the penetration process, and eventually a hole (an orifice) remained in the fabric [????].

5.6.5. Analysis of yarn and fibre failure processes under spike impact using SEM images for SRM509 fabric panels

Figure 5.34 is an example of witness paper destruction, from which it follows that this method of assessing panel destruction is not valid for spiking. The images were taken at different magnifications: a) x50, b) x100 and c) x800.

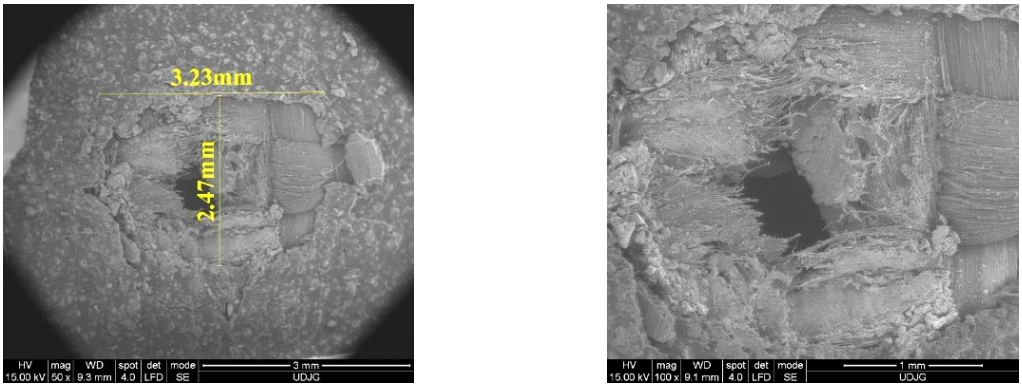

a) b)

Fig. 5.34. a) and b) Aspects of the resulting hole on the face of layer 1 when spiked with 24 J energy for a 16-layer panel of SRM509;

In Fig. 5.34, a) and b), aspects of the resulting hole on the face of layer 1 are shown, when spiked with an energy of 24 J for a 16-layer panel of SRM509.

Figure 5.35 shows SEM images of the penetration orifice of the spike in a 16-layer panel of SRM509 (the view of the entire orifice is given in Fig. 5.34): a) edge from which the different fiber failure mechanism is observed, one by shear others by stretching, on the right side the

breaking mode of the layer with abrasive particles is observed, b) a magnification x1000 shows different fiber breaking modes: A - fiber broken by shearing, B - fiber broken by pulling/stretching in an area where most likely there was a defect on the fiber, C - fiber deformed locally by stretching (to the right of the indicator letter) and D - end broken by shearing with some excessively elongated fibrils, E - breaking by stretching, F - area of fiber deformed by twisting and thinning and breaking by stretching, c) a detail at x2000 magnification of fiber F.

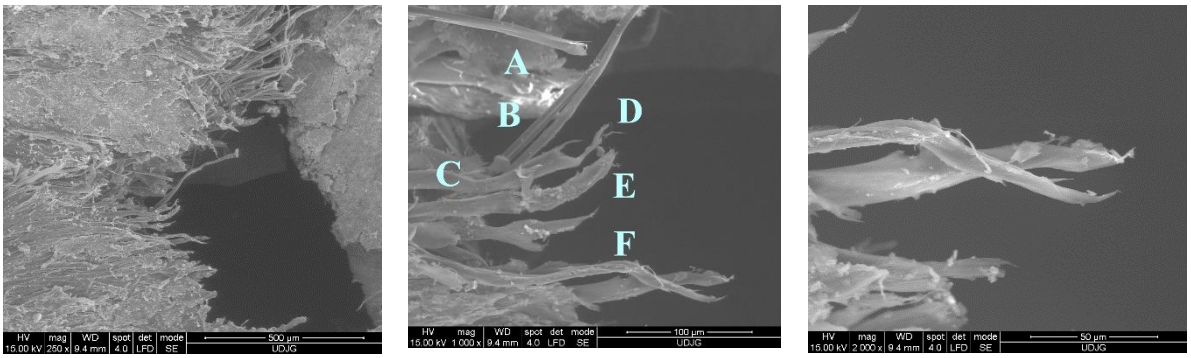

a) b) c)

Fig. 5.35. SEM images of the edge of the penetration hole in a 16-layer panel of SRM509, spiked with an energy of 24 J

Figure 5.36 shows an abrasive particle remaining in the polymer matrix, located just at the edge of the penetration hole on layer 1: a)A1 abrasive particle shattered A2 abrasive particle broken A3 abrasive particle area unaffected, b) the particles are observed with different sizes and shapes, but the particles have sharp edges, which can scratch the knife blade, consuming more of the impact energy by friction compared to the uncoated fabric panel , c) a detail at x2000 magnification of an abrasive particle.

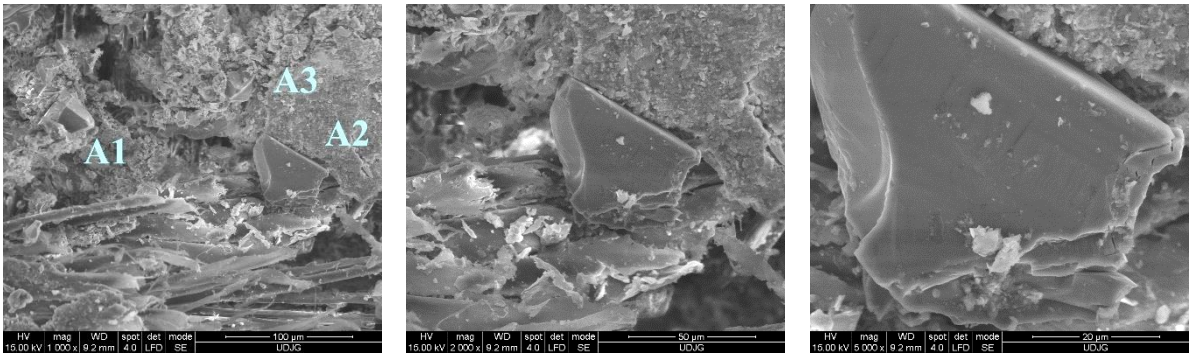

a) b) c)

Fig. 5.36. SEM images of an abrasive particle, broken due to spike action. Imprints on layer 1 of the 16-layer panel of SRM509

Figure 5.37 shows SEM images of fibers, back, broken on stretching due to spike action on layer 1 of the 16-layer panel of SRM509 layer 1, back, 24 J as follows: a) fibers cut by stretching, after being released from the threat the fibers separated chaotically not having a knife-like yarn cut shape, b) and c) fibers broken and splintered, split in particle length, on stretching.

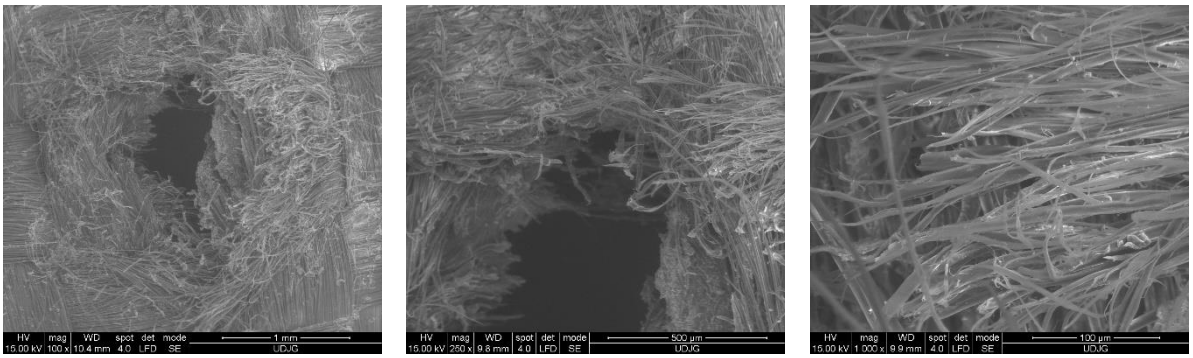

a) b) c)

Fig. 5.37 SEM images of the fibres, back, broken on stretching due to spike action. Images of SRM509 16-layer panel layer 1, back, 24 J

Figure 5.38 shows the appearance of the hole obtained on the face of the last layer (layer 16), when a 16-layer panel is spiked with 24 J at different magnifications: a) x50, b) x100 and c) x250. It can be seen that the composite layer (resin + abrasive particles) is damaged, either by crushing, shearing or/and due to stress differences between the wires and this layer.

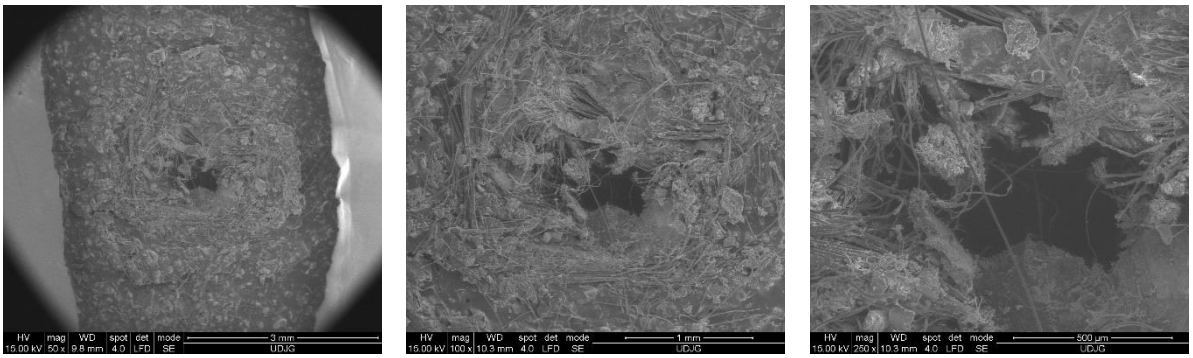

Fig. 5.38. The appearance of the hole obtained on the face of the last layer (layer 16), when a 16-layer panel is spiked, with an energy of 24 J

5.7. Summary of experimental results, obtained on the Instron 9340 drop-test machine

5.7.1. Summary of results obtained in S1 knife tests

Figure 5.39 summarizes the average values of the maximum force recorded for the S1 knife tests as a function of the number of layers and the impact energy. $_{max}$Figure 5.39 shows graphically, as a function of number of plies and impact energy, the average force values calculated for three identical tests, F , for panels made of plies of SRM509 fabric and plies of the same fabric but bonded with adhesive. The dependence has a linear increasing trend from the 16-layer panel to the 40-layer panel for both panel variants.

The impact duration increases with increasing number of layers, with a linear increase. Larger differences are between SRM509 and SRM509 glued . The bonded materials responded differently, due to the bonding factors, between the layers there was not an equally weighted homogeneous solution due to manual spraying of the bonding substance. Some bonded SRM 509 packages came out stiffer and the impact energy was also taken up by this composite

forcing to disperse the packages (bonded). The impact influence on the material decreases with increasing number of layers, having a linear decrease. Fig. 5.40 shows the influence of material on $h_{calculated}$, for tests of 24 J, 33J respectively 43 J.

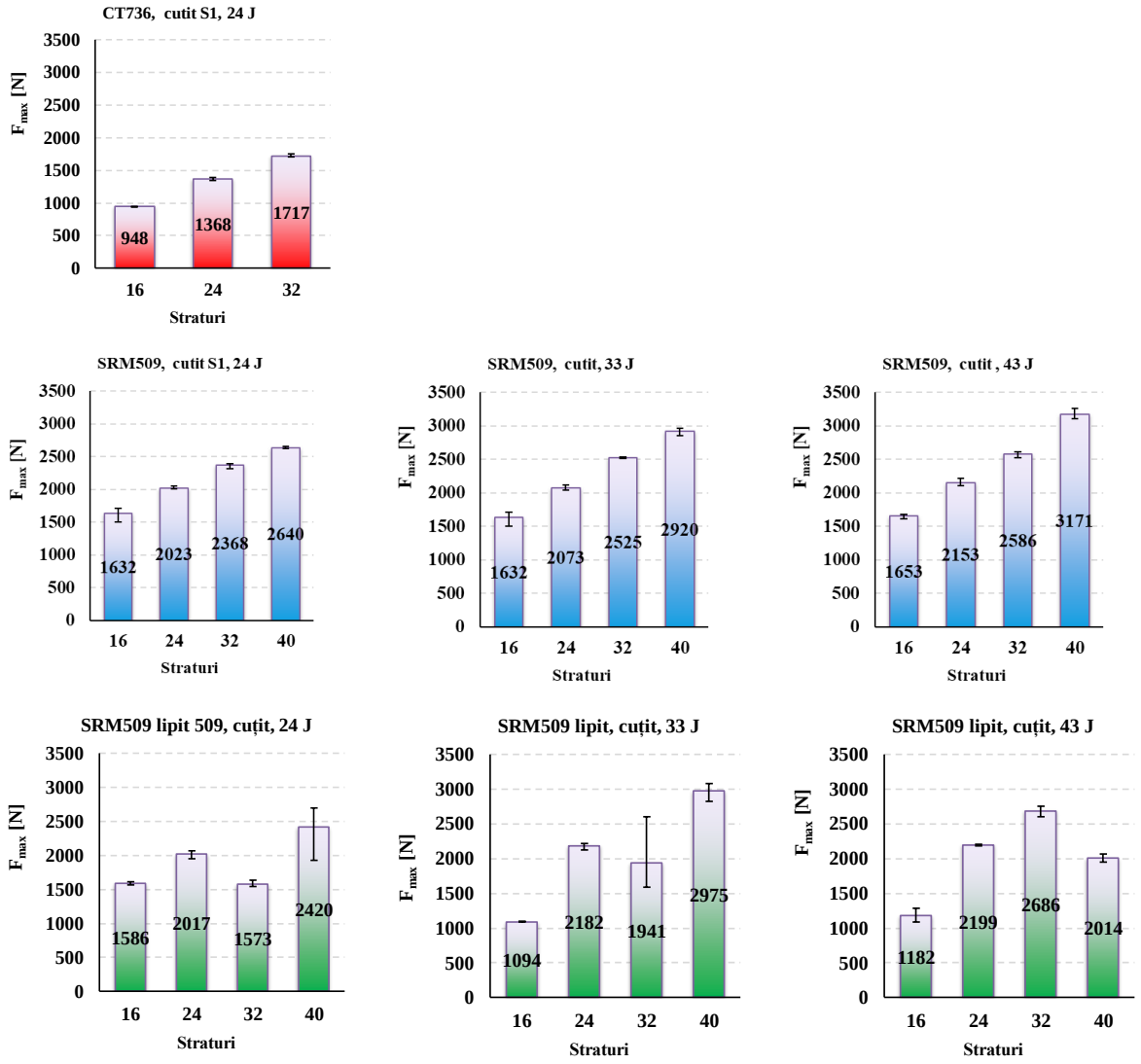

Fig. 5.39. Mean value of the maximum measured force, Fmax, for knife tests S1

5.7. 2. Conclusions drawn for tests performed on the Instron 9340 drop-test machine

Tests carried out on the Instron 9340 drop-test machine allowed the strength of the panels to be analysed on different criteria:

- number of layers of fabric,
- knife penetration depth S1, $h_{calculated}$, for knife tests only, for the spike, this parameter not being relevant due to the cylindrical shape of the spike,
- F_{max} the dependence of parameters such as , the duration of the striking process, t_f , on the panel material, the number of layers in the panel, the striking energy and the shape of the white weapon.
- This analysis shows which material resists better to these destruction processes, but the experimental data only gives a hierarchy of the materials tested, not recommendations on the thickness of the personal protection panels because the samples are relatively

small in area and their grip differs from the grip on the vest wearer, but this hierarchy of material quality is not as costly when testing large area samples as required by the standards [NIJ Standard-0115.00 - Stab Resistance of Personal Protective Vests].

-

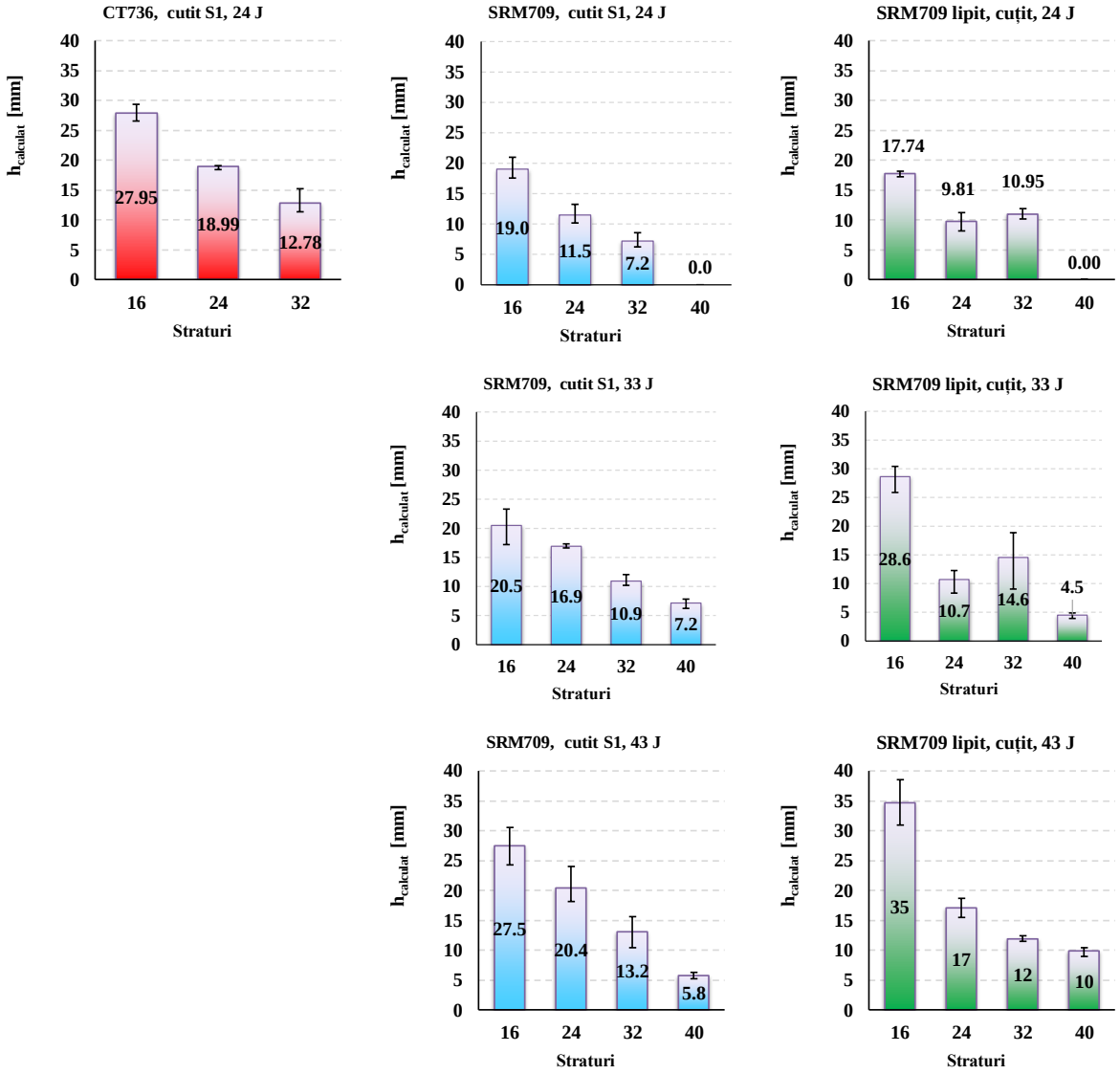

Fig. 5.40. Influence of material on $h_{calculated}$, for 24 J, 33 J and 43 J tests (with S1 knife)

Better results were obtained for uninsulated SRM509 panels. The bonded panels behaved more unpredictably and with higher values for hcalculated, although for some tests (24 J, 16 layers and 24 layers) the values were lower than for the unbonded panels. It is likely that the technology is qualitatively applied to all tests : curing time, uniformity of adhesive coatings, etc.) (Fig. 5.41). In pluys it is added that the panel becomes stiffer, which vastly reduces the movements of the wearer.

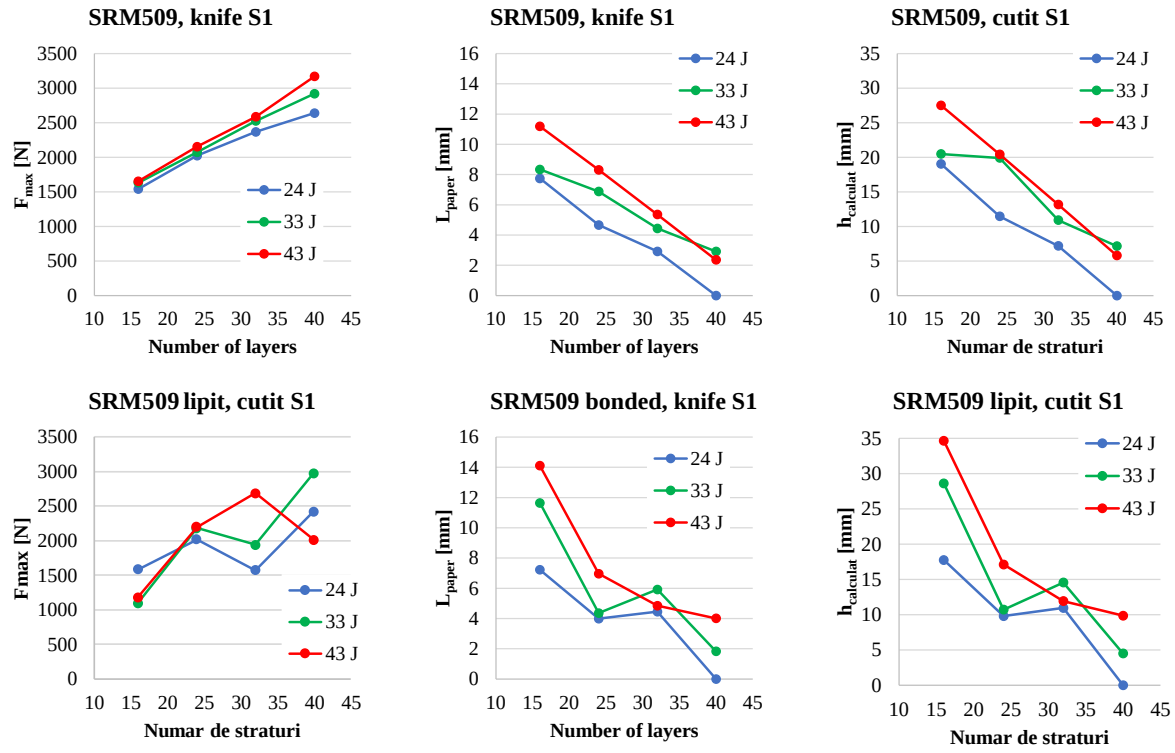

a) b) c)

Fig. 5.41. Summary of experimental results for S1 knife tests for a) SRM509 panels, b) SRM509 panels with adhesive bonded layers.

In Fig. 5.42, the plot is of the impact duration for knife tests, and in Fig. 5.43 the impact duration for spike tests.

Comparing the graphs we can see:

- for each material, increasing the number of layers decreases the calculated parameter $_{h}$,
- At 16 layers, the panel in SRM 509 only laterally bound had this parameter, the lowest for impact energies of 33 J and 43 J,
- of the three panel variants, the lowest values for the same number of layers was obtained for SRMbond 509, but for 32 layers the $_{hcalculated}$ was the same for SRM 509 and SRMbond 509; for these panels it is recommended to repeat the test,
- $_{spate}$for the 40-layer SRMbond 509 panel, on the last layer, Lcalculated=L $_{=Lharsity=0}$, for all three tests.
- The lowest values are obtained for panels glued with adhesive. Further, running the panels to the dimensions for testing them as vest components will also need to establish whether the resulting panels are flexible enough to be worn.
- The quality of the materials used can be seen from the very small ranges of variation for thickness and mass for all the panels tested.

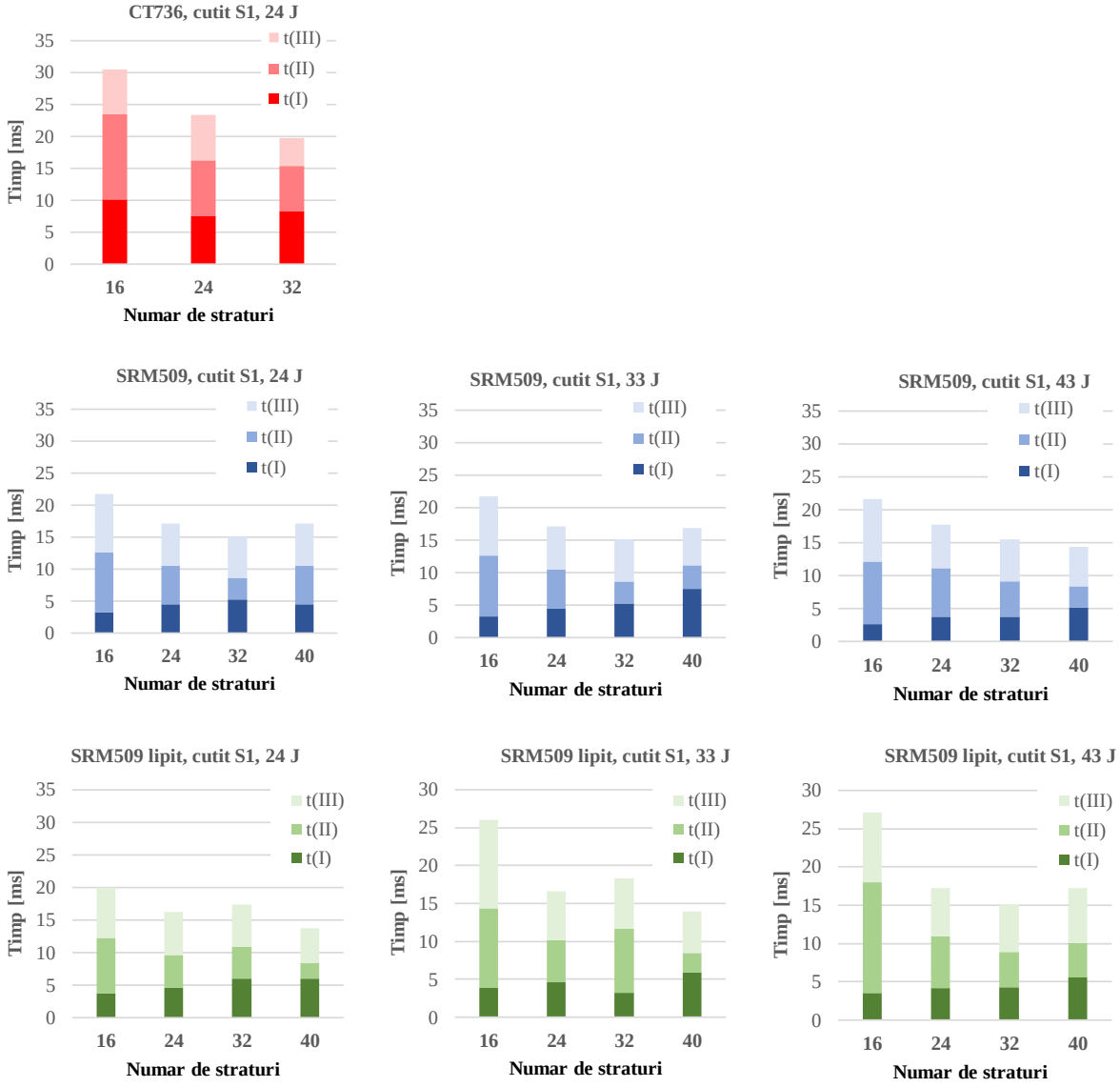

Fig. 5.42. Impact duration for knife tests, represented as the sum of the three stages of the impact process

The following is noted:

- The lowest values were obtained for the bonded SRM 509 fabric panels, but the difference from the SRM 509 panels is very small and the bonded panel set does not behave as uniformly as the unbonded panels.
- The highest values were obtained for panels in TC 736.

Figure 5.42 shows the maximum force (average values for 3 tests) for SRM509 and bonded SRM509 panels. At the same values of the test parameters, the difference between the materials is small, about 10% at most, with lower values for the bonded SRM509 panels. $_{max}$The increasing trend of F seems linear, at least for the range of layer numbers tested.

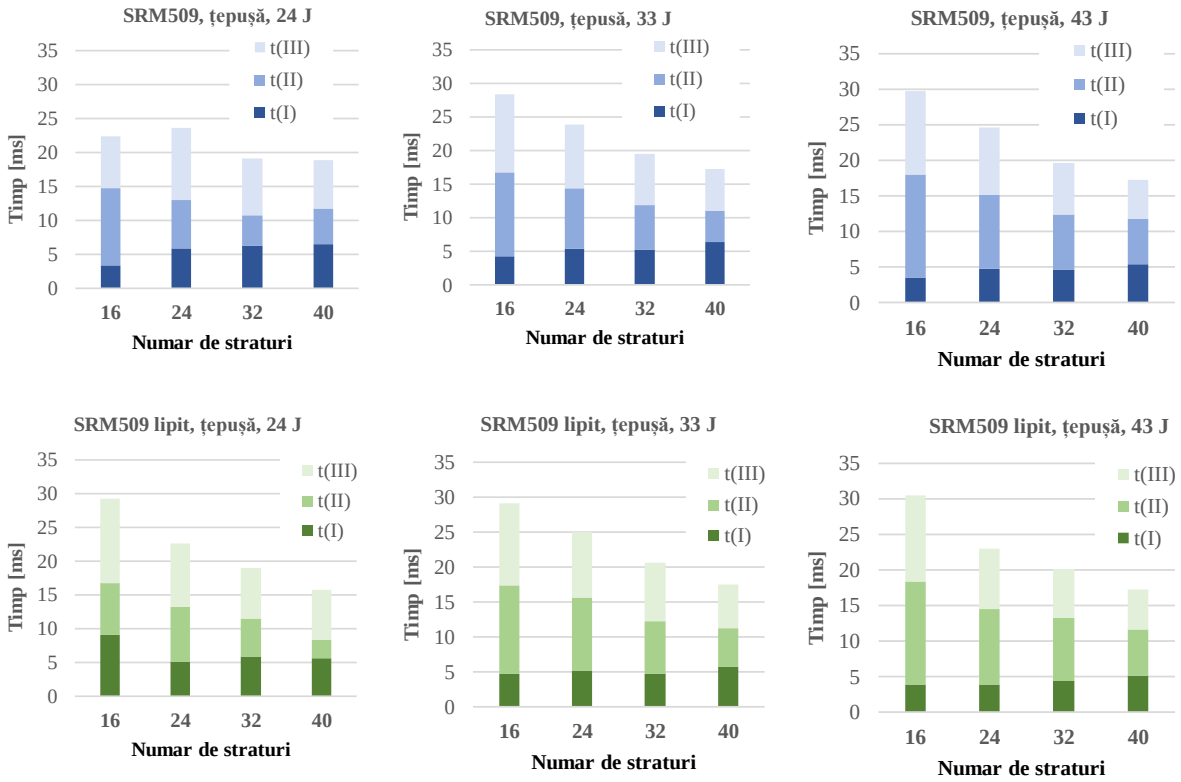

Fig. 5.43. Impact duration for spike tests

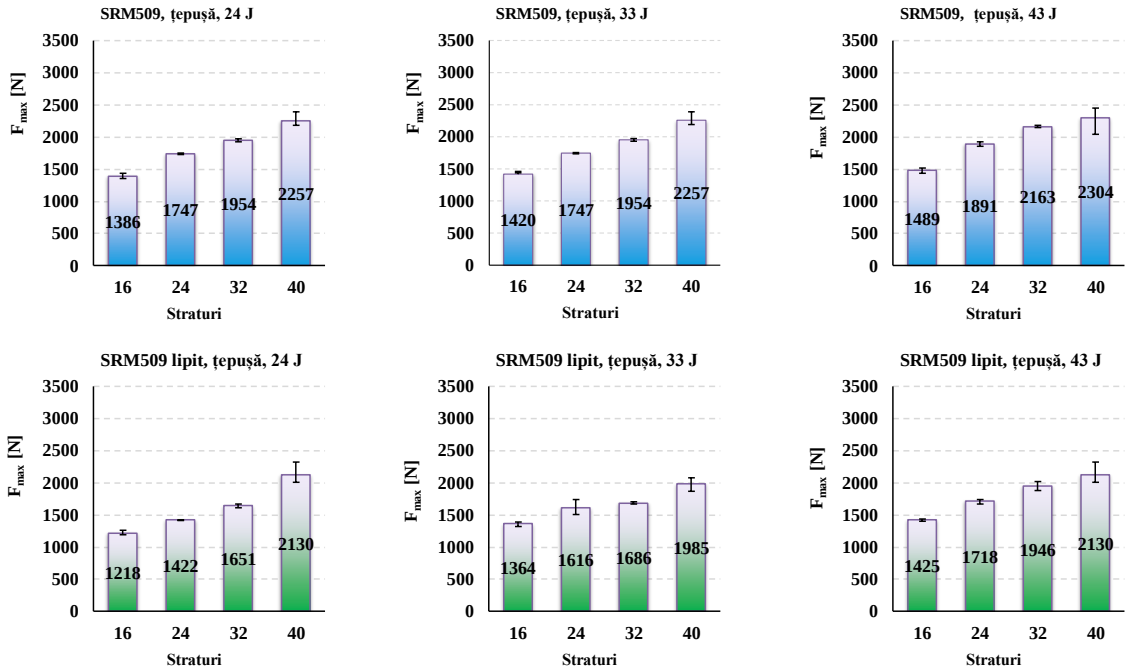

Fig. 5.44. $_{max}$Average value of maximum measured force, F , for spike tests

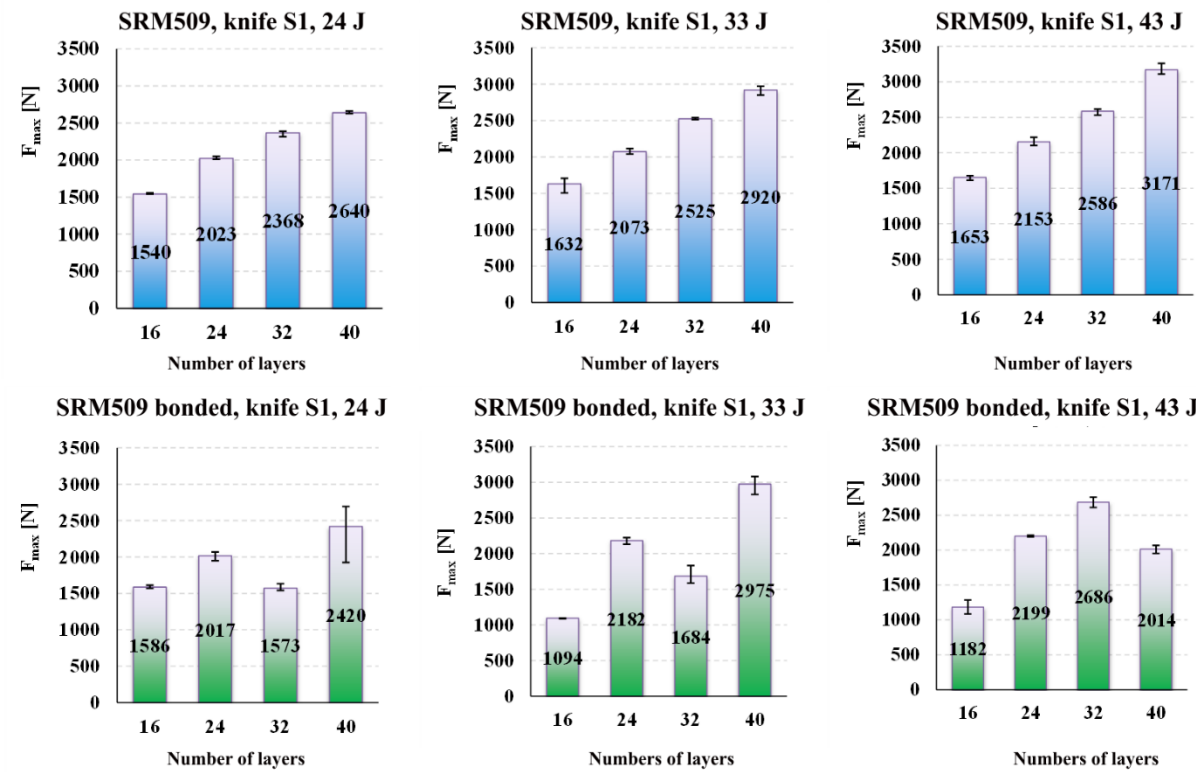

Fig.5.45. Average values and spread ranges for F_{max}, for knife S1 tests

For the knife, F_{max} evolves differently: for SRM panels, the trend still seems linear, but with higher values than for the spike, which can be explained by the fact that fewer wires break in the spike attack. For SRM509 soldered panels there is no clear trend. It can be assumed that the soldering technology is not yet good enough for clear results.

Figure 5.95 shows graphical conclusions on the tests performed on the Instron 9340 machine for the evolution of the mean Fmax value. It is better observed the increasing trend with the number of layers for the SRM509 panels and the increasing value of Fmax with increasing impact energy. For the bonded SRM509 no proportionality of Fmax with impact energy and number of layers was found.

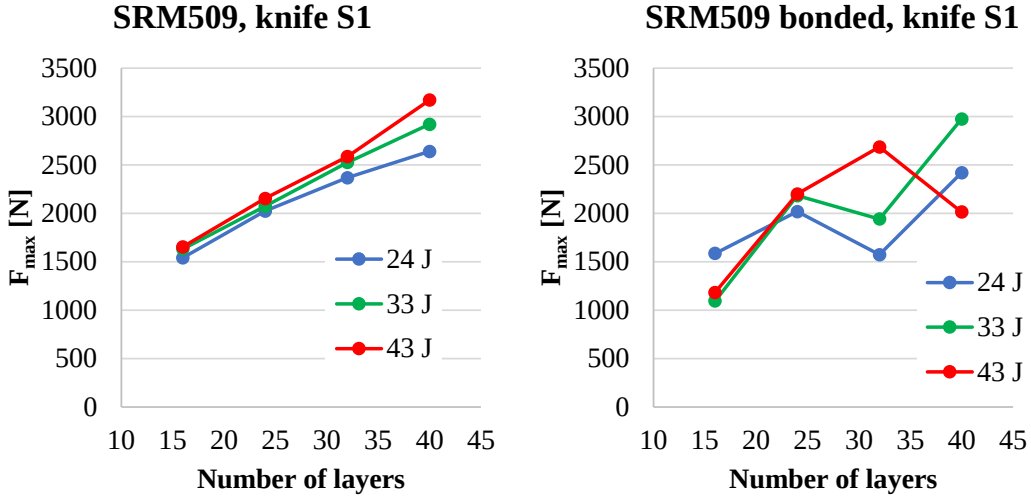

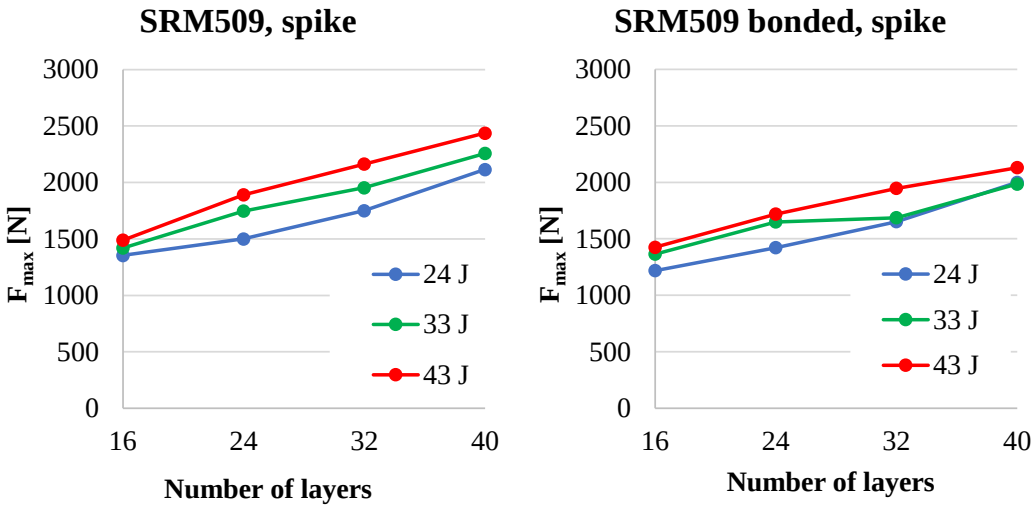

Fig. 5.46. Dependence of maximum striking force on weapon type (knife and spike), number of layers and striking energy

For the spike tests, the response of the two types of panels is similar, an almost linear increase in maximum force with the number of layers and an increasing ordering of values with increasing energy, for the same number of panel layers.

5.8. Tests on the CBRNE installation

As the plant was not instrumented, the relevant parameter was the penetration depth, calculated according to the cut length on the test paper, for the knife tests. For the spike tests, the evaluation was only qualitative (penetration or stopping of the spike in the board, without damage to the last layer.

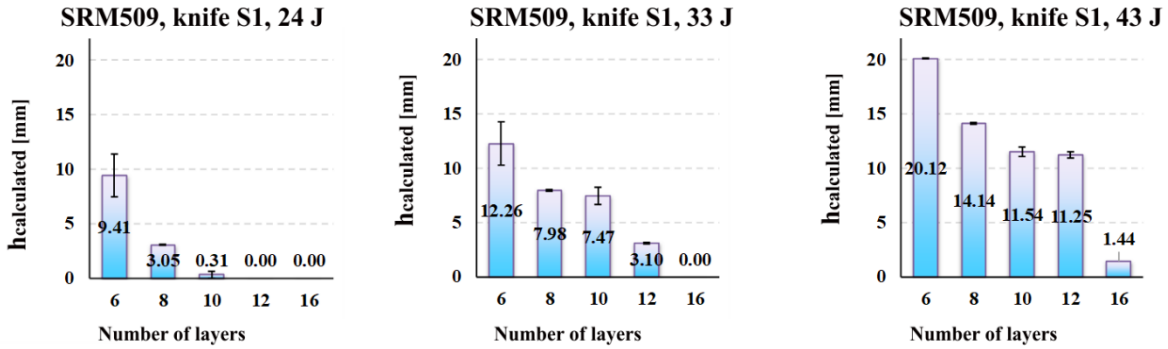

Fig. 5.47. Measured cut lengths for 6, 8, 10, 12, 16 ply panels tested at 24J, 33J, 43 J

The measured cut lengths for 6, 8, 10, 12 and 16 layers panels, tested at 24 J, 33 J and 43 J are shown in Fig. 5.47.

The influence of impact on the material decreases with increasing number of layers, with a linear decrease. Figure 5.47 shows the influence of material on $h_{calculated}$, the length of the cut trace on the back of the material and the breakage of layer 1 (one) for the 6,8,10,12, and 16-layer panels tested at stabbing impact with energy of 24 J, 33 J and 43 J, respevtively.

The samples were scored with the following codes (Fig. 5.48): 1P - hit at energy of 24 J, tested with knife, 2P - hit at energy of 33 J, knife test, 3P - hit at energy of 43 J, knife test, 1S - hit at energy of 24 J, spike test, 2S - hit at energy of 33 J, spike test, 3S - hit at energy of 43 J, spike test.

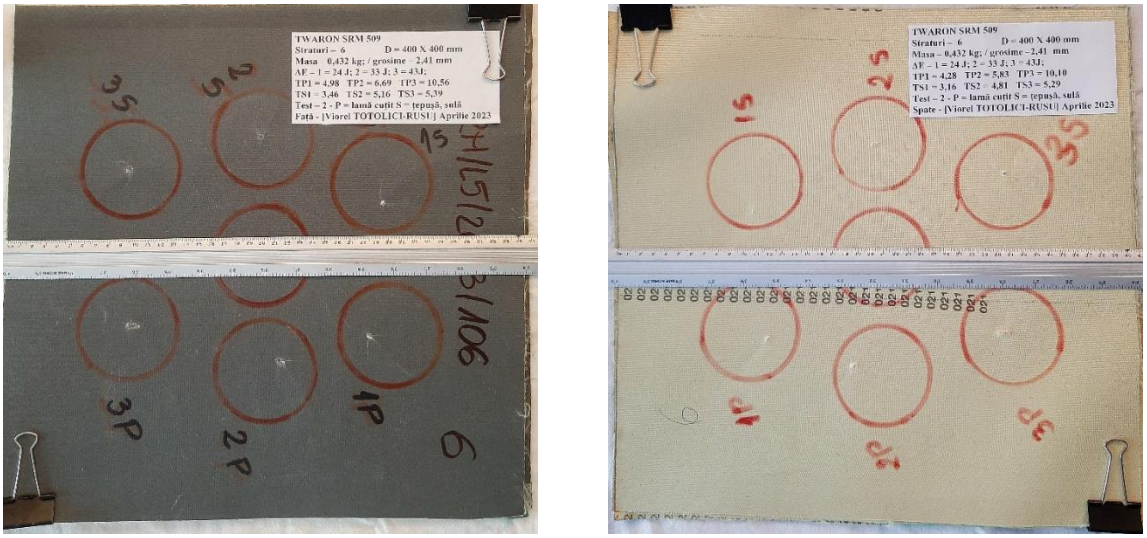

a) face b) Spate

Fig. 5.48 6 layers, SRM 509

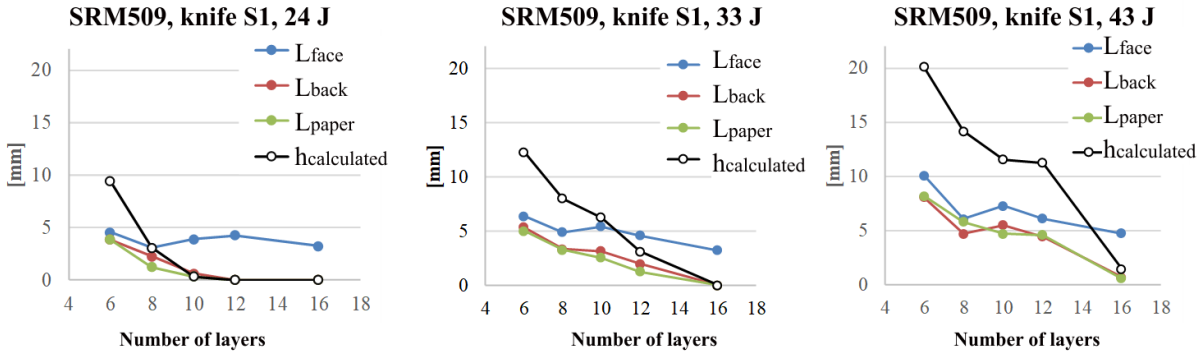

Fig. 5.49. Experimental results (mean values) as a function of the number of layers of SRM509 fabric (tests performed on the CCIACBRNE facility)

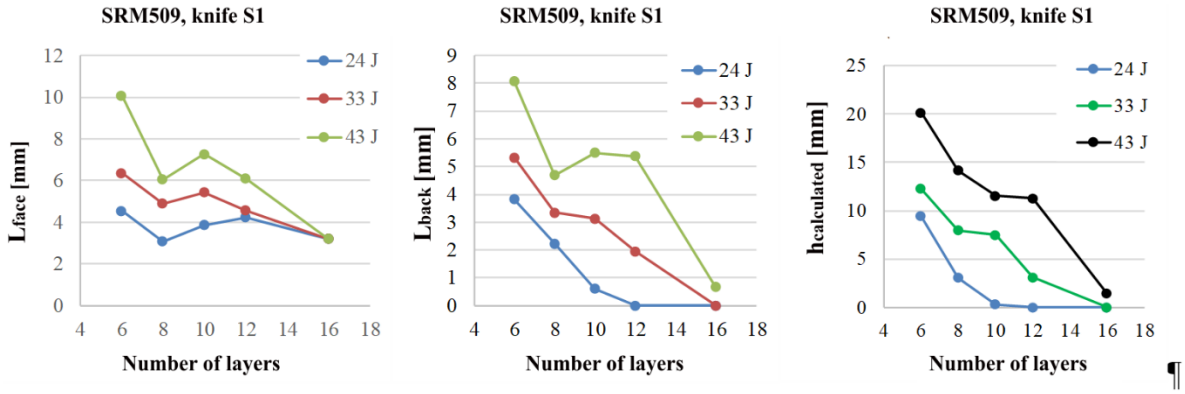

a) b) c)

Fig. 5.50. Experimental results (mean values) as a function of the number of layers of SRM 509 fabric a) front length, b) back length, c) $h_{calculated}$

5.9. Conclusions for Experimental Data

The results show that the higher the number of layers, the better the stab and puncture resistance performance.

Increasing the thickness of the material can prolong the puncture process, absorbing more impact energy. The modes of failure, in the case of a puncture impact, mainly include fibre cracking, sliding, detachment and shear and stretch breakage. The increase in impact energy will lead to an increase in puncture depth and damaged surface, but the mode of failure remains unchanged.

While for 16-layer panels, F_{max} has similar values for both knife impact and spike impact, at all energy levels tested, as the number of layers increases, higher values are obtained for spike impact.

As for the panels obtained from bonded and unbonded SRM509, the results are different.

In the spike test, the bonded SRM509 panels behaved similarly to the unbonded SRM509 panels, but lower values were recorded at 33 J and 43 J. This is explained by the fact that kinetic energy is also dissipated to debond the panels.

The duration till the maximum force in the 40-layer test is almost 10 ms, while in the 32-layer tests, the duration till the maximum force is 7 ms (milliseconds).

The variation of the force F_{max} is not very large from one level of energy to another. From 24 J to 33 J, the energy jump is 37.5% of the initial value, while the jump for force is a 5.9% jump from the maximum force recorded at 24 J.

The pulling-out and friction force of the yarns limited the slippage of the yarns, which caused more yarns to be pushed away in order to dissipate energy.

SEM was chosen to analyse samples because this technique can image at high resolution and offers a greater depth of field than optical microscopy. Thus, the fibre ends could be analysed at high resolution to observe any damage to them. It demonstrates through images, at lower or higher resolutions, the damage to the first and last layers, by white weapon. Penetration and fibre damage differs for each of the weapons involved in test plans.

As for the bonded SRM509 response to stabbing, the results of the performed tests are relatively different, although the three repeated tests recorded very close values.

The panels made of SRM509 have an almost linear, increasing dependence with the number of layers in tests performed at the same parameters. At a higher number of layers, F_{max} is obtained at the highest energy level.

The influence of the number of layers on F_{max} is greater than the influence of the impact energy.

Chapter 6
Conclusions

6.1 Importance of the Theme

Sharp, pointed objects can cause injury to a human, depending on their point or blade (by piercing, stabbing, breaking, cutting or a combination of these mechanisms). The injury potential of a knife or other bladed weapon depends primarily on the shape of the tip and blade. For example, puncture wounds are caused by sharp or rounded points and cuts caused by a sharp point that is forced into the body. The soft tissue penetration mechanism uses a combination of cutting and stabbing, resulting in deep tissue penetration. This penetration trauma depends on the weight, force and distance from which the knife is aimed and the type of tissue encountered. Very important is the area where the stab injury is sustained, so a chest injury, as opposed to an arm injury, for example, can more often lead to severe complications or even death.

In some cases, death is not directly caused by the knife injury, but by blood loss, subsequent infection, sepsis, pneumonia or hypotension.

Therefore, in cases where no gunshot residue or bullet fragments recovered are detected, sharp-edged knives could be considered a potential murder weapon. In these situations, the wearer would need protective clothing. This should be of increased protective capacity, be easy to wear and meet current quality standards.

Damage to the fabric can occur in many different ways, depending on the weapons used, such as tearing, where the tensile force on the fabric causes the yarns to stretch and/or tear, or cutting, where the fibres are cut. Puncture damage to clothing is caused by sharp tools without cutting edges and penetration depends on the shape of the tip and the force applied. The type of clothing affects penetration ability. For example, Twaron SRM509 fabric offers greater protection against stabbing than Twaron CT736CMP. In the experiments carried out in this research, knife cuts were examined, from which it was found that the blade tip attacked the fabric, pushing into the yarns, eventually causing some yarns to fail and, thus, resulting in cutting or tearing of the fabric. Blade penetration ability was influenced by several factors, including blade thickness and tip radius and/or sharpness. It was found that if the tip is more blunt, penetration is more difficult, resulting in greater fabric deformation and worn, stretched yarns rather than cut yarns.

It has been hypothesised that the lightweight coating would provide greater penetration resistance because it would absorb energy, thus reducing the speed and kinetic energy of the knife; that 400 mm x 400 mm test packs would provide greater penetration resistance due to the conversion of the kinetic energy of the weapon into deformation energy of the layers of the panel, the greater the transfer the greater the surface area of the panel and the weaker the lateral grip, so that kinetic energy is also consumed by deformation of the backing material, but this deformation must also be borne by the human body without risking the life of the wearer. Fibres, yarns and fabrics with high tensile strengths and high tensile deformation can therefore absorb considerable amounts of energy.

Personal armour is designed to deal with ballistic and stabbing threats and could be used by personnel operating in risky environments, such as police, soldiers, journalists,

security guards, bodyguards, etc. These threats could act as a combined event, with the effect of each threat acting simultaneously or in a short time on the same protection. The existence of properly made armour helps to preserve bodily integrity and significantly reduces the risk of death in the event of hazardous situations. In addition, it ensures a degree of mental comfort in the performance of the mission.

6.2 Final Conclusions on the Stab Resistance of the Tested Panels

The main research objective of the present work focused on the threat posed by readily available knives, which can be easily purchased from manufacturers, and the testing of stabbing materials that can be used in the production of protective armour. The weapons are usually of high quality and have very sharp cutting edges with fine points and are mechanically sharpened. But the response of materials can also be adapted by various processes to cope with these threats.

The application of the standards has undoubtedly led to improvements in the stab and puncture resistance of armour, although there are still a number of drawbacks, including: a trade-off between protection and mobility, restrictive and cumbersome use, problems and injuries related to inappropriate armour, the financial implications of large-scale deployment for all personnel involved in high-risk actions, poor humidity and temperature management, resulting in heat stress, illness and hampered operational performance.

Using the design possibilities offered today by new technologies, there is a growing opportunity to manufacture armour with a high degree of protection that provides the wearer with manoeuvrability and thermal comfort, and there is also interest in protection systems against combined threats.

The purpose of this work is to determine the stab resistance characteristics of a series of samples, following one of the specifications of the American standard []and to formulate recommendations for determining the minimum thickness required to ensure protection against stabbing and puncture. The stab resistance characteristics were determined during the testing of a series of flat specimens using approved test facilities, one instrumented (Instron 9340), the other non-instrumented (CRBRNE facility). All specimen samples made were tested using the principle of free-fall testing. They were impacted during the experiments with cutting blades, respectively, high-speed steel spikes at different impact energy levels.

This paper has been structured in six chapters, briefly presented below.

Chapter 1 presents the theoretical and experimental framework, which refers to the structure, testing and evaluation of the material characteristics at sharp-edged impact of the fabrics and blanks involved. Theories of various evaluation models, methods of testing materials under stabbing and puncture, and test results are presented. Also in this chapter, issues related to:

- definitions and concepts related to the stab resistance of laminated panels ,
- theories related to the use of stabbing materials and methods,
- types of materials used in technical practice,
- relevant information on the roles and functions of composite materials for protection against cutting impact.

Chapter 2 briefly provides information on the importance of the choice of topic, the objectives pursued and the research methodology. The thesis diagram is also presented here, summarising the stages of the organisation of this work.

Chapter 3 presents the modelling and simulation aspects of layered protection panels that are subjected to stabbing under different conditions. The model is performed at the macro level, in the sense that each layer of the modelled ponour is considered homogeneous and isotropic, but with a behaviour similar to the real one.

Chapter 4 is reserved for the research methodology of the set topic and includes information on the materials and methods of testing. The test methodologies and how to obtain the panels are described in turn.

Chapter 5 presents the analysis and interpretation of the data from the test campaigns. Experimental data on: stabbing and puncture resistance were recorded when testing small 130 mm x 130 mm samples (tests performed on the Instron 9340 machine) and large area samples (400 mm x 400 mm) tested on the CCICBRNE facility. It should be noted that the results obtained for these panels are useful for the design of a prototype, because the sample required in the standards is 500 mm x 500 mm; and the positioning of the blows are those recommended in the American standard. The following parameters of the S1 knife and spike impact were studied: maximum force, penetration depth, duration of the blank attack process. Dependencies of these parameters on the nature of the material (CT736CMP, SRM509 and SRM509 bonded), the number of layers, the weapon (S1 knife and spike) and the striking energy were established. The results obtained from the tests carried out led to the validation of the research direction and the achievement of the objectives set at the beginning of the research approach. The usefulness of the Twaron SRM509 material in preventing and minimising injuries caused by the penetration of sharp objects was demonstrated. A sub-chapter was dedicated to the study of the failure mechanisms of fibres and yarns depending on the material.

In Chapter 6, in order to support the results obtained from the research approach, the importance of the use of laminated panels in stab and/or puncture protection, and the understanding of the stab behaviour of these protective materials and the factors influencing their performance, in such an important area in terms of safety and survival, is highlighted once again.

6.3 Personal Contributions

Given the content of the paper, the author's contributions are:

- literature review on the subject of materials and construction solutions to stabbing and puncture, from accessible databases (Scopus, Elsevier, MDPI), from accessible industry standards, American standards, British standards, European standards, PhD theses and research reports, which have been published in the last 20 years,
- design of two test campaigns, one for the Instron CEAST 9340 machine at the National Institute for Aerospace Research and Development "Elie Carafoli" - INCAS Bucharest and another campaign on the stab test facility at the Institute of Research and Innovation Centre for CBRN Defence and Ecology, Bucharest, in order to observe the

influence of some parameters (number of layers, nature of the material, striking energy) on some characteristics such as the maximum striking force, the duration of the weapon attack process, the penetration depth of the S1 type knife, and the stabbing resistance of the panel,

- the material hierarchy for the panels (Twaron SRM509, Twaron CT736CMP and Twaron SRM 509 solder),

- modeling the stabbing process for a panel at a macro level, considering each panel to be made of isotropic and homogeneous layers, giving a result close to the experimental results performed at CBRN, so that the model is useful in preliminary evaluation in useful ranges of input parameters for the design of stab and puncture resistant panels,

-making the samples, grouped in packs of 16 layers, 24 layers, 32 layers and 40 layers, respectively, with dimensions of 130 mm x 130 mm, due to the fact that larger samples cannot fit on the Instron CEAST 9340 machine at the National Institute for Aerospace Research and Development "Elie Carafoli" - INCAS Bucharest,

- assembly by bonding of samples of Twaron SRM509 material, grouped in bundles of 16 layers, 24 layers, 32 layers and 40 layers respectively, with dimensions of 130 mm x 130 mm for the Instron CEAST 9340 - INCAS Bucharest machine,

- the production of the samples, grouped into 6-layer, 8-layer, 10-layer, 12-layer and 16-layer packages of 400 mm x 400 mm for the stab test facility at the Institute of Research and Innovation Centre for CBRN Defence and Ecology Bucharest,

- test plan for the Instron CEAST 9340 drop-test machine - INCAS Bucharest and for the test facility at CCIACBRNE,

- making of the blank weapons (4 pieces: 2 spikes and 2 S1 knives), which were used in the stabbing and pricking tests,

- photographing samples in detail,

- the study of material failure mechanisms at the macro level by post-test photography and examination at the micro level using scanning electron microscopy (SEM),

- processing of experimental results,

- partial dissemination of results in published papers presented at conferences.

The results obtained on the Instron CEAST 9340 machine have allowed the hierarchy of the tested materials and the study of the failure mechanisms; the surface area of the tested panel being small, it does not favour elastic deformation and, therefore, the behaviour of these samples is not very close to that of the real garment panels.

The tests performed on the larger, lightly smaller panels (400 mm x 400 mm instead of standard 500 mm x 500 mm), carried out on the CCIACBRNE stab test facility, without pressing the whole package panel + support material, is closer to the behaviour of the jacket in reality, therefore, the test results are different; they were better in the sense that the larger area samples behaved better at a lower number of layers.

Twaron SRM509 panels performed better than Twaron CT736CMP, and Twaron SRM 509 bonded panels performed similarly to unbonded panels, but the bonding assembly technology with this adhesive gave more spread-out and less predictable results than panels of the same material, SRM509, but unbonded.

By analyzing SEM images, the author found that the damage at micro levels of yarns and fibers include the same mechanisms, but for the knife, it is dominant the shearing of the

yarns and fibers, especially on the first layers, while for the spike, the fiber breakage is done by shearing as well as by stretching. SEM images revealed that the hard particles on the surface of the SRM509 fabric interact with the weapon and participate in the dissipation of the striking energy, abrasion wear, cracking and breakage of the particle corners were revealed.

6.4. Research Directions Initiated by This Study

Based on the present work, possible research directions are opened, related to the use of stab-resistant aramid materials. Some of these are listed below:

- further study of hybrid panels, also made with carbon fibre fabrics, with other types of coatings to achieve better results at lower surface density,

- the production and testing of other aramid fibre panels (made of a number of different layers) for body protection, in compliance with current standards,

- studying stabbing behaviour for different parameters, such as stabbing angle.

List of scientific papers of the author

Articles in journals indexed in Web of Science (WoS), or Scopus

1. **Totolici-Rusu, V.**, Ojoc, G.G., Cristea, G.C., Chiper, L.T., Botan, M., Muntenita, C. & Deleanu, L. (2022). Characteristics of Stab-resistant Panels Made of Twaron Aramid Fabrics. Plastics Materials, 59(4), 144-154. https://doi.org/10.37358/MP.22.4.5633, WOS:00096503 0700013

2. Ojoc G. G**., Totolici Rusu V.**, Pîrvu C., Deleanu L., How Friction Could Influence the Shape and Failure Mechanism in Impact, With the Help of a Finite Element Model, U.P.B. Sci. Bull., Series D, Vol. 83, Iss. 3, 2021, ISSN 1454-2358, https://www.scientific bulletin. upb.ro /rev_docs_archive/reza6a_789278.pdf

3. Ojoc G.-G., **Totolici-Rusu V.** Popescu C., Pirvu C., Deleanu L., Influence of friction in a case of impact simulation, INCAS Bulletin, Volume 12, Issue 4, 2020, pp. 145-154, DOI: 10.13111/2066-8201.2020.12.4.13; https://doi.org/10.13111/2066-8201.2020.12.4.13

Articles in peer-reviewed journals or international conferences indexed by BDI

1. **Totolici Rusu V.**, Ojoc G. G., Pirvu C., Deleanu L., (2021). Influence of element size in a case of impact simulation. Mechanical Testing and Diagnosis, 10(4), 24-29. https://www.gup.ugal.ro/ugaljournals/index.php/ mtd/article/view/4068

2. **V. Totolici Rusu**,, "Design of a composite and impact tests", published in Mechanical Testing and Diagnosis volume 4, pag. 9-16, 2017.

3. Chiper Titire L., **Totolici Rusu V.**, Sandu S., Influence of material characteristics on impact response for fabrics made of glass and aramid fibers, The 10th International Conference on Advanced Concepts in Mechanical Engineering (ACME 2022). 09 - 10 June, 2022, Online. IOP Conference Series: Materials Science and Engineering, Vol. 1262, IOP Publishing Ltd. DOI 10.1088/1757-899X/1262/1/012045

Participation in international conferences

1. Cantaragiu (Ceoromila) A., Ojoc G. G., Titire (Chiper) L., **Totolici Rusu V.**, Deleanu L., Composites and Polymers Failure Processes in Tribology by Scanning Electron Microscopy, PPE 2021, The 6th International Conference on Polymer Processing in Engineering, 18-19 November 2021, Galati, Romania, http://www.if.ugal.ro/PPE2021/ PPE2021Abstracts.pdf

2. Chiper Titire L., Ojoc G. G., **Totolici Rusu V.**, Deleanu L., Influence of material of unidirectional fabrics in modeling the impact with a sphere, Scientific Conference of Doctoral Schools, Book of Abstract, p. 62, http://www.cssd-udjg.ugal.ro/index.php/2020-2/abstracts-2023 (oral presentation)

3. Ojoc G. G., **Totolici Rusu V.**, Pirvu C., Deleanu L., How Friction Could Influence the Shape and Failure Mechanism in Impact, with the Help of a Finite Element Model. 8th International Conference on Materials Science and Technologies - RoMat 2020, Bucharest (Romania), 26-27 November, 2020, http://www.mse.pub.ro/images/ RoMAT2020/RoMAT-2020_Program-Stiintific.pdf (oral presentation)

4. Chiper Titire L., Ojoc G. G., **Totolici Rusu V.**, Deleanu L., Influence of yarn architecture in simulating the impact with a sphere, 4th International Conference of the Doctoral School "Gheorghe Asachi" Technical University of Iasi, May 19-21, 2021 IASI, ROMANIA, p 44, http://www.csd2021.tuiasi.ro/docs/ CSD2021_Program_Detailed.pdf (oral presentation)

5. Chiper Titire L., **Totolici Rusu V.**, Sandu S., Influence of material characteristics on impact response for fabrics made of glass and aramid fibers, The 10th International Conference on Advanced Concepts in Mechanical Engineering (ACME 2022). 09 - 10 June, 2022, Online. IOP Conference Series: Materials Science and Engineering, Vol. 1262, IOP Publishing Ltd. DOI 10.1088/1757-899X/1262/1/012045

6. **Totolici-Rusu V.**, Determination of dynamic mechanical characteristics of composite materials. National Session of Student Scientific Communications "Anghel Saligny". University "Dunărea de Jos". Galati, 17-18 May 2018.